UNIVERSITY OF CALIFORNIA
RIVERSIDE

Secondary Organic Aerosol Formation From Select Volatile Organic Compounds

A Dissertation submitted in partial satisfaction
of the requirements for the degree of

Doctor of Philosophy

in

Chemical and Environmental Engineering

by

Chia-Li Chen

August 2015

Dissertation Committee:
Dr. David R. Cocker III, Chairperson
Dr. Akua Asa-Awuku
Dr. David Jassby

This Dissertation of Chia-Li Chen is approved:

_____

_____

_____

Committee Chairperson

University of California, Riverside

Acknowledgements

I would like to show my sincere and earnest thankfulness to every individual who helped me in my five years Ph.D. research and student life at UCR CE-CERT. Without his or her help this dissertation would not have been possible.

First, I would like to thank my advisor, Professor David Cocker for educating me, advising me, supporting me with his excellent guidance and patience. He not only educates me in professional air quality research, but also gives me opportunities to learn analytical methods and instrumentation such as method 5, EC/OC, IC analysis and the HR-ToF-AMS. I feel thankful that I have gained these professional skills to which I can then apply and contribute to atmospheric research.

Second, I would like to show my gratitude towards to previous Ph.D. graduate students: Dr. Shunsuke Nakao, Dr. Ping Tang (Annie) and Dr. Xioachen Tang (Esther) for patiently training me on chamber experimental techniques and advising me for my research. Especially I would like to thank Dr. Tang (Annie) as she trained me on a number of AMS instrument troubleshooting skills and data analysis. Thanks must be given to current graduate students Dr. Derek Price, Mary Kacarab, Lijie Li, Weihua Li, for contributing to keeping the chamber running, as well as some of the experiments and data processing for this work. Additionally, I would like to especially thank Ms. Kathy Cocker for analyzing chemical identification for gasoline samples, Ms. Yue Lin for performing TEM images analysis at UCR-CFAMM, and Dr. William P. L. Carter and Dr. Gookyoung Heo for SAPRC model troubleshooting assistance. Completion of this work

will not have happened without the assistance and support of CE-CERT staff members Mr. Kurt Bumiller and Mr. Todd Ambriz.

Third, I would like to thank my advisory committee Dr. Akua Asa-Awuku, Dr. David Jassby for their time and advice, and Dr. Mark R. Matsumoto, Dr. Marko Princevac for giving me valuable comments during my advanced to candidacy exam.

Last but not least, I would like to give my special appreciations to my dear parents and Dr. Nicholas Gysel. Dr. Nicholas Gysel always supports me, encourages me, and takes care of me during those five years. No matter what happened, he was always willing to assist me. Also, my dear parents, family, and friends in Taiwan always support me and encourage me during my Ph.D. years.

Importantly, this study was supported by a number of funding agents. Thanks should be given to W.M. Keck Foundation, National Science Foundation (ATM-0449778, ATM-0901282), UCR-Department of Chemical and Environmental Engineering, California Air Resources Board, and Ford Pierson graduate fellowship.

ABSTRACT OF THE DISSERTATION

Secondary Organic Aerosol Formation From Select Volatile Organic Compounds

by

Chia-Li Chen

Doctor of Philosophy, Graduate Program in Chemical and Environmental Engineering
University of California, Riverside, August 2015
Dr. David R. Cocker III, Chairperson

This thesis enhances our understanding of secondary organic aerosol (SOA) formation from select anthropogenic sources including polycyclic aromatic hydrocarbons (PAHs), PAHs mixed with *m*-xylene and an atmospheric surrogate, and unburned whole gasoline vapors. Major SOA chemical characteristics and physical properties were explored along with SOA formation within the UCR CE-CERT environmental chamber.

SOA formation was significant for all three PAHs precursors during photooxidation under high NO_x, low NO_x and extremely low NO_x conditions with 1-methylnaphthalene forming the most SOA followed by 2-methylnaphthalene and naphthalene. SOA yields greater than 1.0 were observed for extremely low NO_x (H_2O_2) conditions. The atmospheric reactivity influenced by H_2O_2, NO_x levels, initial VOCs/NO ratios, and all impacted the SOA formation from the PAH precursors. Fractal SOA particles were observed for 1-methylnaphthalene or 2-methylnaphthalene high NO_x photooxidation, indicating that SOA in these experiments were solid particles. SOA growth rates (aerosol mass concentration (ΔM_0) versus hydrocarbon reacted (ΔHC)) from different PAHs-*m*-xylene mixtures are correlated with initial *m*-xylene/NO, PAHs/NO, $[OH]/[HO_2]$ ratio, $[NO]/[HO_2]$ ratio and $[HO_2]/[RO_2]$ ratio. Addition of *m*-xylene to

PAHs experiments suppressed SOA formation from the PAH precursor. The chemical composition characteristics such as f_{44} versus f_{43}, H/C ratio, O/C ratio, and the oxidation state of the carbon ($\overline{OS}_c$) show that PAHs-*m*-xylene SOA continuously ages and the SOA exhibits characteristics of both individual precursors.

Finally, the SOA formation from photooxidation of whole gasoline vapor under varying NO_x conditions was found to range from 1.7% to 5.2%. Further, addition of ethanol suppressed the SOA formation. This work shows that the traditional two-product SOA formation model was unable to explain the total SOA formation from the complex gasoline mixture using the actual formation observed for individual aromatic SOA precursors.

Table of Contents

List of Tables

List of Figures

Chapter 1. Introduction

1.1 Introduction of Dissertation

Secondary organic aerosol (SOA) is formed from gas-particle conversion processes of primary organic gases from both anthropogenic and biogenic sources. Organic compounds are also emitted directly in particulate form and are referred as Primary Organic Aerosol (POA) (Kanakidou et al., 2005). Most urban tropospheric aerosols originate from anthropogenic sources. Organic gases are oxidized by hydroxyl radicals (OH), ozone (O_3), nitrate radicals (NO_3) undergoing chemical transformations to form secondary organic aerosols by condensation or nucleation (Seinfeld and Pandis, 2006). It is estimated that organic matter contributes 20~50% of the total fine aerosol mass globally in the lower troposphere at continental mid-latitudes (Kanakidou et al., 2005; Saxena and Hildemann, 1996; Zhang et al., 2007) and as high as 90% in tropical forested areas (Andreae and Crutzen, 1997).

A large mass fraction of fine particulate matter (PM) (aerodynamic diameter ≤ 2.5 μm) is comprised of SOA. PM is a major contributor to changes in radiative forcing (Hoyle et al., 2011; Kanakidou et al., 2005; Schulz et al., 2006) visibility degradation, and is linked to increasing risk of lung cancer, respiratory morbidity and mortality. (Anderson et al., 2001; Moolgavkar and Luebeck, 1996; Pope III, 2002). The presence of organic species in atmospheric aerosol can affect particle hygroscopicity and the internally mixed aerosol particles microphysics properties act as CCN (Merikanto et al., 2009). However, there are uncertainties in the factors related to emission inventories,

radiative forcing, and global modeling and how they correlated with SOA formation that require further study.

Biogenic (mostly monoterpenes) and anthropogenic volatile organic compounds (mostly aromatic hydrocarbons) have been deemed as precursor substances to the SOA formation with their aerosol formation readily measured in chamber studies. The formation of low volatility organic species originate from a variety of chemical processes including "oxidation reactions in the gas phase, reactions in the particle-phase and continuing chemistry over multiple generations of oxidation products" (Kroll and Seinfeld, 2008). Some of these reaction products are able to reversibly partition into the condensed phase. Odum et al. (1996) first established the expression of fractional SOA yield (Y) to describe the gas-particle partitioning absorption model developed by (Odum et al., 1996; Pankow, 1994) with the key assumption that SOA is composed predominantly of semivolatile organics.

Over the past decade, numerous laboratory studies have investigated SOA formation under different high/low NO_x conditions from oxidation of monoterpenes, aromatic hydrocarbons and polycyclic aromatic hydrocarbons (PAHs) (e.g., aromatics: Cocker et al., 2001; Forstner et al., 1997; Hurley et al., 2001; Izumi and Fukuyama, 1990; Ng et al., 2007; Odum et al., 1997; Song et al., 2005, 2007; PAHs: Chan et al., 2009; Kautzman et al., 2010; Kleindienst et al., 2012; Shakya and Griffin, 2010). Atmospheric reactivity conditions including NO_x level, VOC/NO_x ratio, relative humidity, temperature, hydroxyl radical (OH) level, NO_2 photolysis rate are all significant factors to SOA formation from aromatic hydrocarbon precursors (e.g., Warren et al., 2008 (light

intensity); Cocker et al., 2001 (RH); Tang et al., 2015 (OH); Warren et al., 2009 (temperature); Hurley et al., 2001; Kroll et al., 2006; Ng et al., 2007; Presto et al., 2005; Song et al., 2005 (NO_x levels)).

The chemical mechanism for aromatic hydrocarbons and PAHs oxidation is complex and poorly understood. Oxidation commences with OH radical attack of the aromatic hydrocarbons followed by O_2 addition, cyclization, and atmospheric competition for bicyclic peroxy radicals (RO_2) (Henze et al., 2008). The organic peroxy (RO_2) radical is critical for evolution of in low volatility organic aerosol formation and the interplay of NO_x levels in terms of competitive RO_2 chemistry (Kroll and Seinfeld, 2008):

$$\text{Volatile Organic Compounds (VOCs)} + OH \quad \text{(R1)}$$

$$RO_2 + HO_2 \rightarrow ROOH + O_2 , \quad \text{(R2)}$$

$$RO_2 + NO \rightarrow RO + NO_2 , \quad \text{(R3a)}$$

$$RO_2 + NO[+M] \rightarrow RONO_2[+M] \cdot \quad \text{(R3b)}$$

$$RO \xrightarrow{\text{dissociation}} R\cdot\text{(alkyl fragment)} + C{=}O\ \text{(carbonyl)} \quad \text{(R4a)}$$

$$RO \xrightarrow{\text{isomerization}} ROH \cdot \quad \text{(R4b)}$$

$$RO \xrightarrow{O_2} R'O + HO_2 \quad \text{(R4c)}$$

Reaction (R2) forms a low volatility hydroperoxide, which is a major component of SOA formation. In the presence of NO_x condition, RO_2 will react with NO to form alkoxy radical (R3a) or organic nitrate ($RONO_2$) (R3b). The alkoxy (RO) radical can then by

dissociate (R4a), isomerize (R4b), and reacted with oxygen to form a carbonyl and HO_2 (R4c).

Currently, SOA models predict SOA using an empirical parameterization system based on smog chamber experiments to compute mass-based stoichiometric yields to represent some degree of gas-phase oxidation. Two empirical model approaches currently used include the " two-product model" (Odum et al., 1996) and the "volatility basis set" (Donahue et al., 2006). The "two-product model" is based on the equilibrium of gas-phase partitioning of lumped species into condensed organic species. The "volatility basis set" modeling approach is similar to the "two-product model"; however, in this approach semivolatile oxidation products are distributed in logarithmically scaled volatility bins. Previous studies reported that current climate and air quality models often underestimate the total organic aerosols including POA and SOA in urban and remote areas (Heald et al., 2005; Henze et al., 2008; Hodzic et al., 2009; Kleinman et al., 2008; Utembe et al., 2011; Volkamer et al., 2006), mainly due to imperfect parameterization on the chemistry reaction processes and SOA photochemical aging properties that are still not understood (Zhang et al., 2006), and the overestimation of POA (de Gouw et al., 2005). Some "missing" sources of SOA in the National Emission Inventory and SPECIATE species remain unidentified. Polycyclic aromatic hydrocarbons (PAHs) may be a major "missing" source of SOA precursors.

The objectives of this dissertation are focused on three areas of SOA chamber research. First, the chemical characteristics and physical properties of SOA formation from oxidation of PAHs such as naphthalene and methylnaphthalenes under high NO_x

(with HONO), low NO_x, and extremely low NO_x (H_2O_2) condition are investigated. Secondly, the PAHs with different *m*-xylene and surrogate experiments are conducted to explore the SOA chemical composition and physical properties and to further understand the atmospheric condition SOA formation from mixture compounds. Finally, due to, Substantial changes to the U.S.EPA reformulated gasoline program since 1990s include reductions in C_4-C_5 alkenes, benzene, and C_{9+} aromatics from gasoline vapor. Therefore, the final objective was to reevaluate SOA formation from select whole gasoline vapor and fuels using the two-product model and volatility basis set. The ability of these models to predict SOA from complex mixtures using individual precursors us further explored.

Chapter 2 investigates the SOA formation from select polycyclic aromatic hydrocarbons (PAHs) photooxidation under high NO_x, low NO_x, and extremely low NO_x (H_2O_2) conditions. SOA yield is observed to be high for the three PAHs studied (naphthalene, 1-methylnaphthalene, and 2-methylnaphthalene). Traditional two-product model SOA yield curves are established for the different NO_x conditions investigated. The chemical composition and elementary analysis of SOA formation from PAH photooxidation is further characterized by High-Resolution Time-of-Flight Aerosol Mass Spectrometer (HR-ToF-AMS) along with the SOA density and volatility evolution.

Chapter 3 extends the study in Chapter 2 of SOA formation from individual PAH photooxidation to that with different aromatic (*m*-xylene) and surrogate mixtures. The two-product model curves derived from individual PAH and *m*-xylene photooxidation under low NO_x and H_2O_2 condition are used to predict SOA yield from PAHs and *m*-xylene. Both the *m*-xylene and surrogate are found to suppress SOA formation from

individual PAH photooxidation. Additionally, the SAPRC 11 model (Carter, 2010) is used for predicting concentrations of OH radicals, HO_2 radicals, and RO_2 radicals from the mixtures studied. A good linear relationship between SOA growth rate and different radical ratios (e.g., [OH]/[HO_2] ratio, NO/[HO_2] ratio, and [HO_2]/[RO_2] ratios), *m*-xylene/NO, and *m*-xylene/PAHs ratios is observed.

Chapter 4 revisits SOA formation from reformulated whole gasoline vapor photooxidation by selecting representative summer and winter blend gasolines and reference fuels and conduct chamber experiments on them under low NO_x conditions. The basic chemical composition of each gasoline is investigated and along with the aromatic hydrocarbon weight percentage and OH radical concentrations predicted from the SAPRC 11 model and OH rate constant (k_{OH}), the amount of aromatic reacted is estimated. Two-product models for aromatic hydrocarbons (C_{6-7}, C_{8-9}, and C_{10+}) developed by previous work (Tang et al., 2015) is also applied to predict the SOA yield from whole gasoline vapor and reference fuels with and without ethanol.

1.2 References

Anderson, H. R., Bremner, S. A., Atkinson, R. W., Harrison, R. M. and Walters, S.: Particulate matter and daily mortality and hospital admissions in the west midlands conurbation of the United Kingdom: associations with fine and coarse particles, black smoke and sulphate., Occup. Environ. Med., 58(8), 504–510, doi:10.1136/oem.58.8.504, 2001.

Andreae, M. O. and Crutzen, P. J.: Atmospheric Aerosols: Biogeochemical Sources and Role in Atmospheric Chemistry, Science, 276(5315), 1052–1058, doi:10.1126/science.276.5315.1052, 1997.

Carter, W. P. L.: Development of a condensed SAPRC-07 chemical mechanism, Atmos. Environ., 44(40), 5336–5345, doi:10.1016/j.atmosenv.2010.01.024, 2010.

Chan, A. W. H., Kautzman, K. E., Chhabra, P. S., Surratt, J. D., Chan, M. N., Crounse, J. D., Kürten, A., Wennberg, P. O., Flagan, R. C. and Seinfeld, J. H.: Secondary organic aerosol formation from photooxidation of naphthalene and alkylnaphthalenes: Implications for oxidation of intermediate volatility organic compounds (IVOCs), Atmos. Chem. Phys., 9(9), 3049–3060, doi:10.5194/acp-9-3049-2009, 2009.

Cocker, D. R., Mader, B. T., Kalberer, M., Flagan, R. C. and Seinfeld, J. H.: The effect of water on gas-particle partitioning of secondary organic aerosol: II. *m*-xylene and 1,3,5-trimethylbenzene photooxidation systems, Atmos. Environ., 35(35), 6073–6085, doi:10.1016/S1352-2310(01)00405-8, 2001.

Donahue, N. M., Robinson, a L., Stanier, C. O. and Pandis, S. N.: Coupled partitioning, dilution, and chemical aging of semivolatile organics, Environ. Sci. Technol., 40(8), 2635–2643, doi:10.1021/es052297c, 2006.

Forstner, H. J. L., Flagan, R. C. and Seinfeld, J. H.: Secondary Organic Aerosol from the Photooxidation of Aromatic Hydrocarbons: Molecular Composition, Environ. Sci. Technol., 31(5), 1345–1358, doi:10.1021/es9605376, 1997.

De Gouw, J. a., Middlebrook, A. M., Warneke, C., Goldan, P. D., Kuster, W. C., Roberts, J. M., Fehsenfeld, F. C., Worsnop, D. R., Canagaratna, M. R., Pszenny, A. A. P., Keene, W. C., Marchewka, M., Bertman, S. B. and Bates, T. S.: Budget of organic carbon in a polluted atmosphere: Results from the New England Air Quality Study in 2002, J. Geophys. Res. D Atmos., 110(D16), 1–22, doi:10.1029/2004JD005623, 2005.

Heald, C. L., Jacob, D. J., Park, R. J., Russell, L. M., Huebert, B. J., Seinfeld, J. H., Liao, H. and Weber, R. J.: A large organic aerosol source in the free troposphere missing from current models, Geophys. Res. Lett., 32(L18809), doi:10.1029/2005GL023831, 2005.

Henze, D. K., Seinfeld, J. H., Ng, N. L., Kroll, J. H., Fu, T.-M., Jacob, D. J. and Heald, C. L.: Global modeling of secondary organic aerosol formation from aromatic hydrocarbons: high- vs. low-yield pathways, Atmos. Chem. Phys., 8(9), 2405–2420, doi:10.5194/acp-8-2405-2008, 2008.

Hodzic, A., Jimenez, J. L., Madronich, S., Aiken, A. C., Bessagnet, B., Curci, G., Fast, J., Lamarque, J. F., Onasch, T. B., Roux, G. and Ulbrich, I. M.: Modeling organic aerosols during MILAGRO: application of the CHIMERE model and importance of biogenic secondary organic aerosols, Atmos. Chem. Phys. Discuss., 9, 12207–12281, doi:10.5194/acpd-9-12207-2009, 2009.

Hoyle, C. R., Boy, M., Donahue, N. M., Fry, J. L., Glasius, M., Guenther, A., Hallar, A. G., Huff Hartz, K., Petters, M. D., Petäjä, T., Rosenoern, T. and Sullivan, A. P.: A review of the anthropogenic influence on biogenic secondary organic aerosol, Atmos. Chem. Phys., 11(1), 321–343, doi:10.5194/acp-11-321-2011, 2011.

Hurley, M. D., Sokolov, O. and Wallington, T. J.: Organic aerosol formation during the atmospheric degradation of toluene, Environ. Sci. Technol., 35(7), 1358–1366, doi:10.1021/es0013733, 2001.

Izumi, K. and Fukuyama, T.: Photochemical aerosol formation from aromatic hydrocarbons in the presence of NOx, Atmos. Environ. Part A. Gen. Top., 24(6), 1433–1441, doi:10.1016/0960-1686(90)90052-O, 1990.

Kanakidou, M., Seinfeld, J. H., Pandis, S. N., Barnes, I., Dentener, F. J., Facchini, M. C., Van Dingenen, R., Ervens, B., Nenes, a., Nielsen, C. J., Swietlicki, E., Putaud, J. P., Balkanski, Y., Fuzzi, S., Horth, J., Moortgat, G. K., Winterhalter, R., Myhre, C. E. L., Tsigaridis, K., Vignati, E., Stephanou, E. G. and Wilson, J.: Organic aerosol and global climate modelling: a review, Atmos. Chem. Phys., 5(4), 1053–1123, doi:10.5194/acp-5-1053-2005, 2005.

Kautzman, K. E., Surratt, J. D., Chan, M. N., Chan, a W. H., Hersey, S. P., Chhabra, P. S., Dalleska, N. F., Wennberg, P. O., Flagan, R. C. and Seinfeld, J. H.: Chemical composition of gas- and aerosol-phase products from the photooxidation of naphthalene., J. Phys. Chem. A, 114(2), 913–34, doi:10.1021/jp908530s, 2010.

Kleindienst, T. E., Jaoui, M., Lewandowski, M., Offenberg, J. H. and Docherty, K. S.: The formation of SOA and chemical tracer compounds from the photooxidation of naphthalene and its methyl analogs in the presence and absence of nitrogen oxides, Atmos. Chem. Phys. Discuss., 12(5), 12163–12201, doi:10.5194/acpd-12-12163-2012, 2012.

Kleinman, L. I., Springston, S. R., Daum, P. H., Lee, Y.-N., Nunnermacker, L. J., Senum, G. I., Wang, J., Weinstein-Lloyd, J., Alexander, M. L., Hubbe, J., Ortega, J., Canagaratna,

M. R. and Jayne, J.: The time evolution of aerosol composition over the Mexico City plateau, Atmos. Chem. Phys., 8(6), 1559–1575, doi:10.5194/acp-8-1559-2008, 2008.

Kroll, J. H. and Seinfeld, J. H.: Chemistry of secondary organic aerosol : Formation and evolution of low-volatility organics in the atmosphere, , 42, 3593–3624, doi:10.1016/j.atmosenv.2008.01.003, 2008.

Kroll, J. H., Ng, N. L., Murphy, S. M., Flagan, R. C. and Seinfeld, J. H.: Secondary organic aerosol formation from isoprene photooxidation., Environ. Sci. Technol., 40(6), 1869–1877, doi:10.1021/es0524301, 2006.

Merikanto, J., Spracklen, D. V., Mann, G. W., Pickering, S. J. and Carslaw, K. S.: Impact of nucleation on global CCN, Atmos. Chem. Phys. Discuss., 9(3), 12999–13037, doi:10.5194/acpd-9-12999-2009, 2009.

Moolgavkar, S. H. and Luebeck, E. G.: A critical review of the evidence on particulate air pollution and mortality., Epidemiology, 7(4), 420–428, 1996.

Ng, N. L., Kroll, J. H., Chan, a W. H., Chhabra, P. S., Flagan, R. C. and Seinfeld, J. H.: Secondary organic aerosol formation from m-xylene, toluene, and benzene, Atmos. Chem. Phys., 7(3), 3909–3922, doi:10.5194/acp-7-3909-2007, 2007.

Odum, J. R., Hoffmann, T., Bowman, F., Collins, D., Flagan, R. C. and Seinfeld, J. H.: Gas/Particle Partitioning and Secondary Organic Aerosol Yields, Environ. Sci. Technol., 30(8), 2580–2585, doi:10.1021/es950943+, 1996.

Odum, J. R., Jungkamp, T. P. W., Griffin, R. J., Forstner, H. J. L., Flagan, R. C. and Seinfeld, J. H.: Aromatics, Reformulated Gasoline, and Atmospheric Organic Aerosol Formation, Environ. Sci. Technol., 31(7), 1890–1897, doi:10.1021/es960535l, 1997.

Pankow, J. F.: An absorption model of the gas/aerosol partitioning involved in the formation of secondary organic aeroso, Atmos. Environ., 28(2), 189–193, doi:10.1016/1352-2310(94)90094-9, 1994.

Pope III, C. A.: Lung Cancer, Cardiopulmonary Mortality, and Long-term Exposure to Fine Particulate Air Pollution, JAMA J. Am. Med. Assoc., 287(9), 1132–1141, doi:10.1001/jama.287.9.1132, 2002.

Presto, A. A., Huff Hartz, K. E. and Donahue, N. M.: Secondary organic aerosol production from terpene ozonolysis. 2. Effect of NO_x concentration, Environ. Sci. Technol., 39(18), 7046–7054, doi:10.1021/es050400s, 2005.

Saxena, P. and Hildemann, L. M.: Water-soluble organics in atmospheric particles: A critical review of the literature and application of thermodynamics to identify candidate compounds, J. Atmos. Chem., 24(1), 57–109, doi:10.1007/BF00053823, 1996.

Schulz, M., Textor, C., Kinne, S., Balkanski, Y., Bauer, S., Berntsen, T., Berglen, T., Boucher, O., Dentener, F., Guibert, S., Isaksen, I. S. a., Iversen, T., Koch, D., Kirkevåg, a., Liu, X., Montanaro, V., Myhre, G., Penner, J. E., Pitari, G., Reddy, S., Seland, Ø., Stier, P. and Takemura, T.: Radiative forcing by aerosols as derived from the AeroCom present-day and pre-industrial simulations, Atmos. Chem. Phys., 6(12), 5225–5246, doi:10.5194/acp-6-5225-2006, 2006.

Seinfeld, J. H. and Pandis, S. N.: Atmospheric Chemistry and Physics : From Air Pollution to Climate Change (2nd Edition), John Wiley & Sons, Somerset, NJ, USA., 2006.

Shakya, K. M. and Griffin, R. J.: Secondary organic aerosol from photooxidation of polycyclic aromatic hydrocarbons., Environ. Sci. Technol., 44(21), 8134–9, doi:10.1021/es1019417, 2010.

Song, C., Na, K. and Cocker, D. R.: Impact of the hydrocarbon to NOx ratio on secondary organic aerosol formation, Environ. Sci. Technol., 39(9), 3143–3149, doi:10.1021/es0493244, 2005.

Song, C., Na, K., Warren, B., Malloy, Q. and Cocker, D. R.: Impact of propene on secondary organic aerosol formation from m-Xylene, Environ. Sci. Technol., 41(20), 6990–6995, doi:10.1021/es062279a, 2007.

Tang, P., Nakao, S., Chen, C.-L., Carter, W. and Cocker III, D. R.: Role of Alkyl Substituents on Secondary Organic Aerosol Formation from Aromatic Hydrocarbons: Part-I Aerosol Formation Potential in the Presence of NOx., 2015. *(In preparation)*

Utembe, S. R., Cooke, M. C., Archibald, a. T., Shallcross, D. E., Derwent, R. G. and Jenkin, M. E.: Simulating secondary organic aerosol in a 3-D Lagrangian chemistry transport model using the reduced Common Representative Intermediates mechanism (CRI v2-R5), Atmos. Environ., 45(8), 1604–1614, doi:10.1016/j.atmosenv.2010.11.046, 2011.

Volkamer, R., Jimenez, J. L., San Martini, F., Dzepina, K., Zhang, Q., Salcedo, D., Molina, L. T., Worsnop, D. R. and Molina, M. J.: Secondary organic aerosol formation from anthropogenic air pollution: Rapid and higher than expected, Geophys. Res. Lett., 33, 7–10, doi:10.1029/2006GL026899, 2006.

Warren, B., Song, C. and Cocker, D. R.: Light intensity and light source influence on secondary organic aerosol formation for the m-xylene/NOx photooxidation system., Environ. Sci. Technol., 42(15), 5461–5466, doi:10.1021/es702985n, 2008.

Warren, B., Austin, R. L. and Cocker III, D. R.: Temperature dependence of secondary organic aerosol, Atmos. Environ., 43(22-23), 3548–3555, doi:10.1016/j.atmosenv.2009.04.011, 2009.

Zhang, Q., Jimenez, J. L., Canagaratna, M. R., Allan, J. D., Coe, H., Ulbrich, I., Alfarra, M. R., Takami, a., Middlebrook, a. M., Sun, Y. L., Dzepina, K., Dunlea, E., Docherty, K., DeCarlo, P. F., Salcedo, D., Onasch, T., Jayne, J. T., Miyoshi, T., Shimono, a., Hatakeyama, S., Takegawa, N., Kondo, Y., Schneider, J., Drewnick, F., Borrmann, S., Weimer, S., Demerjian, K., Williams, P., Bower, K., Bahreini, R., Cottrell, L., Griffin, R. J., Rautiainen, J., Sun, J. Y., Zhang, Y. M. and Worsnop, D. R.: Ubiquity and dominance of oxygenated species in organic aerosols in anthropogenically-influenced Northern Hemisphere midlatitudes, Geophys. Res. Lett., 34, 1–6, doi:10.1029/2007GL029979, 2007.

Zhang, Y., Liu, P., Queen, A., Misenis, C., Pun, B., Seigneur, C. and Wu, S. Y.: A comprehensive performance evaluation of MM5-CMAQ for the Summer 1999 Southern Oxidants Study episode-Part II: Gas and aerosol predictions, Atmos. Environ., 40(26), 4839–4855, doi:10.1016/j.atmosenv.2005.12.048, 2006.

Chapter 2 SOA Formation from Naphthalene, 1-Methylnaphthalene, and 2-Methylnaphthalene Photooxidation

2.1 Introduction

The formation of secondary organic aerosol (SOA) originates from a variety of chemical processes including gas-phase oxidation reactions of organic species, reactions in the particle (condensed) phase and continuing chemistry over multiple generations of oxidation products (Kroll and Seinfeld, 2008). SOA negatively impacts visibility and can affect global radiative forcing through both direct and indirect effects (Hoyle et al., 2011; Kanakidou et al., 2005; Schulz et al., 2006). Additionally, epidemiological evidence shows a significant risk correlated between fine particles and lung cancer, respiratory illness, and cardiovascular (Lewtas, 2007). Polycyclic aromatic hydrocarbons (PAHs) are an important source of semivolatile gas-phase anthropogenic emissions sources including incomplete combustion emissions from exhaust vehicles (Shah et al., 2005), biomass burning (Conde et al., 2005; Hedberg et al., 2002), and cooking (McDonald et al., 2003). Further, PAH (e.g., naphthalene, 1-methylnaphthalene, 2-methylnaphthalene) may be major unaccounted for source of secondary organic aerosol (SOA) as their contribution to ambient secondary particulate matter is not clearly understood. Pye and Pouliot, 2012 applied the Community Multiscale Air Quality (CMAQ) model and estimated that long-chain alkanes and PAHs accounted for 20~30% of SOA derived from anthropogenic hydrocarbons. The California Air Resources Board (CARB) 2010 California Toxic Inventory (CARB, 2013) estimates total California emission of naphthalene of ~ 910.7 tons/year. Average Southern California Air Basin naphthalene concentrations range from

91~445 ng/m^3 (Eiguren-Fernandez et al., 2004; Lu et al., 2005) with Reisen and Arey (2005) reporting much higher naphthalene concentrations in Los Angeles due to heavy traffic emissions than Riverside (Reisen and Arey, 2005). Further, Lu et al. simulated the distribution of naphthalene emissions over Southern California using the SMOG airshed model and estimated 10-50 kg/day/grid (5-km by 5-km grid cells) in populated urban areas (Lu et al., 2005). Although naphthalene is the most abundant PAHs precursor, a number of petroleum, gasoline, fuels, and kerosene contain significant amounts of methylnaphthalenes. 1-Methylnaphthalene and 2-methylnaphthalene are both generated from natural crude oil, crude oil derivatives, and also found in pyrolysis and combustion products such as cigarette and wood smoke, emissions from combustion engines, roofing and asphalt tars, pesticides, and industry plants (Aislabie et al., 1999; Singer et al., 2003). The methylnaphthalenes emitted from primary sources can react with OH radicals and NO_x to produce methylnitronaphthalenes and dicarbonyl derivates in the atmosphere. Methylnitronaphthalenes and nitronaphthalenes are reported as carcinogens and are associated with mutagenicity and toxic effects in metabolism reactions (Grosovsky et al., 1999; Lin et al., 2009).

Recent research on SOA from PAHs has focused on the evolution and chemical composition of SOA from OH-initiated photooxidation of naphthalene under low-NO_x and high-NO_x conditions (Kautzman et al., 2010) and the naphthalene oxidation by OH radicals (Zhang et al., 2012). Chan et al. reported SOA yields for high-NO_x conditions between 0.19 and 0.3 for naphthalene, 0.19 and 0.39 for 1-methylnaphthalene, and 0.26 and 0.45 for 2-methlynaphthalene. Under low-NO_X conditions, SOA yields were

observed to be 0.73, 0.68, and 0.58 for naphthalene, 1-methylnaphthalene, 2-methylnaphthalene, respectively (Chan et al., 2009). However, lower PAH SOA yields ranging from ~0.02 to ~0.22 were observed by Shakya and Griffin (2010) for aerosol mass concentrations less than 10μg/m^3. Kleindienst et al. (2012) recently reported that naphthalene SOA yields ranging 0.11~0.27 under higher NO_x conditions, which is much lower than reported by Kautzman et al (2010). Further, Kautzman et al report phthalic acid as a major naphthalene photooxidation product for both NO_x conditions. Phthalic acid has been suggested as a potential tracer of ambient naphthalene SOA (Kautzman et al., 2010) due to large observable quantities (e.g., ~ 14 ngm^{-3} in Birmingham, Al). Additionally, 4-nitro-1-naphthol, hydroxyl phthalic acid and hydroxyl nitrobenzoic acid have also been observed in both urban organic aerosols and laboratory SOA from PAH-NO_x photooxidation. OH radical reaction initiates naphthalene and C_1- C_2 alkylnaphthalene atmospheric oxidation. Naphthalene and alkylnaphthalene oxidation mechanism for high NO_x (Kautzman et al., 2010) have been proposed with 2-formylcinnaldehyde (30~60% yield) as the major product (Nishino et al., 2009, 2012; Sasaki et al., 1997). Previous studies have shown that OH radical reaction in the presence of NO_x results in the formation of nitronaphthalenes (0.6%), naphthols (10%) and other ring-opening and ring-remaining products (Sasaki et al., 1997). This study builds in these previous works to reduce uncertainties in the formations and characterizations of SOA derived from PAHs.

2.2 Experimental Methodology

2.2.1 Experimental Setup

All experiments were performed in the UCR/CE-CERT environmental chamber described in detail elsewhere (Carter et al., 2005). The facility includes a 6m×6m×12m thermally insulated enclosure continuously flushed with purified air (Aadco 737 series (Cleves, Ohio) air purification system). Inside the enclosure, there are two 90 m^3 2 mil (54 μm) FEP Teflon® film reactors along with two banks of 115 W 4-ft blacklights. The elevation of the top frames of the reactors are controlled by elevators that slowly move down during the experiments to maintain a positive differential pressure of ~0.02 in H_2O thereby reducing likelihood of dilution due to sampling, leaks, and permeation. Known aliqwots of PAHs were injected into the chamber through a heated glass injection manifold system and flushed into the chamber with pure N_2. 50% wt hydrogen peroxide (H_2O_2) were injected into a glass manifold tube in a 55°C oven, and subsequently flushed into the chamber with purified air. NO was prepared by filling a calibrated glass bulb with a known pressure of pure NO and then subsequently flushed into the chamber with pure N_2. Nitrous acid (HONO) was injected as the OH precursor for high NO_x (NO >350 ppb initially) condition experiments. HONO was prepared by adding 10 ml of 1w% $NaNO_2$ dropwise into 20 ml of 10w% H_2SO_4 aqueous solution (Kautzman et al., 2010). Ammonium sulfate seed aerosol was generated as needed by atomization of a ~0.005 M aqueous ammonium sulfate solution.

2.2.2 Instrumentation

Gas phase: Perfluorohexane (n-C_6F_{14}) was used as an inert chemical tracer. The perfluorohexane and PAH concentrations were monitored using Agilent 6980 (Palo Alto, CA) gas chromatography (GC) equipped with flame ionization detectors (FID) (equipped with: 30 m x 0.53 mm GS-Alumina column used for the analysis of light hydrocarbons and 30 m x 0.53 mm DB-5 column used for the analysis of C_{5+} alkanes and aromatics), and a GC equipped with a thermal desorption system (CDS analytical, ACEM9305, Sorbent Tube MX062171 packed with Tenax-TA/Carbopack/Carbosieve S111), respectively. NO and NO_y-NO were measured by a TECO NO_x analyzer while O_3 was measured by a Dasibi Environmental Corp. Model 1003-AH O_3 analyzer.

Particle phase: Particle size distributions between 27 and 686 nm and number concentrations are measured with an in-house build Scanning Mobility Particle Sizers (SMPS) described by (Cocker et al., 2001). Aerosol particle density was measured with an Aerosol Particle Mass analyzer (APM, Kanomax model 3600) and a SMPS in series. A detailed description of the APM-SMPS system and data algorithms are described elsewhere (Malloy et al., 2009; Nakao et al., 2011). Particle volatility was monitored with a volatility tandem differential mobility analyzer (VTDMA) (Nakao et al., 2011, 2012; Qi et al., 2010b; Rader and McMurry, 1986), in which monodisperse particles of mobility diameter D_{mi} are selected by the 1st differential mobility analyzer (DMA) followed by transport through a Dekati thermodenuder (TD, residence time: ~16 s, at 100 °C). The particle size after the TD (D_{mf}) is then measured by fitting a log-normal size distribution curve acquired by the 2nd DMA. Volume Remaining Faction (VRF) is calculated by

VRF = $(D_{mf}/D_{mi})^3$ where D_{mf} is the particle mobility diameter after the TD and D_{mi} is the initial particle size selected. The FHNW Transmission Electron Microscopy (TEM) sampler was used to collect particles during select experiments. The particulate were subsequently analyzed by TEM (FEI-PHILIPS CM300) at the UCR Central Facility for Advanced Microscopy and Microanalysis (CFAMM).

Particle chemical composition was analyzed with a high-resolution time-of-flight aerosol mass spectrometer operating in "W-mode" (Aiken et al., 2007, 2008; DeCarlo et al., 2006). Details of the HR-ToF-AMS and software analysis are described in (DeCarlo et al., 2006).The HR-ToF-AMS data was analyzed by HR-ToF-AMS analysis toolkit 1.51H and PIKA module for SQUIRREL 1.10 H version.

2.3 Results and Discussion

2.3.1 SOA yields from naphthalene, 1-methylnaphthalene and 2-methylnaphthalene

SOA formation from naphthalene, 1-methylnaphthalene and 2-methylnaphthalene were measured for different gas-phase reactivity conditions in UCR CE-CERT environmental chamber. SOA yields (Y) for individual ROGs were determined as the total aerosol formed divided by PAH consumed. Yield was then plotted versus final organic aerosol mass and fit to the following equations (Odum et al., 1996, 1997):

$$Y = M_0 \sum_i \left(\frac{\alpha_i K_{om,i}}{1 + K_{om,i} M_0} \right) \quad (1)$$

to obtain the best fit two product (i=2) model for α_i and $K_{om,i}$ are the mass-based stoichiometric coefficient and absorption equilibrium partitioning coefficient of product i , respectively.

All experiments were irradiated (K_1= 0.552 min^{-1}) under dry conditions (RH< 0.1%). Table 2.1 lists the experimental conditions and SOA yields for photooxidation experiments conducted for each of the three PAH precursors. The initial PAH concentration in these experiments ranged from 15 ppb to 68 ppb while initial NO_x ranged from > 350 ppb for high NO_x experiments to < 100 ppb for low NO_x conditions, and << 1 ppb for H_2O_2 low NO_x experiments.

2.3.1.1 High NO_x condition

SOA yield ranged from 0.03~0.60 (naphthalene), 0.21~1.52 (1-methylnaphthalene), and 0.34~0.55 (2-methylnaphthalene) under high NO_x (initial PAHs/NO = 0.03~0.17) conditions (Table 2.1). HONO was injected into high NO_x experiments to serve as an •OH source to help increase the reactivity of the experiment. However, the HONO production method also produced variable additional NO and NO_2 that was injected into the chamber. The injected •OH and NO_2/NO ratio impacts aerosol formation from a given PAH precursor (Figure S 2.1). The lowest SOA yield was observed in 1732A naphthalene-high NO_x experiment, which NO and NO_2 were low when injecting HONO into the system, indicating producing lower OH radical and NO, and also the higher additional NO, leading to less aerosol formation. The OH radical initiates reactions of alkylnaphthalene/naphthalene mainly by addition to the ring to form an OH-alkylnaphthalene/OH-naphthalene adduct which subsequently react with NO_2 and

O_2 (Atkinson and Arey, 2007). In this study, SOA yield under high-NO_x conditions is non-linearly related to the HONO, NO, and NO_2 concentration (Figure S 2.1), implying that aerosol formation is expected through NO_2 reaction with OH-naphthalene/OH-alkylnaphthalene adducts leading to nitro-containing and other low volatility products. Previous studies have identified ring-opened products from OH-initiated naphthalene/alkylnaphthalene reactions including 2-formylcinnamaldehyde (30-60%), phthaldialdehyde and phthalic anhydride (Atkinson and Arey, 2007; Nishino et al., 2009, 2012). These products can continue to oxidize and form secondary-generation products that could further to partition into the condensed phase.

2.3.1.2 Low NO_x condition

In the low NO_x (initial PAHs/NO = 0.54~2.20) experiments, SOA yield is 0.04~0.31, 0.14~0.72, and 0.06~0.49 for naphthalene, 1-methylnaphthalene, and 2-methylnaphthalene, respectively. The photooxidation routes to form SOA are expected to be is dominated by RO_2+HO_2 and RO_2+NO reaction pathways (Kroll and Seinfeld, 2008). The SOA formation from the PAH precursors under low-NO_x conditions is lower than that observed for high NO_x (2.3.1.1, see also Figure S 2.1 and Figure S 2.2). Figure S2.2 shows that the initial PAHs/NO ratio significantly influences the SOA growth, which was observed as the initial PAHs/NO ratio increases the aerosol formation increases. For instance, the initial naphthalene/ NO ratio is 3.41 for 1828A and 1.26 for 1592A, the aerosol mass produced for 1828A is much higher than 1592A as shown in Figure S2.2 (a). The SOA yield increases as initial NO level decreases attributable to increasing RO_2 and HO_2 radical concentrations leading to reactions forming products with lower volatilities,

similar to observed NO_x effects on SOA formation from aromatic hydrocarbon (Tang et al., 2015a). Organic aerosol does not grow in the early hours of the experiment (e.g., run 1661) with only slight aerosol formation observed after 3-5 hours, suggesting NO_x might slowly react with intermediate radicals forming organic nitrate products.

2.3.1.3 Effect of seed aerosol

Ammonium sulfate seed aerosol was introduced to four naphthalene low NO_x condition photooxidation with particulate mass of organic aerosol determined by:

$$\text{PM mass}=PM_{(NH_4)_2SO_4}\ \text{mass}+PM_{org}\ \text{mass}+PM_{NO_3}\ \text{mass} \quad (2)$$

$$PM_{org}\ \text{mass}\ (t)=(\text{PM volume corrected}\ \times \rho\ (t))\times(1-f_{(NH_4)_2SO_4}(t)) \quad (3)$$

where $f_{(NH_4)_2SO_4}$ is the fraction of particulate matter that is ammonium sulfate acquired by HR-ToF-AMS and obtained from eq(2). Aerosol density as a function of time (ρ (t)) was directly obtained by the APM-SMPS. Thus, total organic aerosol mass formed (PM_{org} mass (t)) can be calculated by the equation (3). The aerosol formation in the four seeded experiments agrees well with the non-seeded experiments indicating letter loss of semi-volatiles to the chamber walls in contrast to Kautzman et al. 2010. This may be due to large size of the environmental chamber.

2.3.1.4 H_2O_2/ H_2O_2+low NO_x condition

SOA yields in the presence of H_2O_2 increases greatly for naphthalene, 1-methylnaphthalene and 2-methylnaphthalene with some mass-yields exceeding 1.0. High SOA yields occurred in H_2O_2 (only) irradiation condition (1~2 ppm) due to high OH radical concentrations produced by the blacklights (NO_2 photolysis rate is $6.68 \times 10^{-3}\ s^{-1}$).

SOA yield from 1-methylnaphthalene photooxidation is the highest followed by naphthalene and 2-methylnaphthalene. Even higher yields are observed for the low NO_x + H_2O_2 conditions due to even higher OH radical concentrations with SOA highest for 1-methylnaphthalene (1.93), follow by naphthalene (1.15), and 2-methylnaphthalene (1.26). The yields obtained from the H_2O_2 experiments suggest the RO_2+HO_2 chemistry producing substantial amount of low-volatility hydroperoxides and acids. NO quickly drops to sub-ppb levels during first hour irradiation (e.g., run: 1613A), allowing RO_2 and HO_2 to rapidly build and SOA formation to commence. (This is compared with ~ 5 hours for low NO_x experiments when NO depletes and SOA formation accelerates). Additionally, Figure S 2.1(d) shows a linear relationship between instantaneous SOA yield and M_0 concentration. The PAHs were consumed (>99%) after 3 hours irradiation under low NO_x+H_2O_2 conditions (Figure S 2.2 (d)) due to the high OH radical level concentrations. The SOA growth curve (ΔM_0 vs. hydrocarbon reacted ΔHC) indicates that SOA continued to grow after hydrocarbon reacted completely (Figure S2.2 (d) 1613A) suggesting partitioning of some multigenerational oxidation products.

2.3.1.5 Overall comparison

SOA yields are much higher in this work than the studies of Chan et al. (2009), Kleindienst et al.(2012), and Shakya et al. (2010) (Table 2.2). The differences between this study and other studies are attributed to differing chamber conditions such as light intensity (rate of NO_2 photolysis), chamber size (wall-effects), NO_x levels, and hydroxyl radical concentrations. Figure S 2.1 shows that the instantaneous SOA yield trends as: H_2O_2 + low NO_x > H_2O_2 without NO_x > high NO_x> low NO_x conditions. The SOA yield

increases with hydroxyl radical increasing (as well as with increasing reaction rate with OH (k_{OH})). Additionally, the chemical properties such as solid/liquid phase, vapor pressure, and chemical reaction mechanism differ for these three compounds. Applying the two-product model (eq(1)) to all naphthalene, 1-methylnaphthalene and 2-methylnaphthalene photooxidation experiments (Figure 2.1) shows smaller SOA yield fit curves for the three precursors. Zooming in on low M_0 indicates an order of 1-methylnaphthalene > 2-methylnaphthalene ≈ naphthalene.

2.3.2 Density of SOA evolution

The SOA density measured by APM-SMPS is displayed as a function of time (Figure 2.2). The initial SOA densities were ~ 1.58 g/cm^3 for all experiments, decreasing to ~1.3~1.4 g/cm^3 and remaining constant during the remainder of the experiment under most conditions, in agreement with previous aromatic SOA study (Nakao et al., 2013). However, the SOA density decreased continuously for 1-methylnaphthalene photooxidation and 2-merthylnaphthalene under high NO_x conditions (Run ID: 1659A, 1628A, 1623A, 1632A, and 1635A). For these experiments, densities were observed to drop lower than 1 g/cm^3, suggesting that the particles are fractal-like than in typical SOA experiments (e.g., run 1623A density dropped to 0.7 g/cm^3). A power function relationship between effective density and size (equation 4) is used as (Nakao et al., 2011):

$$\rho_{eff} = C d_m^{Df-3} \quad (4)$$

where ρ_{eff} is the effective density of particles, C is a constant, d_m is the mobility diameter of particles, and D_f is the fractal-like dimension. For example, the fractal-like dimension (D_f) in experiment 1623A ranges from 3 to 2.31 over the course of experiment (Figure S 2.3(a)). For these experiments, particle number concentrations of ~10^5 particles /cm^3 are observed (Figure S 2.3(b)) yielding a time constant for coagulation in the order of a few hours (Seinfeld and Pandis, 2006). If the SOA is solid, then it is possible that coagulating particles could form such fractal particles for these conditions and timescales with decreasing particle density. Particle density as their mobility diameter increased from 40 nm to 235 nm (Figure S 2.3(a)). Further evidence of fractal 1-methylnaphthalene SOA was observed by injecting *m*-xylene into the chamber at the end of an experiment. The 1-methylnaphthalene SOA density rapidly increased from 1.15 g/cm^3 to 1.51 g/cm^3 as m-xylene coated to the 1-methylnaphthalene SOA filling the fractal voids (Figure S 2.4). Finally, a TEM sample was collected during the 1st hour of particle formation, 5-6 hours, and 6-7 hours irradiation time. Figure 2.2 shows the TEM images collected of SOA formed from 1-methylnaphthalene/high NO_x photooxidation, confirming the formation of fractal SOA particles coagulated after 5~6 hours of photooxidation. This study shown the importance of measuring density for individual experiments to determine mass based aerosol yield.

2.3.3 SOA volatility evolution

The volatility trends of strongly decreasing volatility as the experiment progressed were similar from naphthalene, 1-methylnaphthalene and 2-methylnaphthlene

photooxidations under high NO_x, H_2O_2 and low NO_x+ H_2O_2 conditions. For example, VRF increased from < 25 % to > 85% (Figure 2.3(a)) for naphthalene, 1-methylnaphthalene, and 2-methylnaphthalene photooxidation for high-NO_x conditions even for experiments when the fractal like agglomerate formed. This indicates that the vast majority of SOA formed how low volatility even @100 ° C. Additional VTDMA experiments with the thermal denuder temperature set to 150 ° C were performed to further explain the volatility of SOA from naphthalene, 1-methylnaphthalene, and 2-methylnaphthalene (Figure 2.3(b)), which more SOA evaporated at higher temperature, the SOA at the end of the experiment was still very low volatility (VRF > 60%). The volatility of the SOA was far lower than that measured for monoaromatic compounds (Qi et al., 2010a; Tang et al., 2015b).

2.3.4 Chemical composition characteristics of SOA formation

The HR-ToF-AMS measures the ion fragments from impaction of particles after vaporization on a heated surface (~600 °C) and electron ionization (70 eV) (DeCarlo et al., 2006). Traces of specific *mass-to-charge* ratios (*m*/*z*) are often used to characterize SOA evolution. Numerous studies have used *m/z* 44 (mostly CO_2^+, 43.989) associated with carboxylic acids and *m/z* 43 ($C_2H_3O^+$(43.018) or $C_3H_7^+$(43.054)) associated with oxygenated non-acids (such as aldehydes and ketones) as important indicators of chemical composition and aging of chamber SOA and ambient SOA (e.g., Ng et al., 2010, 2011). The *m/z* 44 is the key signature of the oxygenated organic compounds formed from PAH SOA formation and the most abundant fragment observed in this study.

Typical normalized m/z distributions of naphthalene, 1-methylnaphthalene and 2-methylnaphthalene SOA averaged over the course of the reaction for high-NO_x conditions are shown in Figure 2.4. The high *m/z* 44 signal was paired with a high *m/z* 18 (H_2O^+) peak implying thermal decomposition of the carboxylic acid group at the vaporizer (Alfarra et al., 2004). Additional major ion fragments detected included *m/z* 43 ($C_2H_3O^+$, 43.018), *m/z* 50 ($C_4H_2^+$, 50.156), *m/z* 51($C_4H_3^+$, 51.023), the typical aromatics series $C_6H_5C_nH_{2n}^+$ (*m/z* 77 ($C_6H_5^+$,77.039), 91($C_7H_7^+$,91.054), 105 ($C_8H_9^+$,105.070)) (McLafferty and Turecek., 1993), *m/z* 76 ($C_6H_4^+$,76.031) , *m/z* 115 ($C_9H_7^+$,115.054), *m/z* 104 (C_8H_8 (104.062) and $C_7H_4O^+$(104.026)), and *m/z* 105 ($C_7H_5O^+$(105.033) and $C_8H_9^+$(105.070) isomer). Interestingly, nitro-organic compounds ion fragments were also observed at *m/z* 131 ($C_9H_7O^+$(131.049) and $C_4H_5NO_4^+$(131.021)), *m/z* 133 ($C_4H_7NO_4^+$ (133.037)) and *m/z* 145 ($C_{10}H_9O^+$(145.065) and $C_5H_7NO_4^+$(145.037)), corresponding to the N-containing compounds like 2-nitrophenol and 4-nitro-1-naphthol observed during OH-initiated naphthalene-high NO_x photooxidation in Kautzman et al. (2010) study. Three possible PAHs photooxidation products are proposed in this study based on *m/z* comparison to NIST library WebBook- *trans*-cinnamic acid, phthalic acid, and benzoic acid (Figure S 2.5). Firstly, the *m/z* 147 ($C_9H_7O_2^+$(147.044)) is the expected major ion fragment of *trans*-cinnamic acid ($C_9H_8O_2$, MW 148) with additional fragments of *m/z* 148, *m/z* 103, *m/z* 77, *m/z* 51, all present in reasonable ratios in the PAH SOA *m/z* spectrum. Second, phthalic acid ($C_8H_6O_4$, M.W. 166) is suggested by the major mass spectrum peak at *m/z* 104 ($C_7H_4O^+$) along with additional at *m/z* 76, *m/z* 18, *m/z* 50, and *m/z* 148 (Figure S 2.5 ,S 2.6). The *m/z* 104 mass spectrum intensity from each high-NO_x

PAH experiment shows that the fraction 104 (f_{104}) is 1.82%, 1.14% and 1.28% for naphthalene, 1-methylnaphthalene, and 2-methylnaphthalene, respectively (Figure S 2.7). The third suggested product of this study is benzoic acid, whose major m/z is expected at *m/z* 105. These three compounds have also been identified as major PAH SOA product in previous OH radical-initiated naphthalene reactions (Kautzman et al., 2010; Wang et al., 2007). It is therefore suggested that the *m/z* 104 can be used as a potential indicator of phthalic anhydride or phthalic acid in HR-ToF AMS mass spectra distribution from PAH photooxidation.

The triangle plot (f_{44} vs. f_{43}) of SOA formation from naphthalene, 1-methylnaphthalene and 2-methylanpthalene photooxidation for different conditions is shown in Figure S 2.8. The naphthalene SOA lies on the top of triangle area, the 1-methylnaphthalene SOA sits on the left edge of triangle and 2-methylnaphthalene SOA locates on the right edge of triangle range, which is ambient OOA as (Ng et al., 2010). It is suggested that PAHs SOA is highly oxidized SOA since $f_{43} < 0.05$ and the H:C is ~1. Interestingly, f_{43} of 2-methylnaphthalene SOA was much higher than 1-methylnaphthalnene and naphthalene, suggesting more aldehydes or ketones (CH_2CHO^+ or CH_3CO^+) as well as saturated hydrocarbons ($C_3H_7^+$) (Alfarra et al., 2004) products are formed from 2-methylnaphthalene than the other two PAHs. Under high NO_x conditions, the SOA f_{44} continuously increased from 0.17 to 0.32 during naphthalene photoxodation, which is a much larger increase than observed for 1-methylnaphthalene and 2-methylnaphthalene. The same f_{44} aging trend occurs for the three PAHs precursors under

high NO_x, H_2O_2, and low NO_x + H_2O_2 conditions experiments, indicating that the formation of highly oxidized.

SOA characteristics including oxygen-to-carbon ratio (O/C), hydrogen-to-carbon ratio (H/C), and VRF (Volume Remaining Fraction) are summarized in Table S 2.1. The average O/C ratios of naphthalene and methylnaphthalene SOA increased from 0.33 to 0.63 during the course of the experiment. The average mean oxidation state of carbon ($\overline{OS}_c$), calculated as $\overline{OS}_c \approx 2\ O/C - H/C$ (Kroll et al., 2011), increases from -0.5 to 0.5 over the course of experiment. Figure S 2.9 shows the Van Krevelen diagram from PAHs photooxidation for each of the PAH precursors. The increasing $\overline{OS}_c$ is consistent with SOA aging during the course of experiment. The naphthalene and methylnaphthalenes SOA was suggested to be between low volatility oxygenated OA (LV-OOA) and SV-OOA compared to ambient OOA in the triangle plot and Van Krevelen diagram as Ng et al. The O/C ratios increased with irradiation time is consistent with f_{44} formation, which further demonstrated that oxidized organic aerosol aging property during PAHs photooxidation under both NO_x conditions and absence of NO_x conditions.

2.4 Conclusion

The characteristics of naphthalene, 1-methylnaphthalene and 2-methylnaphthalene SOA under high NO_x, low NO_x and absence of NO_x conditions are reported. SOA yields from naphthalene and methylnaphthalene are very high with increasing yield of 1-methylnaphthalene> naphthalene~ 2-methylnaphthalene, differing from the results of earlier studies due to the differences in chamber experimental

conditions. SOA yields increase with increasing the hydroxyl radical concentrations for H_2O_2 condition, H_2O_2+low NO_x and high NO_x condition with HONO. It is noted that 1-methylnaphthalene is the highest PAHs precursor that leads to higher SOA potential formation. The CARB emission inventory for toxic shows that naphthalene is the most abundant precursor (910.7 tons/year) among PAHs followed by 2-methylnaphthalene accounting for 81.1 tons/year. Given their high SOA yields, near 1.0, these PAHs can significantly contribute to the aerosol inventory through secondary atmospheric reactions.

Further, it was determined that 1-methylnaphthalene and 2-methylnaphthalene/high NO_x SOA decreases is solid allowing it to form fractal-like SOA when particle number is high enough to promote coagulation. Formation of fractal SOA particles requires careful evaluation of SOA density to accurately represent SOA mass yields. The *m/z* 104 is identified as a possible indicator of phthalic acid and phthalic anhydride from naphthalene photooxidation by HR-ToF-AMS measurement. Finally, the triangle plot, Van Krevelen diagram, and $\overline{OS}_c$ shows significant evolution of the SOA density during the course of the experiment.

2.5 References

Aiken, A. C., DeCarlo, P. F. and Jimenez, J. L.: Elemental analysis of organic species with electron ionization high-resolution mass spectrometry., Anal. Chem., 79(21), 8350–8, doi:10.1021/ac071150w, 2007.

Aiken, A. C., Decarlo, P. F., Kroll, J. H., Worsnop, D. R., Huffman, J. A., Docherty, K. S., Ulbrich, I. M., Mohr, C., Kimmel, J. R., Sueper, D., Sun, Y., Zhang, Q., Trimborn, A., Northway, M., Ziemann, P. J., Canagaratna, M. R., Onasch, T. B., Alfarra, M. R., Prevot, A. S. H., Dommen, J., Duplissy, J., Metzger, A., Baltensperger, U. and Jimenez, J. L.: O/C and OM/OC ratios of primary, secondary, and ambient organic aerosols with high-resolution time-of-flight aerosol mass spectrometry, Environ. Sci. Technol., 42(12), 4478–4485, doi:10.1021/es703009q, 2008.

Aislabie, J., Balks, M., Astori, N., Stevenson, G. and Symons, R.: Polycyclic aromatic hydrocarbons in fuel-oil contaminated soils, Antarctica, Chemosphere, 39(13), 2201–2207, 1999.

Alfarra, M., Coe, H., Allan, J., Bower, K., Boudries, H., Canagaratna, M., Jimenez, J., Jayne, J., Garforth, a and Li, S.: Characterization of urban and rural organic particulate in the Lower Fraser Valley using two Aerodyne Aerosol Mass Spectrometers, Atmos. Environ., 38(34), 5745–5758, doi:10.1016/j.atmosenv.2004.01.054, 2004.

Atkinson, R. and Arey, J.: Mechanisms of the Gas-Phase Reactions of Aromatic Hydrocarbons and PAHs with OH and NO_3 Radicals, Polycycl. Aromat. Compd., 27(1), 15–40, doi:10.1080/10406630601134243, 2007.

CARB: California Toxics Inventory "Draft 2010 CTI Summary Table," Calif. Air Resour. Board [online] Available from: http://www.arb.ca.gov/toxics/cti/cti.htm, 2013.

Carter, W. P. L., CockerIII, D. R., Fitz, D. R., Malkina, I. L., Bumiller, K., Sauer, C. G., Pisano, J. T., Bufalino, C. and Song, C.: A new environmental chamber for evaluation of gas-phase chemical mechanisms and secondary aerosol formation, Atmos. Environ., 39(40), 7768–7788, doi:10.1016/j.atmosenv.2005.08.040, 2005.

Chan, A. W. H., Kautzman, K. E., Chhabra, P. S., Surratt, J. D., Chan, M. N., Crounse, J. D., Kürten, A., Wennberg, P. O., Flagan, R. C. and Seinfeld, J. H.: Secondary organic aerosol formation from photooxidation of naphthalene and alkylnaphthalenes: Implications for oxidation of intermediate volatility organic compounds (IVOCs), Atmos. Chem. Phys., 9(9), 3049–3060, doi:10.5194/acp-9-3049-2009, 2009.

Cocker, D. R., Flagan, R. C. and Seinfeld, J. H.: State-of-the-art chamber facility for studying atmospheric aerosol chemistry, Environ. Sci. Technol., 35(12), 2594–2601, doi:10.1021/es0019169, 2001.

Conde, F. J., Ayala, J. H., Afonso, A. M. and González, V.: Emissions of polycyclic aromatic hydrocarbons from combustion of agricultural and sylvicultural debris, Atmos. Environ., 39(35), 6654–6663, doi:10.1016/j.atmosenv.2005.07.043, 2005.

DeCarlo, P. F., Kimmel, J. R., Trimborn, A., Northway, M. J., Jayne, J. T., Aiken, A. C., Gonin, M., Fuhrer, K., Horvath, T., Docherty, K. S., Worsnop, D. R. and Jimenez, J. L.: Field-deployable, high-resolution, time-of-flight aerosol mass spectrometer, Anal. Chem., 78(24), 8281–8289, doi:10.1021/ac061249n, 2006.

Eiguren-Fernandez, A., Miguel, A. H., Froines, J. R., Thurairatnam, S. and Avol, E. L.: Seasonal and Spatial Variation of Polycyclic Aromatic Hydrocarbons in Vapor-Phase and $PM_{2.5}$ in Southern California Urban and Rural Communities, Aerosol Sci. Technol., 38(5), 447–455, doi:10.1080/02786820490449511, 2004.

Grosovsky, A. J., Sasaki, J. C., Arey, J., Eastmond, D. A., Parks, K. K. and Atkinson, R.: Evaluation of the potential health effects of the atmospheric reaction products of polycyclic aromatic hydrocarbons, Res. Rep. Health. Eff. Inst., (84), i–iv, 1–22; discussion 23–27, 1999.

Hedberg, E., Kristensson, A., Ohlsson, M., Johansson, C., Johansson, P. Å., Swietlicki, E., Vesely, V., Wideqvist, U. and Westerholm, R.: Chemical and physical characterization of emissions from birch wood combustion in a wood stove, Atmos. Environ., 36(30), 4823–4837, doi:10.1016/S1352-2310(02)00417-X, 2002.

Hoyle, C. R., Boy, M., Donahue, N. M., Fry, J. L., Glasius, M., Guenther, A., Hallar, A. G., Huff Hartz, K., Petters, M. D., Petäjä, T., Rosenoern, T. and Sullivan, A. P.: A review of the anthropogenic influence on biogenic secondary organic aerosol, Atmos. Chem. Phys., 11(1), 321–343, doi:10.5194/acp-11-321-2011, 2011.

Kanakidou, M., Seinfeld, J. H., Pandis, S. N., Barnes, I., Dentener, F. J., Facchini, M. C., Van Dingenen, R., Ervens, B., Nenes, a., Nielsen, C. J., Swietlicki, E., Putaud, J. P., Balkanski, Y., Fuzzi, S., Horth, J., Moortgat, G. K., Winterhalter, R., Myhre, C. E. L., Tsigaridis, K., Vignati, E., Stephanou, E. G. and Wilson, J.: Organic aerosol and global climate modelling: a review, Atmos. Chem. Phys., 5(4), 1053–1123, doi:10.5194/acp-5-1053-2005, 2005.

Kautzman, K. E., Surratt, J. D., Chan, M. N., Chan, a W. H., Hersey, S. P., Chhabra, P. S., Dalleska, N. F., Wennberg, P. O., Flagan, R. C. and Seinfeld, J. H.: Chemical composition of gas- and aerosol-phase products from the photooxidation of naphthalene., J. Phys. Chem. A, 114(2), 913–34, doi:10.1021/jp908530s, 2010.

Kleindienst, T. E., Jaoui, M., Lewandowski, M., Offenberg, J. H. and Docherty, K. S.: The formation of SOA and chemical tracer compounds from the photooxidation of naphthalene and its methyl analogs in the presence and absence of nitrogen oxides, Atmos. Chem. Phys., 12(18), 8711–8726, doi:10.5194/acp-12-8711-2012, 2012.

Kroll, J., Donahue, N. and Jimenez, J.: Carbon oxidation state as a metric for describing the chemistry of atmospheric organic aerosol., Nat. Chem., 3(February), 133–139, doi:10.1038/nchem.948, 2011.

Kroll, J. H. and Seinfeld, J. H.: Chemistry of secondary organic aerosol: Formation and evolution of low-volatility organics in the atmosphere, Atmos. Environ., 42(16), 3593–3624, doi:10.1016/j.atmosenv.2008.01.003, 2008.

Lewtas, J.: Air pollution combustion emissions: characterization of causative agents and mechanisms associated with cancer, reproductive, and cardiovascular effects., Mutat. Res., 636(1-3), 95–133, doi:10.1016/j.mrrev.2007.08.003, 2007.

Lin, C. Y., Wheelock, A. M., Morin, D., Baldwin, R. M., Lee, M. G., Taff, A., Plopper, C., Buckpitt, A. and Rohde, A.: Toxicity and metabolism of methylnaphthalenes: comparison with naphthalene and 1-nitronaphthalene, Toxicology, 260(1-3), 16–27, doi:10.1016/j.tox.2009.03.002, 2009.

Lu, R., Wu, J., Turco, R. P., Winer, A. M., Atkinson, R., Arey, J., Paulson, S. E., Lurmann, F. W., Miguel, A. H. and Eiguren-Fernandez, A.: Naphthalene distributions and human exposure in Southern California, Atmos. Environ., 39(3), 489–507, doi:10.1016/j.atmosenv.2004.09.045, 2005.

Malloy, Q. G. J., Nakao, S., Qi, L., Austin, R., Stothers, C., Hagino, H. and Cocker, D. R.: Real-Time Aerosol Density Determination Utilizing a Modified Scanning Mobility Particle Sizer—Aerosol Particle Mass Analyzer System, Aerosol Sci. Technol., 43(7), 673–678, doi:10.1080/02786820902832960, 2009.

McDonald, J. D., Zielinska, B., Fujita, E. M., Sagebiel, J. C., Chow, J. C. and Watson, J. G.: Emissions from charbroiling and grilling of chicken and beef., J. Air Waste Manag. Assoc., 53(2), 185–194, doi:10.1080/10473289.2003.10466141, 2003.

McLafferty, F. W. and Turecek., F.: Interpretation of mass spectra, University Science Books, Sausalito, California., 1993.

Nakao, S., Shrivastava, M., Nguyen, A., Jung, H. and Cocker, D.: Interpretation of Secondary Organic Aerosol Formation from Diesel Exhaust Photooxidation in an Environmental Chamber, Aerosol Sci. Technol., 45(8), 964–972, doi:10.1080/02786826.2011.573510, 2011.

Nakao, S., Liu, Y., Tang, P., Chen, C.-L., Zhang, J. and Cocker III, D. R.: Chamber studies of SOA formation from aromatic hydrocarbons: observation of limited glyoxal uptake, Atmos. Chem. Phys., 12(9), 3927–3937, doi:10.5194/acp-12-3927-2012, 2012.

Nakao, S., Tang, P., Tang, X., Clark, C. H., Qi, L., Seo, E., Asa-Awuku, A. and Cocker, D.: Density and elemental ratios of secondary organic aerosol: Application of a density

prediction method, Atmos. Environ., 68, 273–277, doi:10.1016/j.atmosenv.2012.11.006, 2013.

Ng, N. L., Canagaratna, M. R., Zhang, Q., Jimenez, J. L., Tian, J., Ulbrich, I. M., Kroll, J. H., Docherty, K. S., Chhabra, P. S., Bahreini, R., Murphy, S. M., Seinfeld, J. H., Hildebrandt, L., Donahue, N. M., DeCarlo, P. F., Lanz, V. A., Prévôt, A. S. H., Dinar, E., Rudich, Y. and Worsnop, D. R.: Organic aerosol components observed in Northern Hemispheric datasets from Aerosol Mass Spectrometry, Atmos. Chem. Phys., 10(10), 4625–4641, doi:10.5194/acp-10-4625-2010, 2010.

Ng, N. L., Canagaratna, M. R., Jimenez, J. L., Chhabra, P. S., Seinfeld, J. H. and Worsnop, D. R.: Changes in organic aerosol composition with aging inferred from aerosol mass spectra, Atmos. Chem. Phys., 11(13), 6465–6474, doi:10.5194/acp-11-6465-2011, 2011.

Nishino, N., Arey, J. and Atkinson, R.: Yields of glyoxal and ring-cleavage co-products from the OH radical-initiated reactions of naphthalene and selected alkylnaphthalenes., Environ. Sci. Technol., 43(22), 8554–60, doi:10.1021/es902018v, 2009.

Nishino, N., Arey, J. and Atkinson, R.: 2-Formylcinnamaldehyde formation yield from the OH radical-initiated reaction of naphthalene: effect of NO_2 concentration., Environ. Sci. Technol., 46(15), 8198–204, doi:10.1021/es301865t, 2012.

Pye, H. O. T. and Pouliot, G. a: Modeling the role of alkanes, polycyclic aromatic hydrocarbons, and their oligomers in secondary organic aerosol formation, Environ. Sci. Technol., 46(11), 6041–7, doi:10.1021/es300409w, 2012.

Qi, L., Nakao, S., Malloy, Q., Warren, B. and Cocker III, D. R.: Can secondary organic aerosol formed in an atmospheric simulation chamber continuously age?, Atmos. Environ., 44(25), 2990–2996, doi:10.1016/j.atmosenv.2010.05.020, 2010a.

Qi, L., Nakao, S., Tang, P. and Cocker III, D. R.: Temperature effect on physical and chemical properties of secondary organic aerosol from *m*-xylene photooxidation, Atmos. Chem. Phys. Discuss., 10(1), 863–883, doi:10.5194/acpd-10-863-2010, 2010b.

Rader, D. J. and McMurry, P. H.: Application of the tandem differential mobility analyzer to studies of droplet growth or evaporation, J. Aerosol Sci., 17(5), 771–787, doi:10.1016/0021-8502(86)90031-5, 1986.

Reisen, F. and Arey, J.: Atmospheric Reactions Influence Seasonal PAH and Nitro-PAH Concentrations in the Los Angeles Basin, Environ. Sci. Technol., 39(1), 64–73, doi:10.1021/es035454l, 2005.

Sasaki, J., Aschmann, S. M., Kwok, E. S. C., Atkinson, R. and Arey, J.: Products of the gas-phase OH and NO_3 radical-initiated reactions of naphthalene, Environ. Sci. Technol., 31(11), 3173–3179, doi:10.1021/es9701523, 1997.

Schulz, M., Textor, C., Kinne, S., Balkanski, Y., Bauer, S., Berntsen, T., Berglen, T., Boucher, O., Dentener, F., Guibert, S., Isaksen, I. S. a., Iversen, T., Koch, D., Kirkevåg, a., Liu, X., Montanaro, V., Myhre, G., Penner, J. E., Pitari, G., Reddy, S., Seland, Ø., Stier, P. and Takemura, T.: Radiative forcing by aerosols as derived from the AeroCom present-day and pre-industrial simulations, Atmos. Chem. Phys., 6(12), 5225–5246, doi:10.5194/acp-6-5225-2006, 2006.

Seinfeld, J. H. and Pandis, S. N.: Atmospheric Chemistry and Physics : From Air Pollution to Climate Change (2nd Edition), John Wiley & Sons, Somerset, NJ, USA., 2006.

Shah, S. D., Ogunyoku, T. a, Miller, J. W. and Cocker, D. R.: On-road emission rates of PAH and n-alkane compounds from heavy-duty diesel vehicles., Environ. Sci. Technol., 39(14), 5276–84, doi:10.1021/es048086+, 2005.

Shakya, K. M. and Griffin, R. J.: Secondary organic aerosol from photooxidation of polycyclic aromatic hydrocarbons., Environ. Sci. Technol., 44(21), 8134–9, doi:10.1021/es1019417, 2010.

Singer, B. C., Hodgson, A. T. and Nazaroff, W. W.: Gas-phase organics in environmental tobacco smoke: 2. Exposure-relevant emission factors and indirect exposures from habitual smoking, Atmos. Environ., 37(39-40), 5551–5561, doi:10.1016/j.atmosenv.2003.07.015, 2003.

Tang, P., Nakao, S., Chen, C.-L., Carter, W. and Cocker III, D. R.: Role of Alkyl Substituents on Secondary Organic Aerosol Formation from Aromatic Hydrocarbons: Part-I Aerosol Formation Potential in the Presence of NO_x., 2015a.(*In preparation*)

Tang, P., Nakao, S., Qi, L., Chen, C.-L. and Cocker III, D. R.: Role of Alkyl substituents on Secondary Organic Aerosol Formation from Aromatic Hydrocarbons: Part-II Chemical Composition., 2015b.(*In preparation)*

Wang, L., Atkinson, R. and Arey, J.: Dicarbonyl products of the OH radical-initiated reactions of naphthalene and the C1- and C2-alkylnaphthalenes, Environ. Sci. Technol., 41(8), 2803–2810, doi:10.1021/es0628102, 2007.

Zhang, Z., Lin, L. and Wang, L.: Atmospheric oxidation mechanism of naphthalene initiated by OH radical. A theoretical study., Phys. Chem. Chem. Phys., 14(8), 2645–50, doi:10.1039/c2cp23271e, 2012.

2.6 Tables and Figures

Table 2.1 Initial experimental conditions and SOA yield for all experiments

High-NO_x (with HONO)		HC_0	ΔHC	NO[a]	NO_2[a]	NO[b]	NO_2[b]	ΔM_0	SOA yield[c]	Density
Run ID	Compound	ppb	μg/m^3	ppb	ppb	ppb	ppb	μg/m^3		g/cm^3
1586A	naphthalene	45.3	168	73	94	510	188	94.8	0.60	1.48[d]
1588A	naphthalene	29.1	126	N.D.	104	610	166	59.4	0.47	1.48[d]
1590A	naphthalene	25.9	116	20	142	420	338	47.1	0.41	1.47
1732A	naphthalene	29.6	105	25	38	624	152	3.0	0.03	1.51
1737A	naphthalene	22.6	80	50	88	576	207	20.3	0.25	1.40
1623A	1-methylnaphthalene	67.7	362	44	177	396	440	375.2	1.04	0.92 (1.47→0.71)
1628A	1-methylnaphthalene	40.0	203	26	103	397	372	173.7	0.78	1.07 (1.49 →0.83)
1652A	1-methylnaphthalene	14.2	52	68	50	476	284	10.4	0.21	1.25[e]
1659A	1-methylnaphthalene	26.8	111	63	81	445	341	74.1	0.65	1.25 (1.54→1.06)
1770A	1-methylnaphthalene	47.0	253	294	202	400	216	383.2	1.52	1.23 (1.48→1.12)
1632A	2-methylnaphthalene	30.6	148	28	77	380	321	51.1	0.35	1.32
1635A	2-methylnaphthalene	41.2	211	47	83	403	348	89.7	0.43	1.26
1768A	2-methylnaphthalene	47.7	182	145	104	530	168	61.1	0.34	1.35
1775A	2-methylnaphthalene	43.7	163	148	117	515	145	89.1	0.55	1.32
Low NO_x condition		HC_0	ΔHC	NO[a]	AS[g] seed(μm^3/cm^3)			ΔM_0	Y	Density
1592A	naphthalene	28.0	135	22				5.7	0.04	1.48
1660A	naphthalene + AS	17.1	86	14	17.3			15.5	0.18	1.58
1661A	naphthalene	14.7	76	13				21.1	0.28	1.47
1668A	naphthalene + AS	15.9	77	21	41.9			9.7	0.13	1.61
1718A	naphthalene	27.1	140	19				30.8	0.22	1.48
1828A	naphthalene	34.7	173	10				50.1	0.29	1.48[d]
1992A	naphthalene + AS	27.0	125	18	15.4			34.5	0.28	1.58
1992B	naphthalene	28.7	142	18				27.1	0.19	1.48
2040A	naphthalene + AS	14.6	69	10	3.4			22.7	0.33	1.48
2040B	naphthalene	16.9	84	11				26.2	0.31	1.48 [d]
1616A	1-methylnaphthalene	34.8	114	63				18.7	0.14	1.41
1616B	1-methylnaphthalene	35.0	185	29				34.8	0.19	1.4[f]
1742A	1-methylnaphthalene	45.3	218	71				44.1	0.20	1.44
1664A	1-methylnaphthalene	25.9	148	13				107.0	0.72	1.40
1666A	2-methylnaphthalene	20.0	115	12				56.3	0.49	1.37
1744A	2-methylnaphthalene	26.4	152	49				8.5	0.06	1.40
1745A	2-methylnaphthalene	29.1	157	13				43.4	0.28	1.33
H_2O_2 / H_2O_2 +low NO_x conditions				NO[a]	H_2O_2 (ppm)			ΔM_0	Y	Density
1584A	naphthalene	24.6	114	-	2			68.5	0.62	1.48[d]
1585A	naphthalene	48.0	313	-	2			201.0	0.96	1.48[d]
1754A	naphthalene	20.8	100	-	1			87.4	0.58	1.48[d]
1776A	naphthalene	46.5	207	-	1			190.3	0.95	1.49
1596A	1-methylnaphthalene	35.6	201	-	1			234.5	1.19	1.4[f]
1598A	1-methylnaphthalene	24.8	139	-	1			164.9	1.19	1.4[f]
1600A	1-methylnaphthalene	50.7	274	-	1			483.2	1.81	1.37
1608A	2-methylnaphthalene	28.6	162	-	1			128.7	0.81	1.39
1772A	2-methylnaphthalene	40.9	232	-	1			202.8	0.87	1.37
1613A	naphthalene	34.8	181	59	1			208.3	1.15	1.43
1650A	1-methylnaphthalene	36.6	209	38	1			403.4	1.93	1.26(1.49→1.05)
1643A	2-methylnaphthalene	34.0	195	55	1			246.5	1.26	1.30

a: initial NO and NO_2 concentration when injecting HONO; b: initial NO and NO_2 concentration after injecting additional NO and mixing reactors before turning blacklights on; c : SOA yield is calculated at the end of each experiment. Each experiment irradiates for 6 to 8 hours. d: assume average density of naphthalene SOA is 1.48 g/cm^3.e: assume average density of 1-methylnaphthalene high NO_x SOA is 1.25 g/cm^3; f: assume density of 1-methylnaphthalene H_2O_2+ low NO_x SOA is 1.4 g/cm^3; g: AS: ammonium sulfate.

Table 2.2 Comparison of SOA yield from PAHs photooxidation

PAHs	Condition	SOA yield (Chan et al., 2009)[a]	SOA yield (Kleindienst et al., 2012)[b]	SOA yield (Shakya and Griffin, 2010)[d]	SOA yield (this study)
naphthalene	high NO_x	0.19~0.30	0.28[c]	0.08~0.16	0.03~0.60
naphthalene	low NO_x+H_2O_2	0.73	---	---	1.15
naphthalene	low NO_x	---	---	---	0.04~0.33
naphthalene	H_2O_2	---	0.18-0.36	---	0.58~0.96
1-methylnaphthalene	high NO_x	0.19~0.39	0.20	0.03-0.22	0.21~1.52
1-methylnaphthalene	low NO_x+H_2O_2	0.68	0.41	---	1.93
1-methylnaphthalene	H_2O_2	---	---	---	1.19~1.81
1-methylnaphthalene	low NO_x	---	---	---	0.14~0.72
2-methylnaphthalene	high NO_x	0.26~0.45	0.15	0.04-0.13	0.34~0.55
2-methylnaphthalene	low NO_x+H_2O_2	0.58	0.64	---	1.26
2-methylnaphthalene	H_2O_2	---	---	---	0.81~0.87
2-methylnaphthalene	low NO_x	---	---	---	0.06~0.49

a: aerosol mass loadings (ΔM_0) : 10~40 μg/m^3 ; b: aerosol mass loadings (ΔM_0) : 39~130 μg/m^3 ; c: 0.14ppm; CH_3ONO, 0.3 ppm NO, for ΔM_0 100 μg/cm^3 ; d : aerosol mass loadings (ΔM_0) : 4~18 μg/m^3. (Kleindienst et al., 2012)

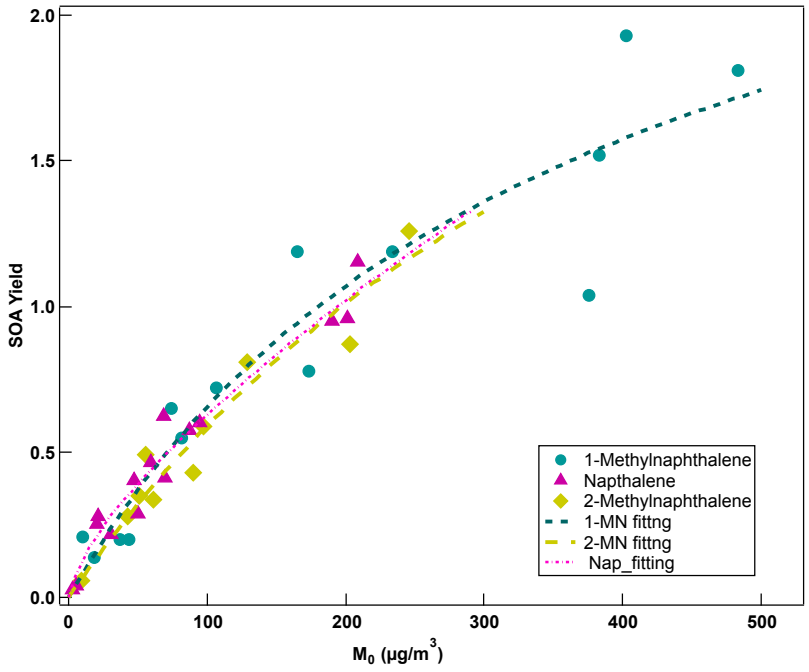

Figure 2.1 Two-product model curve for SOA yield from naphthalene, 1-methylnaphthalene and 2-methylnaphthalene photooxidation. Coefficients of α_1, $K_{om,1}$, α_2, $K_{om,2}$ for naphthalene are 0.2235, 0.0558, 6.0176, 0.0008 for naphthalene, and 0.8096, 0.0008, 2.4436, 0.0032 for 1-methylnaphthalene, 1.0074, 0.0014, 2.600, 0.0022 for 2-methylnaphthalene, respectively.

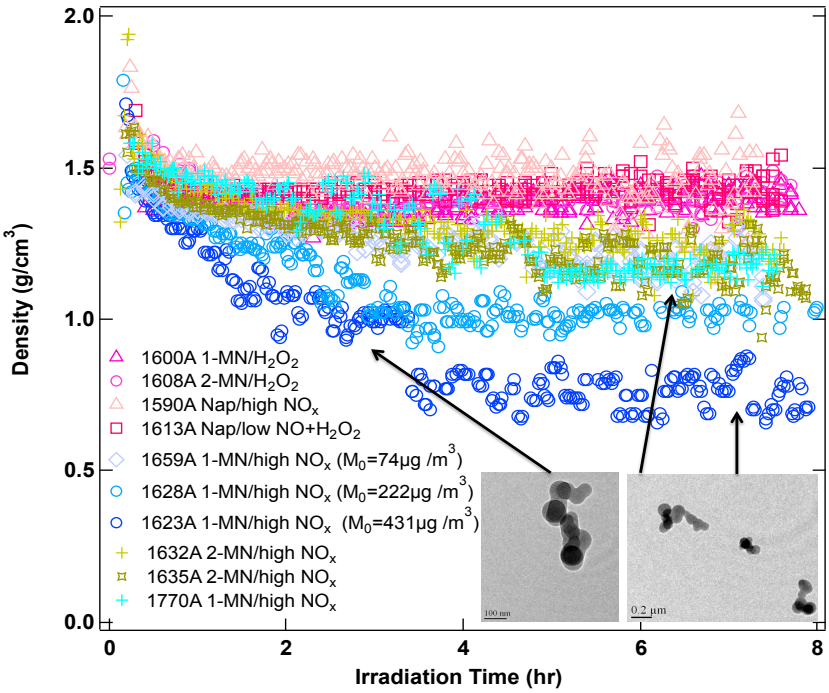

Figure 2.2 Time series of the densities of SOA from naphthalene, 1-methylnaphthalene and 2-methlnaphthalene photooxidation under different conditions.

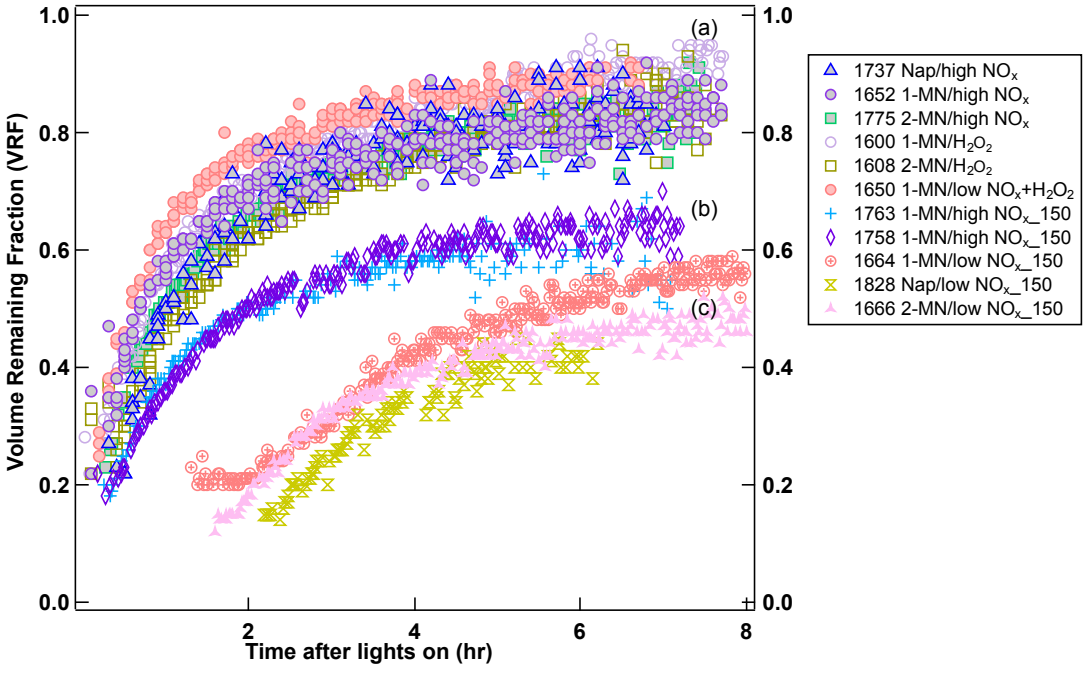

Figure 2.3 Volume remaining fraction (VRF) evolution of SOA during the courses of experiments under (a) high NO_x, H_2O_2, low NO_x and H_2O_2 conditions at thermodenuder temperature of 100 °C, (b) high NOx conditions at 150 °C, (c) low NO_x conditions at 150 °C.

(a) 1629A Naphthalene/high-NO_x

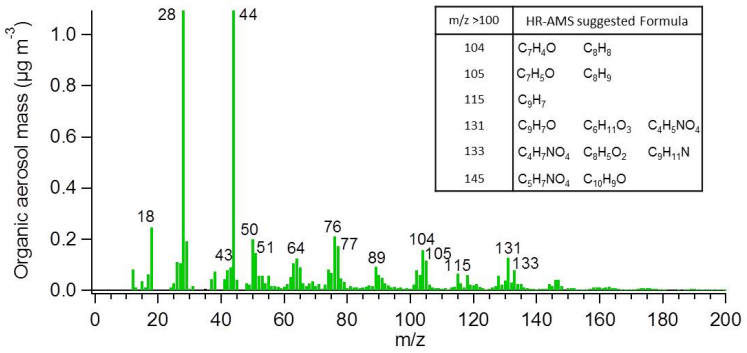

(b) 1628A 1-Methylnaphthalene/high-NO_x

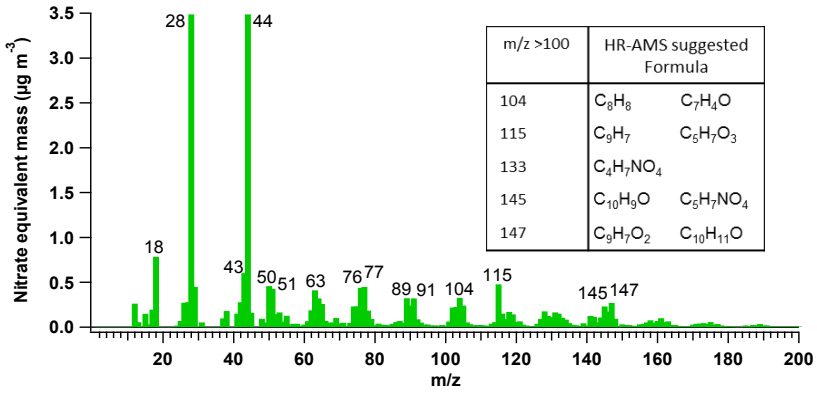

(c) 1768A 2-Methylnaphthalene/high-NO_x

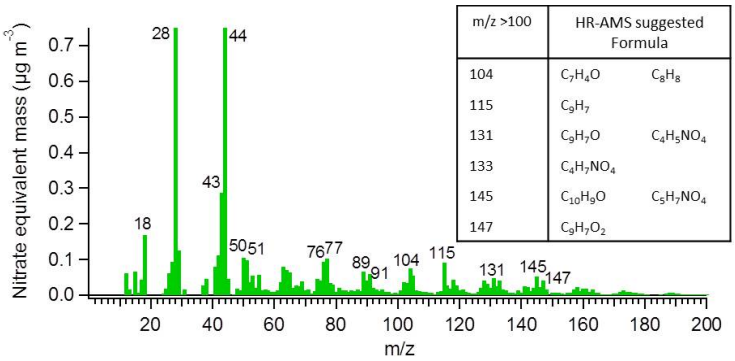

Figure 2.4 Normalized HR-ToF-AMS mass spectra distribution of three representative high-NO_x SOA experiments. (a) naphthalene high-NO_x; (b) 1-methylnaphthalene high-NO_x; (c) 2-methylnaphthalene high-NO_x. (see also Figure S2.10-S2.12)

2.7 Supporting Information

Table S 2.1 Characteristics results of O/C, H/C ratio and volume remaining fraction (VRF) from PAHs photooxidation experiments.

Run ID	Compound	Condition	O/C initial	O/C final	H/C initial	H/C final	VRF initial	VRF final	VTDMA Thermo-denuder temperature
1590A	naphthalene	high NO_x	0.40	0.69	0.94	1.08	N/A	N/A	
1629A	naphthalene	high NO_x	0.25	0.64	1.06	0.86	N/A	N/A	
1737A	naphthalene	high NO_x	N/A	N/A	N/A	N/A	0.27	0.81	100 °C
1628A	1-methylnaphthalene	high NO_x	0.38	0.70	0.87	0.86	N/A	N/A	
1631A	1-methylnaphthalene	high NO_x	0.32	0.67	0.89	0.89	N/A	N/A	
1652A	1-methylnaphthalene	high NO_x	N/A	N/A	N/A	N/A	0.22	0.83	100 °C
1659A	1-methylnaphthalene	high NO_x	0.36	0.49	1.17	1.09	N/A	N/A	
1768A	2-methylnaphthalene	high NO_x	0.36	0.54	1.01	1.07	N/A	N/A	
1775A	2-methylnaphthalene	high NO_x	N/A	N/A	N/A	N/A	0.23	0.85	100 °C
1661A	naphthalene	low NO_x	0.43	0.63	1.19	1.04	0.18	0.51	150 °C
1718A	naphthalene	low NO_x	N/A	N/A	N/A	N/A	0.35	0.70	100 °C
1828A	naphthalene	low NO_x	N/A	N/A	N/A	N/A	0.15	0.44	150 °C
1616A	1-methylnaphthalene	low NO_x	N/A	N/A	N/A	N/A	0.54	0.81	100 °C
1664A	1-methylnaphthalene	low NO_x	N/A	N/A	N/A	N/A	0.23	0.61	150 °C
1666A	2-methylnaphthalene	low NO_x	N/A	N/A	N/A	N/A	0.12	0.44	150 °C
1744A	2-methylnaphthalene	low NO_x	N/A	N/A	N/A	N/A	0.36	0.70	100 °C
1594A	1-methylnaphthalene	H_2O_2	0.25	0.69	1.02	0.86	N/A	N/A	
1600A	1-methylnaphthalene	H_2O_2	0.23	0.65	1.00	0.84	0.28	0.93	100 °C
1608A	2-methylnaphthalene	H_2O_2	0.33	0.56	1.22	0.95	0.22	0.83	100 °C
1613A	naphthalene	H_2O_2+ low NO_x	0.35	0.64	0.85	0.82	N/A	N/A	
1650A	1-methylnaphthalene	H_2O_2+ low NO_x	0.26	0.65	1.13	0.89	0.25	0.91	100 °C

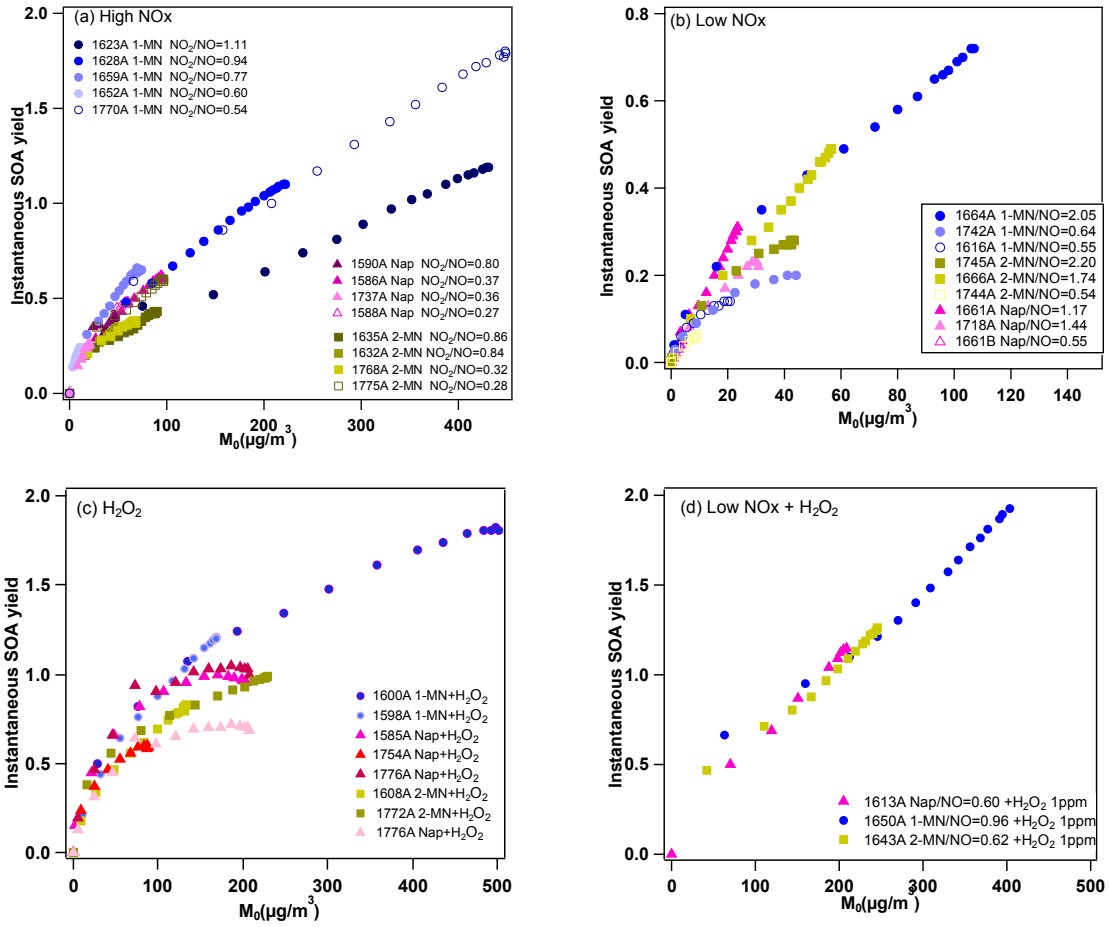

Figure S 2.1 Instantaneous SOA yield for naphthalene, 1-methylnaphthalene, and 2-methylnaphthalene photooxidation under (a) high NO_x conditions, (b) low NO_x conditions, (c) H_2O_2 conditions, (d) low NO_x + H_2O_2 conditions.

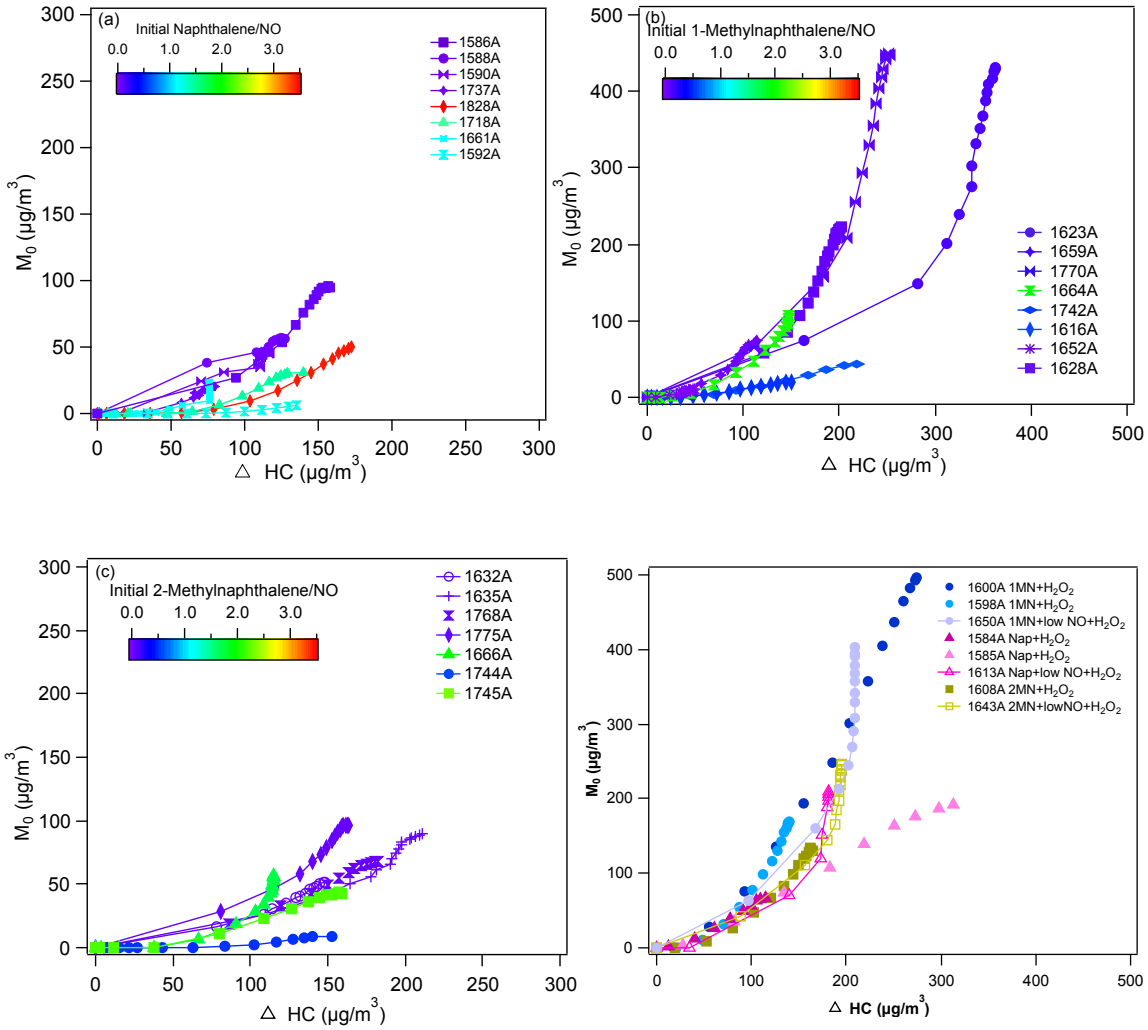

Figure S 2.2 SOA growth curve with irradiation time for naphthalene, 1-methylnaphthalene and 2-methylnaphtlaene under high-NO_x and low-NO_x experiments. Color scale represents the initial PAHs/NO ratio: (a) naphthalene, (b) 1-methylnaphthalene, and (c) 2-methylnaphthalene for each experiment. (d) SOA growth curve with irradiation time for PAHs photooxidation under H_2O_2 and low NO_x+H_2O_2 conditions.

(a) (b)

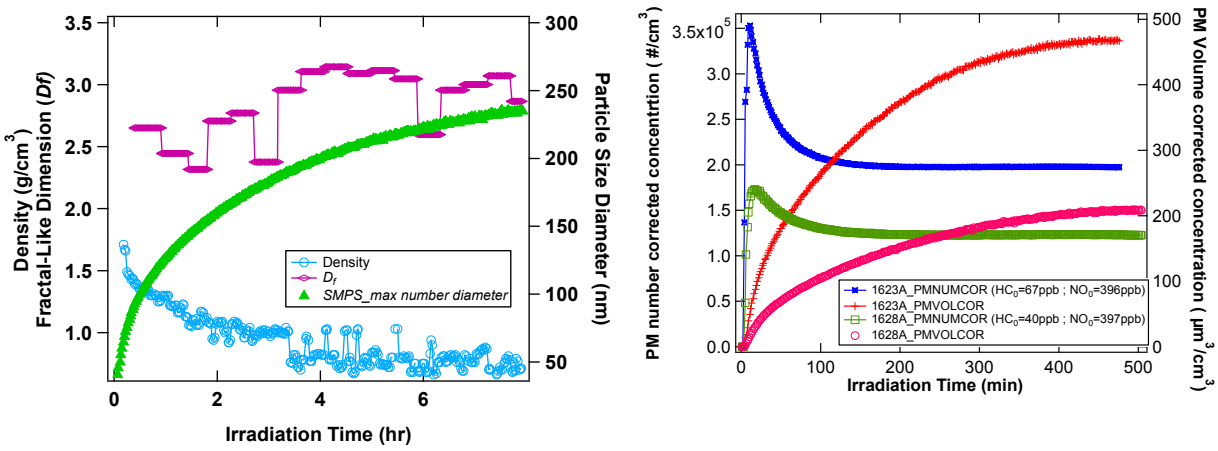

Figure S 2.3 (a) Density, particle maximum number size and fractal-like dimension change over time (1623A). (b) Particulate matter formation from 1-methylnaphthalene photooxidation under high NO_x with HONO condition.

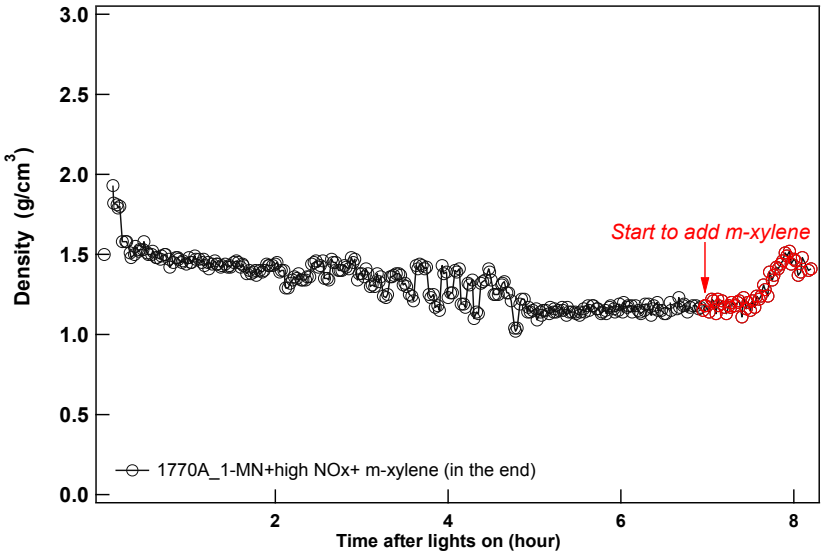

Figure S 2.4 Time series of density changes during 1-methylnaphtlaene-high NO_x with *m*-xylene experiment (run 1770A).

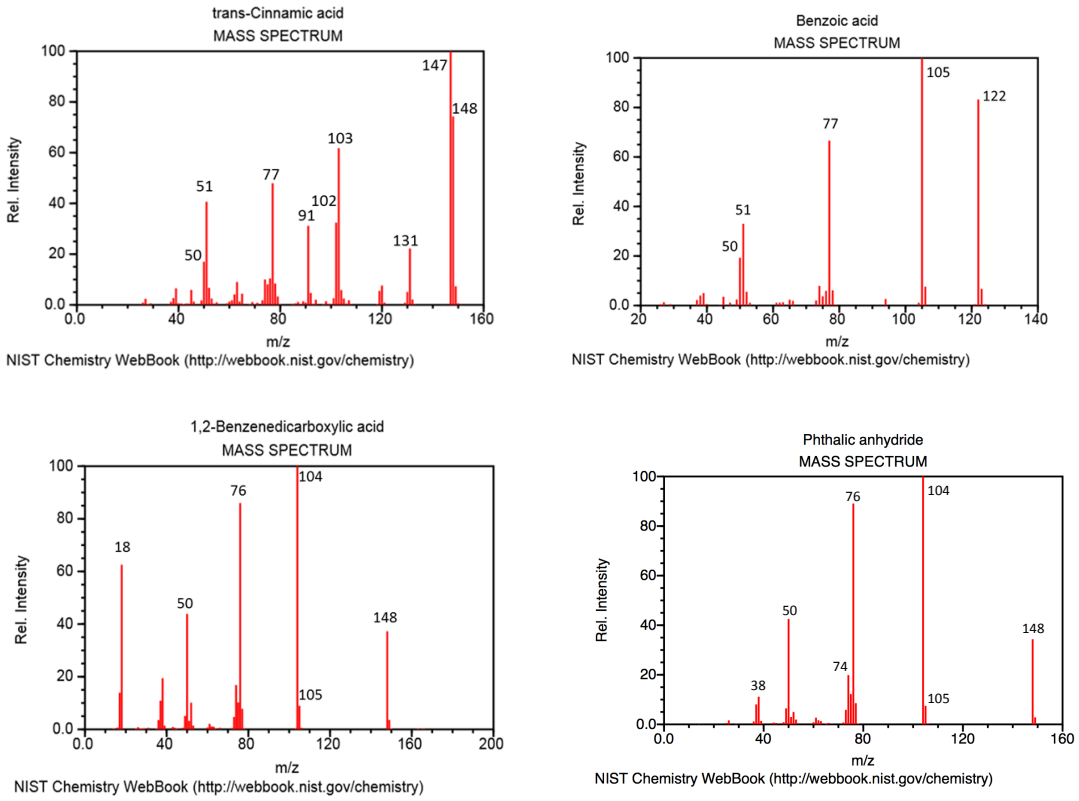

Figure S 2.5 Mass spectra of trans-cinnamic acid, benzoic acid, phthalic acid (1,2-benzenedicarboxylc acid), and phthalic anhydride.

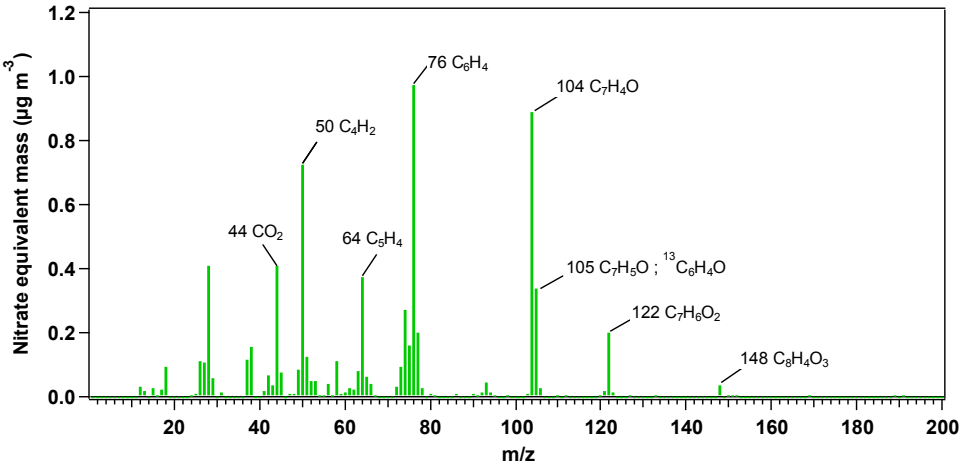

Figure S 2.6 The mass-to-charge distribution of pure phthalic acid measured by HR-ToF-AMS.

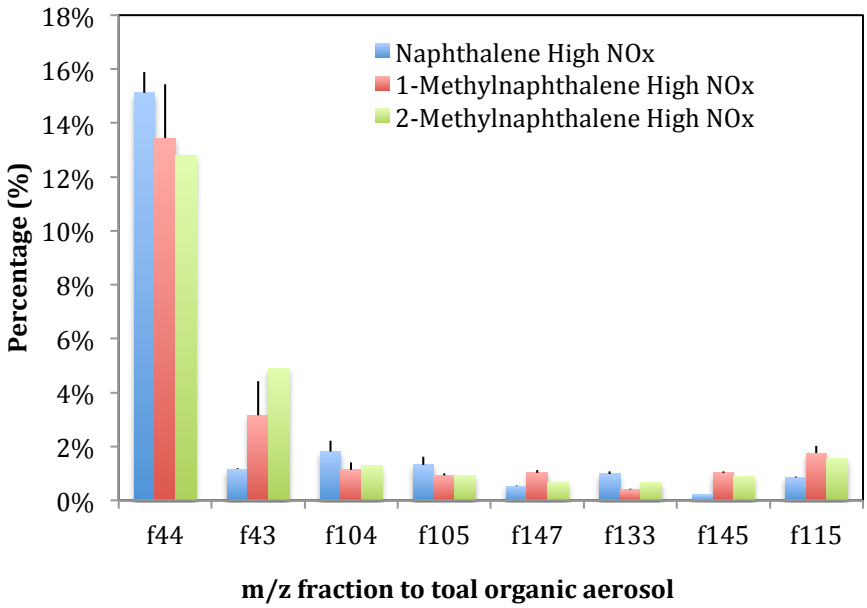

Figure S 2.7 The average specific *m/z* fraction to total organic aerosol for PAHs photooxidation under high NO_x condition.

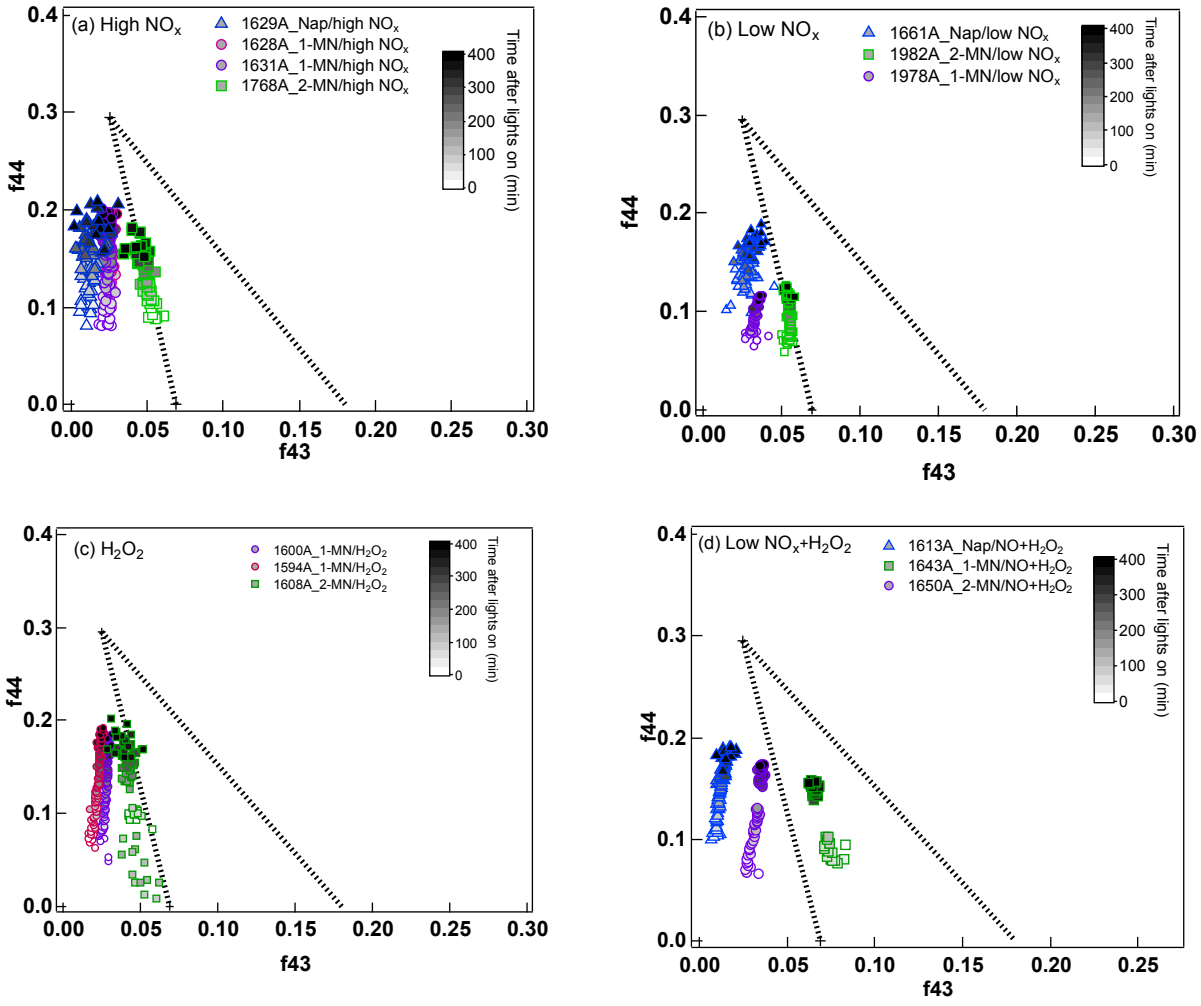

Figure S 2.8 Triangle plot of SOA formed from naphthalene, 1-methylnaphthalene and 2-methylnaphthalene photooxidation. Dashed lines represent triangle region from (Ng et al., 2010) of ambient OA. Color from light grey to black represents the irradiation time of each experiment. (a) High NO_x conditions. (b) Low NO_x conditions. (c) H_2O_2 conditions. (d) Low NO_x and H_2O_2 conditions.

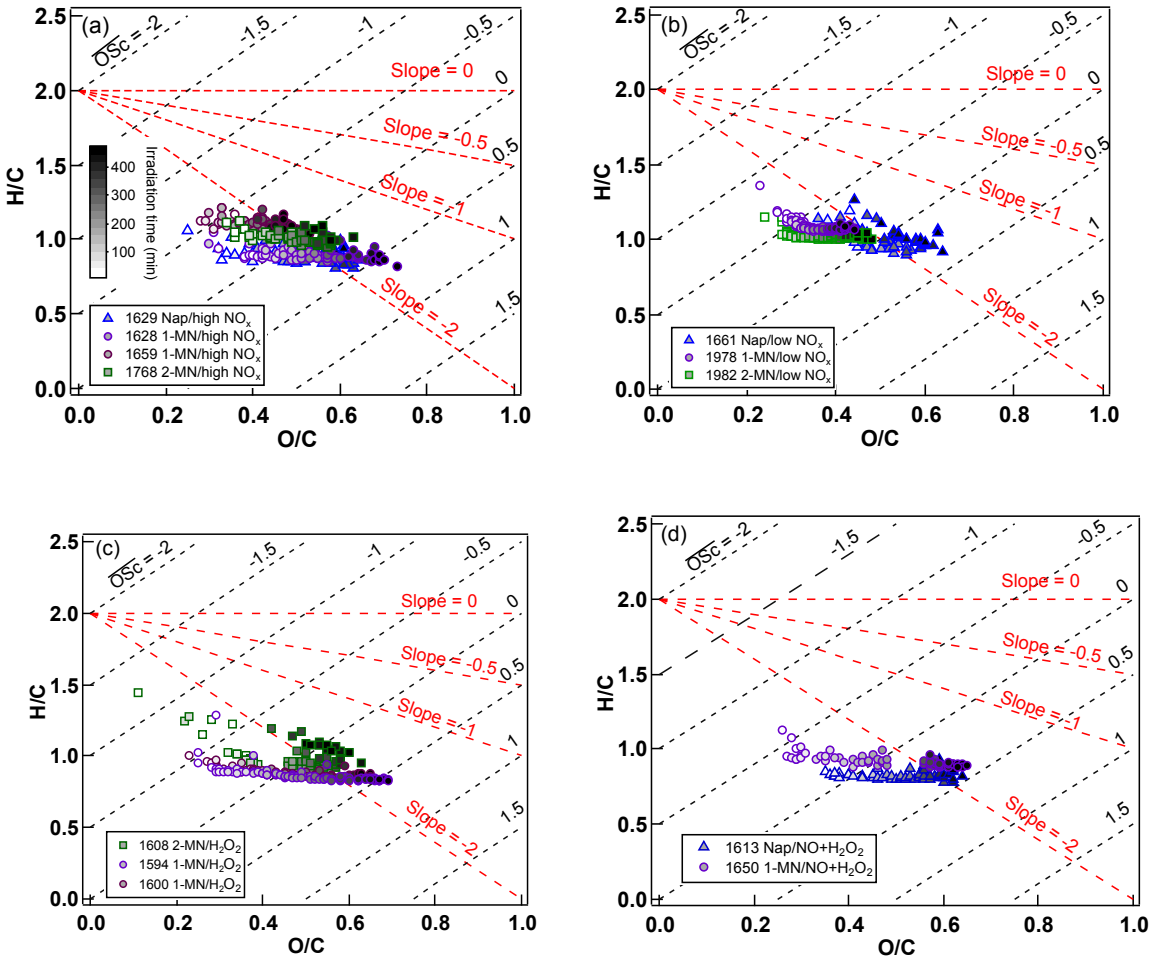

Figure S 2.9 Van Krevelen diagram (Ng et al., 2011) SOA formation from naphthalene, 1-methylnaphthalene and 2-methylnaphthalene photooxidations. $\overline{\mathrm{OS}}_c \approx 2\ \mathrm{O/C} - \mathrm{H/C}$ (Kroll et al., 2011). Color from light grey to black represents the irradiation time of each experiment. (a) High NO_x conditions. (b) Low NO_x conditions. (c) H_2O_2 conditions. (d) Low NO_x and H_2O_2 conditions.

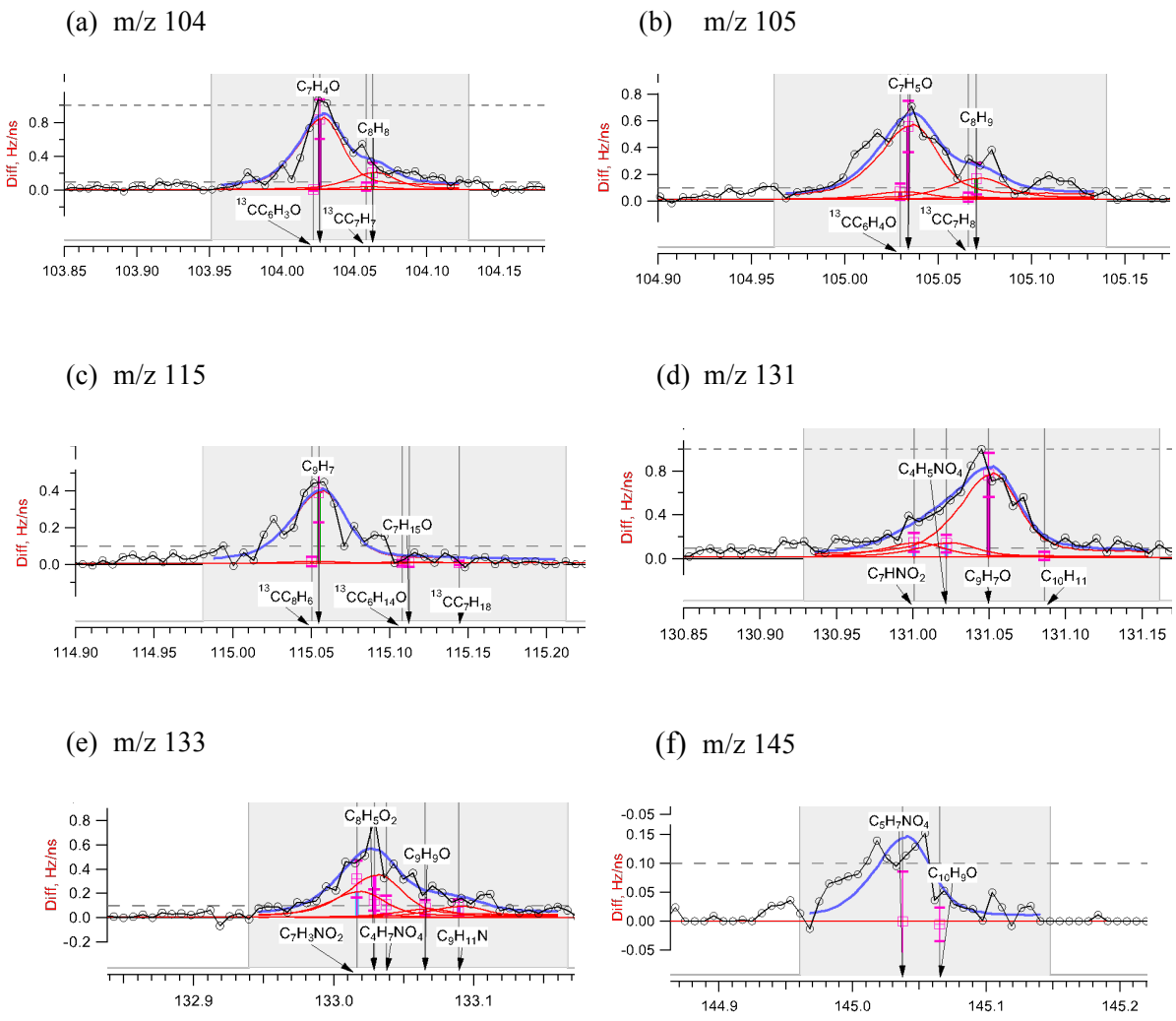

Figure S 2.10 High-Resolution spectra (a-f) of N-containing m/z ratios for naphthalene high-NO_x SOA (1629A).

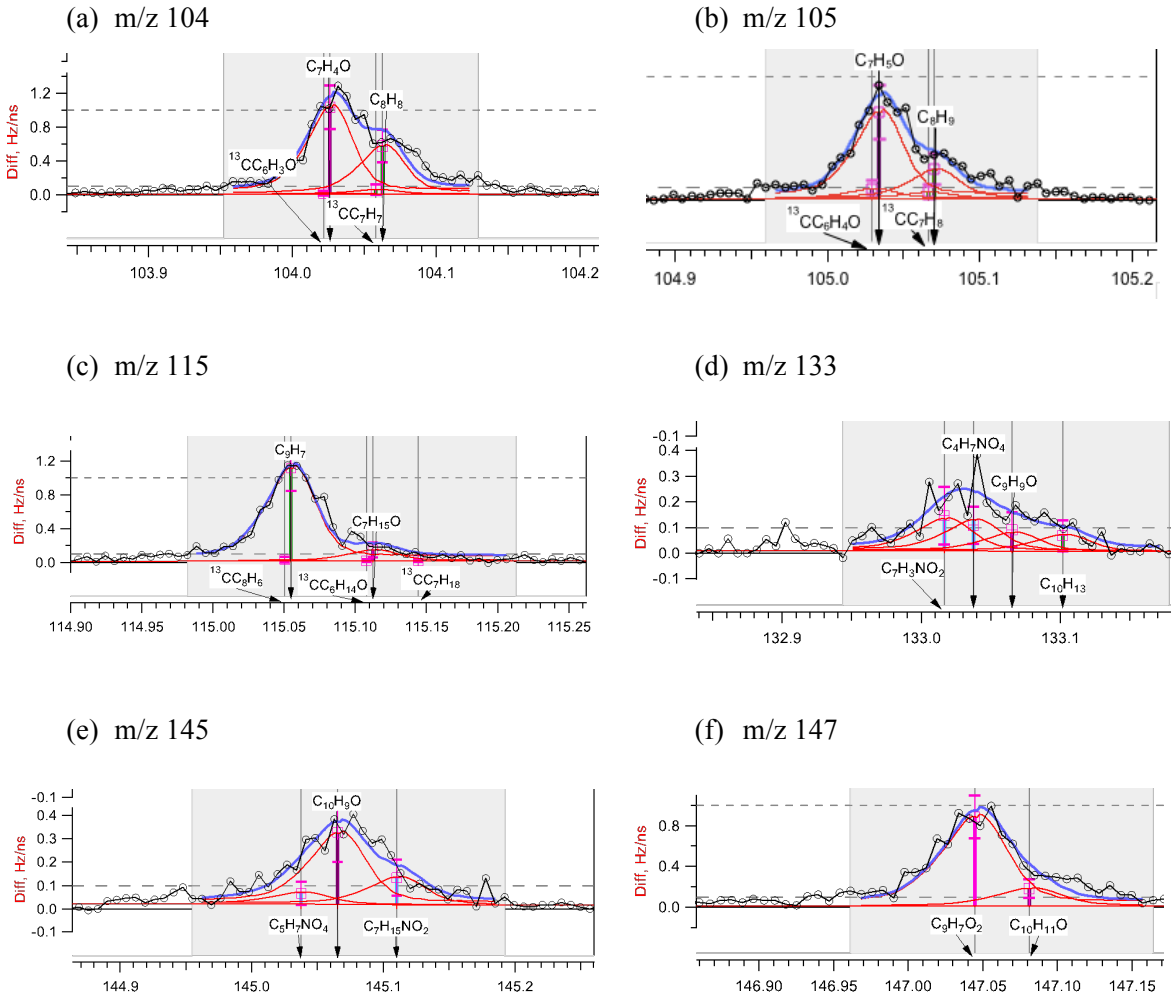

Figure S 2.11 High-Resolution spectra (a-f) of N-containing m/z ratios for 1-methylnaphthalene high NO_x SOA (1628A).

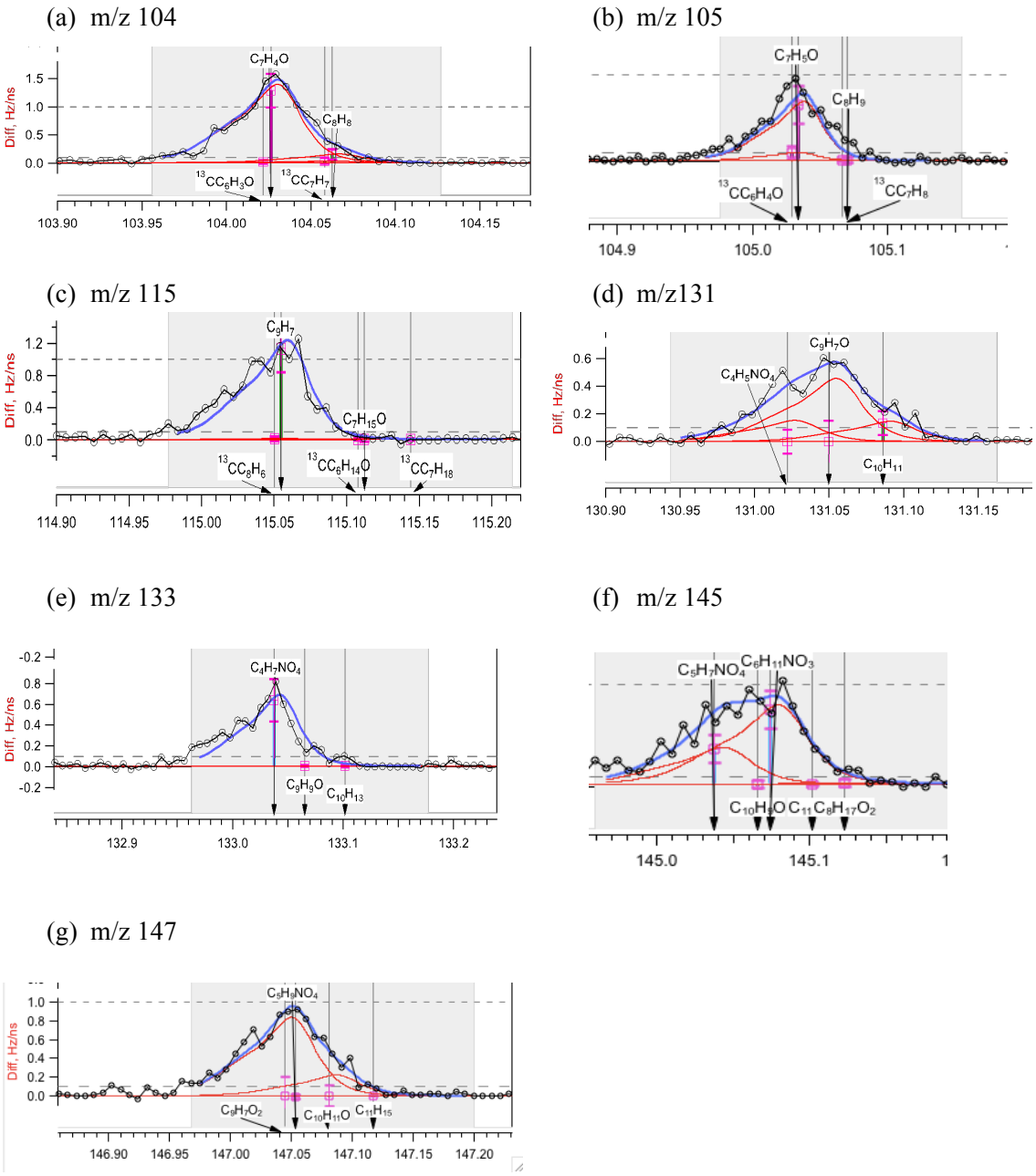

Figure S 2.12 High-Resolution spectra (a-g) of N-containing m/z ratios for 2-methylnaphthalene high-NO_x SOA (1768A).

Chapter 3 SOA Formation from Photooxidation of Naphthalene and Methylnaphthalenes with *m*-Xylene and Surrogate Mixtures

3.1 Introduction

Previous research has shown that SOA yield for naphthalene, 1-methylnaphthalene, and 2-methylnaphthalene range from 0.04~1.81 (Chen et al., 2015). Polycyclic aromatic hydrocarbons (PAHs) are significant components of semivolatile gas-phase emissions from anthropogenic sources including incomplete combustion emissions from heavy-duty diesel exhaust vehicles (Shah et al., 2005), biomass burning (Conde et al., 2005; Hedberg et al., 2002), and meat cooking (McDonald et al., 2003), and may be a major "missing" source of SOA. A number of petroleum products including gasoline, jet fuel and kerosene contain significant quantities of naphthalene and methylnaphthalenes. Formation of naphthalene and its alkyl derivatives are favored among PAHs and can represent as much as 80 % of the total PAHs in a combustion smoke sample (Conde et al., 2005).

Numerous studies have shown nitrogen oxides (NO_x) levels to play an important role on SOA formation from small hydrocarbons (10 carbons or fewer) (Kroll et al., 2006; Ng et al., 2007; Song et al., 2005). SOA yields are generally observed to decrease as NO_x increases; however, some studies observe reverse NO_x dependence at low NO_x level due to low OH levels (Kroll et al., 2006). Generally, $RO_2\cdot$ + NO and $RO_2\cdot$ + $HO_2\cdot$ oxidation mechanisms dominate the reaction pathway in forming VOCs oxidation products. The chemical composition and aging properties of SOA formed from *m*-xylene

photooxidation has been investigated previously (Bahreini et al., 2005; Loza et al., 2012; Qi et al., 2010); however, SOA formation from aromatics (e.g., with PAHs) are poorly understood. Previous chamber studies have reported that NO_x level influences SOA formation from *m*-xylene photooxidation—SOA formation per *m*-xylene reacted increases with decreasing NO_x levels (Song et al., 2005; Tang et al., 2015). Song et al. (2007) studied SOA formation from *m*-xylene in the absence of NO_x. The experiments utilized H_2O_2 photolysis as a hydroxyl radical source, leading to higher hydroxyl radical concentrations relative to NO_x experiments, observed that greater SOA formation attributed to measured production. Further, Henze et al., 2008 reports that SOA yield increases when aromatic hydrocarbons react with OH under lower [NO]/[HO_2] ratios. Hence, atmospheric reactivity conditions are significant factors to SOA formation from aromatic hydrocarbon precursors. Additionally, the OH radical reactions occurred mainly by OH radical addition pathway (>90%) to the aromatic ring(s) for both monocyclic aromatic hydrocarbons and PAHs (Atkinson and Arey, 2007). Previous studies reported that major three products (approximately 75%) of SOA from *m*-xylene oxidation includes 3-methyl-2,5-furandione, *m*-toluic acid, and 2,5-furandione (Forstner et al., 1997). For naphthalene SOA under low NO_x condition (with H_2O_2) ~26.2% is associated with organic peroxide compounds, and others are mainly from acids, such as hydroxyphthalic acid and phthalic acid (Kautzman et al., 2010).

Numerous studies report that current climate and air quality models underestimate the total organic aerosols including POA and SOA in urban and remote areas (e.g., Heald et al., 2005 ;Volkamer et al., 2006; Kleinman et al., 2008; Utembe et al., 2011; Hodzic et

al., 2009; Henze et al. 2008). It is hypothesized that the underestimation is attributable to missing chemical reaction processes and errors in SOA photochemical (Zhang et al., 2006) as well as overestimation of POA (de Gouw et al., 2005). Hodzic et al., (2009) reported that biogenic SOA were underestimated by about a factor of 2-10 by the meso-scale chemistry-transport model CHIMERE while anthropogenic SOA is underestimated by a factor of two in the late morning with the discrepancy increases rapidly during the day. Volkamer et al. (2006) also estimated that anthropogenic SOA is underestimated by a factor of 5 after the start of photochemistry increasing to an order magnitude after a few hours of photooxidation processing.

Currently, SOA formation potentials are measured from single precursors where the atmospheric reactivity of the chamber study is set by the individual oxidizing species and NO_x/oxidants injected. However, these precursors react in a complex atmospheric mixture dictated by atmospheric NO_x as well as the many other vehicle organic compounds present in the atmosphere. Therefore, this study investigates how the individual SOA formation from select PAHs and influenced by the presence of other VOCs. This study takes advantage of the extensive *m*-xylene experimental database and previous literature studies to identify how a simple VOC mixture impacts SOA formation from PAH precursors. Further, an atmospheric surrogate based on (Carter, 2010) developed for O_3 reactivity studies is used to influence atmospheric reactivity during PAH formation and explore its impact on SOA formation from individual PAH.

3.2 Experimental Methodology

3.2.1 Experimental setup

All mixtures and individual PAH experiments were conducted in the UCR/CE-CERT environmental chamber described in detail elsewhere (Carter,2005). The facility includes a 6m×6m×12m thermally insulated enclosure, which is continuously flushed with purified air (Aadco 737 series (Cleves, Ohio) air purification system). Inside the enclosure, there are two 90 m^3 2 mil (54 μm) FEP Teflon® film reactors, and two banks of 115 W 4-ft blacklights for driving NO_2 photolysis within the reactor. The top frames of the chamber are controlled by elevators that maintain a positive differential pressure of ~0.02 in H_2O. Aliquots of volatile organic compound are injected into the chamber through a heated glass injection manifold system and flushed into the chamber with pure N_2. PAHs and hydrogen peroxide (50 wt% H_2O_2) are injected into a glass manifold tube with a 55°C oven, and flushed into the chamber with purified air. NO is prepared by filling a calibrated glass bulb to a known pressure of pure NO followed by flushing into the chamber with pure N_2. The full surrogate used for select experiments consists of *n*-butane (135 ppb), *n*-octane (36ppb), ethane (25 ppb), propene (20 ppb), *trans*-2-butene (20 ppb), toluene (33 ppb), and *m*-xylene (31 ppbb) (Carter, 2010). 100 ppb Perfluorohexane was injected into the chamber as an inert tracer.

3.2.2 Instrumentation

Gas phase: Hydrocarbon decay and perfluorohexane were monitored with dual Agilent 6980 (Palo Alto, CA) gas chromatographs (GC) equipped with flame ionization

detectors (FIDs). NO and NO_x were measured by a TECO model 42 chemiluminescence NO_x analyzer while O_3 was monitored with a Dasibi Environmental Corp. Model 1003-AH O_3 analyzer.

Particle phase: Particle size distributions (27- 686 nm) and number concentrations are measured with an in-house build Scanning Mobility Particle Sizers (SMPS) that described by Cocker et al. (2001). Aerosol particle density was measured with an aerosol particle mass analyzer (APM, Kanomax model 3600) (Ehara et al., 1996) and SMPS in series. A detailed description of the APM-SMPS system and data algorithms for density determination are described elsewhere (Malloy et al., 2009 ; Nakao et al., 2011). Particle volatility was monitored with a volatility tandem differential mobility analyzer (VTDMA) (Nakao et al., 2012) for which monodisperse particles of mobility diameter (D_{mi}) are selected by the 1st differential mobility analyzer (DMA) followed by transport through a Dekati thermodenuder (TD, residence time: ~16 s, at 100 °C) and resizing after the TD in the second DMA column (D_{mf}). Volume Remaining Fraction (VRF) is then calculated as $VRF = (D_{mf}/D_{mi})^3$.

High-Resolution Time-of-Flight Aerosol Mass Spectrometer (HR-ToF-AMS) has been widely used to provide quantitative chemical composition and size-resolved mass distributions with high time resolution (Aiken et al., 2007, 2008; DeCarlo et al., 2006). Details of the HR-ToF-AMS and software analysis are described in DeCarlo et al. (2006). This study used W-mode for higher mass resolution analysis, including *mass-to-charge* (*m*/*z*) distribution, elementary analysis of elemental carbon (EC) and organic carbon (OC). Data was analyzed with ToF-AMS analysis toolkit squirrel 1.56D /PIKA 1.15D version.

3.2.3 Gas-phase kinetic modeling of radical species

The OH radical concentration was estimated by fitting the *m*-xylene decays, using the SAPRC gas-phase mechanism (Carter and Heo, 2013). SAPRC 12 was then used to estimate HO_2 and RO_2 radical concentration. Further, the model used a kinetic and equilibrium approach to predict secondary particulate matter formation and ozone (Carter and Heo, 2013; Carter, 2010).

3.2.4 SOA yield

SOA formation is evaluated assuming gas-particle partitioning equilibrium of semivolatile partitioning products is achieved. Odum et al. (1996, 1997) established the expression of fractional SOA yield (Y) to describe the gas-particle partitioning absorption model. SOA yield for individual hydrocarbons is defined by equation (1), where ΔM_0 ($\mu g/m^3$) is the total organic aerosol mass concentration, ΔHC ($\mu g/m^3$) is the amount of hydrocarbon reacted, and α_i and $K_{om,i}$ ($m^3/\mu g$) are the mass-based stoichiometric coefficient and absorption equilibrium partitioning coefficient of product *i* , respectively.

$$Y = \frac{\Delta M_0}{\Delta HC} = \sum_i^n Y_i = M_0 \sum_{i=1}^n \frac{\alpha_i K_{om,i}}{1+K_{om,i} M_0} \quad (1)$$

Total organic aerosol formation for multicomponent mixture is estimated from individual VOC yields by:

$$M_{0\ \text{total estimated}} = \sum Y_{HC,i}\ \Delta HC_{HC,i} \quad (2)$$

$$M_{0\ \text{predicted}} = Y_{HC,1} \times \Delta\ HC_{HC,1} + Y_{HC,2} \times \Delta HC_{HC,2} \quad (3)$$

where $Y_{HC,i}$ is estimated from the α_i and $K_{om,i}$ in (eq1) and total aerosol mass concentration measured.

3.3 Results and Discussion

3.3.1 SOA formation from mixtures of *m*-xylene and individual PAH

All experiments were conducted for 6-8 hours at UCR CE-CERT environmental chamber at T= 27°C and RH< 0.1%. Table 3.1 summarizes the key parameters of the SOA experiments along with total organic aerosol mass formed, SOA yields, and average density. Empirical fits to the two-product model (eq1) for naphthalene, 1-methylnaphthalene, and 2-methylnaphthalene under various conditions has been explored previously within the same chamber under the same light, RH, and temperature conditions (Table S 3.1) (Chen et al., 2015). Figure 3.1 shows the two-product model curves for three individual PAH under different conditions including H_2O_2/H_2O_2 without NO addition (curve1), high NO_x + HONO (curve 2), low NO_x (curve 3), along with *m*-xylene SOA yield curves obtained for similar conditions (Song et al., 2005). The two-product model SOA yield curve 3 for low NO_x condition and curve 1 for H_2O_2 condition was used for predicting the total organic aerosol formation for individual PAH and *m*-xylene. The predicted to measured organic aerosol mass concentration (M_0) for mixtures of individual PAH with *m*-xylene are summarized (Table 3.3). $Y_{predicted}/Y_{measured}$ ranges from 1.23~1.61, 0.78 to 1.15, and 1.08~1.59 for naphthalene/*m*-xylene mixture, 1-methylnaphthalene/*m*-xylene, and 2-methylnaphthalene/*m*-xylene, respectively for low NO_x conditions. Measured versus predicted SOA formation for each PAH/*m*-xylene photooxidation experiment (Figure 3.2) shows a linear correlation with a 1.07 slope (slight underprediction) and R^2=0.89. 1-methylnaphthalene/*m*-xylene > 2-

methylnaphthalene/*m*-xylene ≈ naphthalene/*m*-xylene, were consistent with individual PAH photooxidation SOA yield (Chen et al., 2015). SOA formation from PAH and *m*-xylene mixtures are expected to be affected by the initial PAHs/NO ratio, *m*-xylene/NO ratio, *m*-xylene/PAHs mixing ratio and other changes to the reactivity of the system. Therefore, differences between reactivity from individual precursor/NO_x system and those induced by addition of different hydrocarbons biases estimation of aerosol formation using the simple gas-particle partitioning approach where the hydrocarbon mixture aerosol formation is predicted from the sum of individual precursors. The two-product model for this particular matter over predicts the experimentally observed SOA formation. The bias increases with increasing *m*-xylene/PAH ratio. The bias may be induced by changes to the reactivity of the overall system (e.g., HO_2/HO ratios, OH concentration, HO_2/NO or RO_2/NO ratio, etc) or by additional cross-reaction between oxidation products from the two individual precursors.

3.3.2 Relationship between M_0 and initial *m*-xylene/naphthalene

The relationship between SOA yield and the initial *m*-xylene/PAHs (0.7~3.7) is shown in Figure 3.3. Initial PAH hydrocarbon concentration at low NO_x conditions is the key metric for estimating the SOA formation from aromatic/PAH hydrocarbon photooxidation. $Y_{m\text{-xylene predicted}}$ is constant with initial *m*-xylene/PAHs since the SOA yield for *m*-xylene is located on the plateau of two-product curve for the given aerosol mass concentration. The SOA yield for naphthalene prediction ($Y_{\text{naphthalene predicted}}$)

decreases from 0.34 to 0.26, indicating *m*-xylene addition suppresses naphthalene SOA yield. Overall, the total SOA yield (Y_{total}) and total M_0 decrease as the initial *m*-xylene/PAHs increases. Additionally, the $M_{0\_predicted}$ is higher than the $M_{0\_measured}$ for naphthalene+*m*-xylene mixture by 23% to 61% and is not a function of total ΔHC (Figure 3.4). Figure 3.4 also shows that $M_{0\_m\text{-xylene predicted}}$ decreases as initial *m*-xylene/PAHs increases, and is a function of $\Delta HC_{m\text{-xylene}}$. In contrast, the $M_{0\_naphthalene\ predicted}$ increases as the initial *m*-xylene/PAHs decreases and $\Delta HC_{naphthalene}$ increases, implying naphthalene SOA dominates the SOA formation from mixture. This study suggests that *m*-xylene not only suppressed the SOA formation from naphthalene.

3.3.3 Overall and instantaneous aerosol formation after onset of aerosol growth

The timing for the onset of new particle formation was identified as the time at which aerosol mass concentration (ΔM_0) equaled 2 $\mu g/m^3$. Aerosol yield can then be estimated as the amount growth after the new particle induction period versus the hydrocarbon consumed after new particle formation commences. The irradiation time and aerosol yield after onset of aerosol formation are summarized in the supplemental information section (Table S 3.2). The onset of new particle formation varies widely—for example, exp. 1784A (naphthalene 36.6 ppb, *m*-xylene 114.8 ppb, NO 12.5 ppb) has an irradiation of 41 min while exp. 1784B (naphthalene 37.7 ppb, no *m*-xylene, NO 12.4 ppb) has an induction time of 156 min. Figure 3.5 compares aerosol growth with and without shifting for timing of new particle formation. Remarkably, the aerosol growth curve

appears linear after offset with linear regression for each system. The slope of the line then indicates the aerosol yield accounting only for hydrocarbon decay after the meet of aerosol formation. This implies three very important observations: 1) Aerosol formation is independent of the HC consumed prior to aerosol formation; 2) the aerosol formation after particle formation is not strongly influenced by organic aerosol present for these systems; and 3) addition of species that influence the timing of aerosol formation by altering the reactivity of the system will directly impact total aerosol formation from a given quantity of hydrocarbon by changing the time and therefore **Δ**HC precursor reacted prior to the onset of aerosol formation. *m*-Xylene decay is observed (Table S 3.2 and Figure 3.5) to be greater than naphthalene when the initial naphthalene to *m*-xylene (ppbv/ppbv) mixing ratio is less than 1 (i.e. naphthalene < *m*-xylene) (e.g., 1784A, 1791A, and 1800A). Conversely, for mixing ratios greater than 1 the naphthalene is observed to decay more than the *m*-xylene. Therefore, the initial hydrocarbon mixing ratio is a significant factor of SOA formation for constant NO range.

3.3.4 Gas-phase chemistry

Time series of NO and naphthalene decay along with increasing NO_2 and total organic aerosol mass concentration is provided (Figure 3.6). Aerosol mass concentration starts to increase for the naphthalene/*m*-xylene mixture experiment, only after the NO decreases from 12.5 ppb to 1 ppb (t = 33 min). The irradiation time for NO to consume to sub-ppb level from naphthalene only side is much longer than the mixture (188min).

SAPRC-12 gas-phase chemical model predicts RO_2 and HO_2 radicals to sharply increase to 10^9 molecules/cm^3 level when NO is depleted (Figure 3.7). Competition for available hydroxyl radical led to consumption of only 50% and 65% of the precursor *m*-xylene and naphthalene, respectively versus 94% naphthalene consumption in the naphthalene-NO_x only experiment. The mixture experiment's rapid conversion of NO to NO_2 greatly enhanced HO_2+RO_2 reaction while the slow conversion of NO to NO_2 in naphthalene only experiment led to greater contribution of RO_2+NO chemistry. Therefore, it is expected that mixture experiment will lead to lower volatility hydroperoxides products compared with the reactivity higher volatility RO_2+NO products.

3.3.5 SOA growth rate for different PAHs mixtures

Hydroxyl radicals initiate aromatic oxidation and play a significant role in forming secondary organic aerosol from aromatic hydrocarbons. The hydroxyl radical reaction rate constant (k_{OH}) is 2.31×10^{-11} cm^3 $molecule^{-1}$ s^{-1} for *m*-xylene, and 2.30×10^{-11} cm^3 $molecule^{-1}$ s^{-1} for naphthalene, 5.3×10^{-11} cm^3 $molecule^{-1}$ s^{-1} for 1-methylnaphthalene and 5.23×10^{-11} cm^3 $molecule^{-1}$ s^{-1} for 2-methylnaphthalene, respectively. The average OH concentration in each experiment was obtained using the SAPRC-11 model (Table S 3.3). The SOA mass concentration of PAHs/*m*-xylene mixture experiments were plotted as a function of total hydrocarbon reacted (Figure 3.8). SOA mass concentration (ΔM_0) as a function of total hydrocarbon reacted for naphthalene/*m*-xylene photooxidation experiments is shown for different mixing ratio

(1.5:1, 1:1, 1:3.3 and 1:4) all with similar initial NO levels (Figure 3.8(a)). The hydrocarbon reacted lag phase (ΔHC', the hydrocarbon reacted when $\Delta M_0 >= 2$ μg/m^3) was subtracted from total HC reacted (ΔHC) (Figure 3.8 (a), right panel). The M_0 vs. ΔHC−ΔHC' was linearly curve fit with the slope representing the SOA formation rate for each experiment after onset of particle growth. The slope is the highest (0.38) when the mixing ratio is 1:1. The relationship of SOA formation rate to average OH concentration (Figure 3.9) suggests that the OH radical concentration is not the determining factor for aerosol production in the naphthalene/*m*-xylene mixture photooxidation. Integrated [OH]/[HO_2] ratio (Figure 3.9(b)) ranges from 1.03×10^{-3} to 6.43×10^{-3} for the various mixtures with SOA growth rate slightly increasing with increasing [OH]/[HO_2] ratio. Furthermore, if we consider [NO]/[HO_2] (Figure 3.9(c)), the SOA growth rate is observed to increase with [NO]/[HO_2] ratio. The [NO]/[HO_2] trend is opposite of that suggested by Henze et al. (2008), which suggests based on global modeling that aromatic species produce more SOA when they react with OH radicals in regions where the [NO]/[HO_2] ratios are lower. A strong positive correlation between SOA formation and [HO_2]/[RO_2] ratios is observed (Figure 3.9 (d)), suggesting increasing HO_2+RO_2 chemistry enhances SOA formation and high initial PAHs/NO ratio (Figure 3.9(e)) the low initial *m*-xylene/NO ratio (Figure 3.9 (f)) are also weakly associated with more SOA formation, suggesting *m*-xylene inhibits OH radical availability for PAH reaction in the PAH/*m*-xylene low NO_x condition.

3.3.6 Mixtures under absence of NO_x

Song et al. (2007) observed that SOA mass concentration from aromatics is enhanced by injecting H_2O_2 as in increases hydroxyl radical levels which in turn increase organic peroxide formation rates (Song et al., 2007). SOA yields from PAH precursors were suppressed as more *m*-xylene was added, consistent with observations from the low NO_x condition (Table 2). The two-product model overestimates aerosol formation for naphthalene/*m*-xylene photooxidation by 34% to 78% based on individual PAH/H_2O_2 and *m*-xylene /H_2O_2 two-product model curves (as Table S 3.1 and Figure S 3.2). Adding *m*-xylene to PAHs photooxidation reduces the OH radicals for all PAH/m-xylene mixtures H_2O_2 experiments (Figure S3.3), and therefore SOA formation from the precursors. Therefore, the overprediction of SOA formation from the two-product model derives from changes to OH radical levels by the mixture of precursors versus of the individual precursor.

3.3.7 Individual PAH/surrogate mixture

An ambient surrogate mixture (Carter, 2010) was introduced into the PAH system to further understand the effect of mixture compounds in the atmosphere. The initial condition and experimental results for individual PAH and surrogate mixture photooxidation experiments in the absence and presence of NO_x are summarized (Table 3.2). The H_2O_2 (runs: B) was injected as an additional OH radical sources, thereby increasing both OH and hydroperoxyl (HO_2) radicals. CO was introduced with H_2O_2 (run

1814A) to further promote HO_2 radical concentration through the CO oxidation cycle. SOA formation from the naphthalene/surrogate is less than 5 μg/m^3 with addition of CO and H_2O_2 condition (run:1814A), while the experiment without CO addition formed for more aerosol mass concentration (73.1 μg/m^3, run:1814B) (Figure S3.4). The large differences in aerosol formation are attributed to greatly reduced OH superceding any additional aerosol formation through increasing HO_2. HO_2 radical increases rapidly at the onset of aerosol formation (Figure S 3.4), which indicating the CO and surrogate reacted with OH radical and form more HO_2 leading to lower SOA formation. The surrogate mixture in the presence of NO_x inhibits SOA formation from individual PAH photooxidation, which indicates that SOA formation from PAHs is less pronounced for the atmospheric reactivity conditions produced by the ambient surrogate.

3.3.8 Volatility and density evolution

Figure 3.10 shows the volume remaining fraction (VRF) evolution of SOA generated from different PAHs/*m*-xylene mixtures photooxidation. VRF increased from 0.26 to 0.69 for the 1.5:1 (naphthalene:*m*-xylene) mixing ratio. Previously, our group reported the VRF increasing from 0.35 to 0.7 for naphthalene/low NO_x experiment (Chen et al., 2015) and from 0.21 to 0.4 for *m*-xylene/low NO_x experiment (Tang et al., 2015). Therefore, the mixture VRF of 0.69 is indicative of low volatility aerosol mainly from naphthalene photooxidation. Decreasing the mixing ratio (PAH: *m*-xylene) from 1:1 to 1:4 decreased the final VRF from 0.66 to 0.55, 0.74 to 0.65, and 0.70 to 0.56,

respectively for m-xylene mixtures with naphthalene, 1-methylnaphthalene, 2-methylnaphthalene. The 1-methylnapthalene/*m*-xylene mixture formed the lowest volatility products, consistent with the VRF order from individual PAH (Chen et al., 2015).

Densities for each PAHs/*m*-xylene mixture experiment (Table 3.1) and density evolution (Figure S 3.6) are provided for low NO_x conditions. The average density ranges from 1.32 to 1.42 for naphthalene/*m*-xylene mixture, from 1.30 to 1.40 for 1-methylnaphthalene/*m*-xylene mixture, and from 1.35 to 1.37 for 2-methylnaphthalene/*m*-xylene mixture. No obvious changes in density occur as each PAH/*m*-xylene experiment progresses (Figure S 3.6).

3.3.9 Chemical composition of PAHs mixtures

3.3.9.1 Cross-reaction effect evaluation

The HR-ToF-AMS was used to characterize the chemical composition of PAHs/*m*-xylene mixtures. Three representative average spectral distributions of 2-methylnaphthalene, *m*-xylene and 2-methylnaphthalene+*m*-xylene is shown (Figure 3.11). M/z 43 and *m*/*z* 44 are the two dominant fragments from *m*-xylene and 2-methylnaphthalene photooxidation. The *m*/*z* 43 ($C_2H_3O^+$ or $C_3H_7^+$) indicates of oxidized organic compounds such as aldehydes and ketones (CH_2CHO^+ or CH_3CO^+) and saturated hydrocarbon compounds ($C_3H_7^+$) (Alfarra et al., 2004). The *m*/z distribution from the 2-methylnaphthalene/*m*-xylene mixture combines fragments from individual 2-

methylnaphthalene and *m*-xylene photooxidation experiments with the higher *m*/*z* fragment (*m*/*z*>100) is dominated by PAHs. To explore the relative SOA production from each mixture components, and from cross reaction, the unique *m*/*z* indicators were chosen and analyzed by a mass-balance approach:

(M_0 contribution of m-xylene to AMS signal of mixed exp.)+(M_0 contribution of PAHs to AMS signal of mixed exp.)

+ M_0cross reaction=total M_0 (5)

$$\frac{signal\ mixture\ experiment\ (\sum i)}{\frac{\sum i}{M_0\_mxylene\ only}} + \frac{signal\ mixture\ experiment\ (\sum i)}{\frac{\sum i}{M_0\_PAHs\ only}} + M_0 cross\ reaction = total\ M_0 \quad (6)$$

where M_0 is total organic aerosol mass concentration (μg/m^3), and $\sum i$ are the unique *m*/*z* indicators for each individual *m*-xylene or PAHs. In this study, *m*-xylene has unique *m*/*z* at 95; and naphthalene has unique *m*/*z* at 76, 104, 105; 1-methylnaphthalene has unique *m*/*z* at 76, 104, 105, 115, and 147; and 2-methylnapthalene has unique *m*/*z* at 76, 104, 105, 115, and 147. The $M_{0\ \text{cross-reaction}}$ was calculated by equation (5) and (6) based on individual *m*-xylene (1193A and 1930A) and PAH experiments (Table S 3.5). The aerosol mass concentration $M_{0\ \text{cross-reaction}}$ is from 0.65 to -9.66 μg/m^3 for naphthalene/*m*-xylene mixture experiment, suggesting little to no effect of cross-reaction between naphthalene and *m*-xylene precursors. However, since the *m*/*z* 95 is a minor *m*-xylene SOA fragment, significant discrepancies are observed from each individual experiment. Therefore, the M_0 contribution prediction from two-product model is compared with the AMS evaluation method (Table S 3.5). The two-product model prediction of the individual contribution to aerosol mass concentration is more plausible; however, the AMS method has to great of uncertainties associated with unique *m*/*z* fragments leading

to significant the percentage discrepancy in estimates of individual contributors between experiments.

3.3.9.2 Triangle plot and Van Krevelen diagram analysis

PAHs/*m*-xylene photooxidation experiments were evaluated with two common AMS analyses (“ Triangle plot” and “Van Krevelen diagram” (Ng et al., 2010))(Figure 3.12). SOA from all three PAHs/*m*-xylene mixtures lies on the lower side of triangle area indicating these SOA mixtures are semivolatile oxygenated organic aerosol (SV-OOA). Chen et al. (2015) has investigated each individual PAH (naphthalene, 1-methylnaphthalene, and 2-methylnaphthalene) SOA all of which are located on the upper side of triangle area. Chhabra et al. (2010) and Kautzman et al. (2010) report that SOA continuously ages (higher fragment *m/z* 44 (CO_2^+) intensity) with 33% organic acid SOA from low NO_x with H_2O_2 naphthalene photooxidation. This study observes that SOA from PAHs/*m*-xylene mixtures age with increasing f_{44} ands f_{43}. Elevated *m*/*z* 44 (CO_2^+) is considered “aged” organic aerosol and classified as low volatility oxygenated organic aerosol (LV-OOA) while SV-OOA is associated with “fresh” OOA with elevated *m*/*z* 43 ($C_2H_3O^+$) signal intensity (Chhabra et al., 2011). *m*/*z* 44 (CO_2^+) fragments are associated with thermal decarboxylation of many different oxo-, di-, and poly carboxylic acids, hydroxyl-acids, and acyl peroxides (Alfarra et al., 2004; Aiken et al., 2007 ; Takegawa et al., 2007; Duplissy et al., 2011). Recent studies (Loza et al., 2012; Tang et al., 2015) have shown that *m*-xylene SOA lies on the right of the triangle region with f_{43} higher than the ambient SOA reported by Ng et al. 2010.

Previous studies have observed that atmospheric organic aerosol lies on the -1 slope of Van Krevelen diagram (H:C versus O:C). Heald et al. (2010) suggests that the slope the addition of carboxylic acid or equal addition of hydroxyl and carbonyl functional groups to an aliphatic (unfunctionalized) carbon. PAHs/*m*-xylene mixtures in this study occupy the area between a slope of -1 and -2 on Van Krevelen diagram (Figure 3.12 (b)). The slope of -1 for naphthalene and 2-methylnaphthalene indicates greater addition of carboxylic acid groups to the precursor. However, the 1-methylnaphthalene/*m*-xylene mixture SOA lies on the area with slope -2, which indicates less formation of carboxylic acid and more ketone/aldehyde functionality to the precursor molecule.

Furthermore, SOA with higher f_{44} increases O/C values and the state of the carbon ($\overline{OS}_c$) (Ng et al., 2010; Kroll et al., 2011). The simplified equation describing $\overline{OS}_c$ is:

$$\overline{OS}_c \approx 2\ O/C - H/C \quad (7)$$

The $\overline{OS}_c$ of SOA from photooxidation of PAHs/*m*-xylene mixture increases from -0.54 to -0.37 for naphthalene/*m*-xylene, from -0.77 to 0.11 for 1-methylnaphthalene/*m*-xylene, and from -0.41 to -0.43 for 2-methylnaphthalene/*m*-xylene SOA. Kroll et al. (2011) reports ambient organic aerosol $\overline{OS}_c$ values from -0.5 to 0 for SV-OOA and 0.5 to 0.9 for LV-OOA. Therefore, the PAH mixture SOA has similar $\overline{OS}_c$ to ambient SV-OOA, just as the SOA was consistent with the SV-OOA portion of triangle plot.

3.4 Conclusion

Previous studies have demonstrated that the SOA yield is potentially high for naphthalene and methylnaphthalenes photooxidation, and that the system reactivity (e.g., hydroxyl radical concentration, NO_x concentration) significantly impact the secondary organic aerosol formed from these precursors. This study explores the SOA formation t from PAHs mixed with either *m*-xylene or an atmospheric surrogate mixture during photooxidation under low NO_x conditions with and without H_2O_2. Traditional two-product models as well as *m*/*z* HR-ToF-AMS fragment analysis were applied to evaluate the aerosol mass contribution from individual PAH and *m*-xylene during PAH/*m*-xylene photooxidations. Our results indicate that SOA growth rate from PAH photooxidation was inhibited by *m*-xylene addition for low NO_x and H_2O_2 experiments, despite promoting earlier particles nucleation. Furthermore, the traditional two-product model using parameters derived from individual precursors over-predicted M_0 for PAHs/*m*-xylene photooxidation, suggesting that gas-phase cross-reaction chemistry or changes in the radical chemistry hinder the ability of the individual precursors to form SOA.

3.5 References

Aiken, A. C., DeCarlo, P. F. and Jimenez, J. L.: Elemental analysis of organic species with electron ionization high-resolution mass spectrometry., Anal. Chem., 79(21), 8350–8, doi:10.1021/ac071150w, 2007.

Aiken, A. C., Decarlo, P. F., Kroll, J. H., Worsnop, D. R., Huffman, J. A., Docherty, K. S., Ulbrich, I. M., Mohr, C., Kimmel, J. R., Sueper, D., Sun, Y., Zhang, Q., Trimborn, A., Northway, M., Ziemann, P. J., Canagaratna, M. R., Onasch, T. B., Alfarra, M. R., Prevot, A. S. H., Dommen, J., Duplissy, J., Metzger, A., Baltensperger, U. and Jimenez, J. L.: O/C and OM/OC ratios of primary, secondary, and ambient organic aerosols with high-resolution time-of-flight aerosol mass spectrometry, Environ. Sci. Technol., 42(12), 4478–4485, doi:10.1021/es703009q, 2008.

Alfarra, M.: Insights Into Atmospheric Organic Aerosols Using An Aerosol Mass Spectrometer, University of Manchester, UK., 2004.

Alfarra, M., Coe, H., Allan, J., Bower, K., Boudries, H., Canagaratna, M., Jimenez, J., Jayne, J., Garforth, a and Li, S.: Characterization of urban and rural organic particulate in the Lower Fraser Valley using two Aerodyne Aerosol Mass Spectrometers, Atmos. Environ., 38(34), 5745–5758, doi:10.1016/j.atmosenv.2004.01.054, 2004.

Atkinson, R. and Arey, J.: Mechanisms of the Gas-Phase Reactions of Aromatic Hydrocarbons and PAHS with OH and NO3 Radicals, Polycycl. Aromat. Compd., 27(1), 15–40, doi:10.1080/10406630601134243, 2007.

Bahreini, R., Keywood, M. D., Ng, N. L., Varutbangkul, V., Gao, S., Flagan, R. C., Seinfeld, J. H., Worsnop, D. R. and Jimenez, J. L.: Measurements of secondary organic aerosol from oxidation of cycloalkenes, terpenes, and m-xylene using an aerodyne aerosol mass spectrometer, Environ. Sci. Technol., 39(15), 5674–5688, doi:10.1021/es048061a, 2005.

Carter, W. P. L.: Development of a condensed SAPRC-07 chemical mechanism, Atmos. Environ., 44(40), 5336–5345, doi:10.1016/j.atmosenv.2010.01.024, 2010.

Carter, W. P. L. and Heo, G.: Development of revised SAPRC aromatics mechanisms, Atmos. Environ., 77, 404–414, doi:10.1016/j.atmosenv.2013.05.021, 2013.

Carter, W. P. L., CockerIII, D. R., Fitz, D. R., Malkina, I. L., Bumiller, K., Sauer, C. G., Pisano, J. T., Bufalino, C. and Song, C.: A new environmental chamber for evaluation of gas-phase chemical mechanisms and secondary aerosol formation, Atmos. Environ., 39(40), 7768–7788, doi:10.1016/j.atmosenv.2005.08.040, 2005.

Chen, C.-L., Kacarab, M., Tang, P. and Cocker III, D. R.: SOA Formation from Naphthalene, 1-Methylnaphthalene, and 2-Methylnaphthalene Photooxidation., 2015. *(In preparation)*

Chhabra, P. S., Flagan, R. C. and Seinfeld, J. H.: Elemental analysis of chamber organic aerosol using an aerodyne high-resolution aerosol mass spectrometer, Atmos. Chem. Phys., 10(9), 4111–4131, doi:10.5194/acp-10-4111-2010, 2010.

Chhabra, P. S., Ng, N. L., Canagaratna, M. R., Corrigan, a. L., Russell, L. M., Worsnop, D. R., Flagan, R. C. and Seinfeld, J. H.: Elemental composition and oxidation of chamber organic aerosol, Atmos. Chem. Phys., 11(17), 8827–8845, doi:10.5194/acp-11-8827-2011, 2011.

Cocker, D. R., Flagan, R. C. and Seinfeld, J. H.: State-of-the-art chamber facility for studying atmospheric aerosol chemistry, Environ. Sci. Technol., 35(12), 2594–2601, doi:10.1021/es0019169, 2001.

Conde, F. J., Ayala, J. H., Afonso, A. M. and González, V.: Emissions of polycyclic aromatic hydrocarbons from combustion of agricultural and sylvicultural debris, Atmos. Environ., 39(35), 6654–6663, doi:10.1016/j.atmosenv.2005.07.043, 2005.

DeCarlo, P. F., Kimmel, J. R., Trimborn, A., Northway, M. J., Jayne, J. T., Aiken, A. C., Gonin, M., Fuhrer, K., Horvath, T., Docherty, K. S., Worsnop, D. R. and Jimenez, J. L.: Field-deployable, high-resolution, time-of-flight aerosol mass spectrometer, Anal. Chem., 78(24), 8281–8289, doi:10.1021/ac061249n, 2006.

Duplissy, J., De Carlo, P. F., Dommen, J., Alfarra, M. R., Metzger, a., Barmpadimos, I., Prevot, a. S. H., Weingartner, E., Tritscher, T., Gysel, M., Aiken, a. C., Jimenez, J. L., Canagaratna, M. R., Worsnop, D. R., Collins, D. R., Tomlinson, J. and Baltensperger, U.: Relating hygroscopicity and composition of organic aerosol particulate matter, Atmos. Chem. Phys., 11, 1155–1165, doi:10.5194/acp-11-1155-2011, 2011.

Forstner, H. J. L., Flagan, R. C. and Seinfeld, J. H.: Secondary Organic Aerosol from the Photooxidation of Aromatic Hydrocarbons: Molecular Composition, Environ. Sci. Technol., 31(5), 1345–1358, doi:10.1021/es9605376, 1997.

De Gouw, J. a., Middlebrook, A. M., Warneke, C., Goldan, P. D., Kuster, W. C., Roberts, J. M., Fehsenfeld, F. C., Worsnop, D. R., Canagaratna, M. R., Pszenny, A. A. P., Keene, W. C., Marchewka, M., Bertman, S. B. and Bates, T. S.: Budget of organic carbon in a polluted atmosphere: Results from the New England Air Quality Study in 2002, J. Geophys. Res. D Atmos., 110(D16), 1–22, doi:10.1029/2004JD005623, 2005.

Heald, C. L., Jacob, D. J., Park, R. J., Russell, L. M., Huebert, B. J., Seinfeld, J. H., Liao, H. and Weber, R. J.: A large organic aerosol source in the free troposphere missing from current models, Geophys. Res. Lett., 32(L18809), doi:10.1029/2005GL023831, 2005.

Heald, C. L., Kroll, J. H., Jimenez, J. L., Docherty, K. S., Decarlo, P. F., Aiken, A. C., Chen, Q., Martin, S. T., Farmer, D. K. and Artaxo, P.: A simplified description of the evolution of organic aerosol composition in the atmosphere, Geophys. Res. Lett., 37(L08 803), doi:10.1029/2010GL042737, 2010.

Hedberg, E., Kristensson, A., Ohlsson, M., Johansson, C., Johansson, P. Å., Swietlicki, E., Vesely, V., Wideqvist, U. and Westerholm, R.: Chemical and physical characterization of emissions from birch wood combustion in a wood stove, Atmos. Environ., 36(30), 4823–4837, doi:10.1016/S1352-2310(02)00417-X, 2002.

Henze, D. K., Seinfeld, J. H., Ng, N. L., Kroll, J. H., Fu, T.-M., Jacob, D. J. and Heald, C. L.: Global modeling of secondary organic aerosol formation from aromatic hydrocarbons: high- vs. low-yield pathways, Atmos. Chem. Phys., 8(9), 2405–2420, doi:10.5194/acp-8-2405-2008, 2008.

Hodzic, A., Jimenez, J. L., Madronich, S., Aiken, A. C., Bessagnet, B., Curci, G., Fast, J., Lamarque, J. F., Onasch, T. B., Roux, G. and Ulbrich, I. M.: Modeling organic aerosols during MILAGRO: application of the CHIMERE model and importance of biogenic secondary organic aerosols, Atmos. Chem. Phys. Discuss., 9, 12207–12281, doi:10.5194/acpd-9-12207-2009, 2009.

Kautzman, K. E., Surratt, J. D., Chan, M. N., Chan, a W. H., Hersey, S. P., Chhabra, P. S., Dalleska, N. F., Wennberg, P. O., Flagan, R. C. and Seinfeld, J. H.: Chemical composition of gas- and aerosol-phase products from the photooxidation of naphthalene., J. Phys. Chem. A, 114(2), 913–34, doi:10.1021/jp908530s, 2010.

Kleinman, L. I., Springston, S. R., Daum, P. H., Lee, Y.-N., Nunnermacker, L. J., Senum, G. I., Wang, J., Weinstein-Lloyd, J., Alexander, M. L., Hubbe, J., Ortega, J., Canagaratna, M. R. and Jayne, J.: The time evolution of aerosol composition over the Mexico City plateau, Atmos. Chem. Phys., 8(6), 1559–1575, doi:10.5194/acp-8-1559-2008, 2008.

Kroll, J., Donahue, N. and Jimenez, J.: Carbon oxidation state as a metric for describing the chemistry of atmospheric organic aerosol., Nat. Chem., 3(February), 133–139, doi:10.1038/nchem.948, 2011.

Kroll, J. H., Ng, N. L., Murphy, S. M., Flagan, R. C. and Seinfeld, J. H.: Secondary organic aerosol formation from isoprene photooxidation., Environ. Sci. Technol., 40(6), 1869–1877, doi:10.1021/es0524301, 2006.

Loza, C. L., Chhabra, P. S., Yee, L. D., Craven, J. S., Flagan, R. C. and Seinfeld, J. H.: Chemical aging of m-xylene secondary organic aerosol: Laboratory chamber study, Atmos. Chem. Phys., 12, 151–167, doi:10.5194/acp-12-151-2012, 2012.

Malloy, Q. G. J., Nakao, S., Qi, L., Austin, R., Stothers, C., Hagino, H. and Cocker, D. R.: Real-Time Aerosol Density Determination Utilizing a Modified Scanning Mobility

Particle Sizer—Aerosol Particle Mass Analyzer System, Aerosol Sci. Technol., 43(7), 673–678, doi:10.1080/02786820902832960, 2009.

McDonald, J. D., Zielinska, B., Fujita, E. M., Sagebiel, J. C., Chow, J. C. and Watson, J. G.: Emissions from charbroiling and grilling of chicken and beef., J. Air Waste Manag. Assoc., 53(2), 185–194, doi:10.1080/10473289.2003.10466141, 2003.

Nakao, S., Shrivastava, M., Nguyen, A., Jung, H. and Cocker, D.: Interpretation of Secondary Organic Aerosol Formation from Diesel Exhaust Photooxidation in an Environmental Chamber, Aerosol Sci. Technol., 45(8), 964–972, doi:10.1080/02786826.2011.573510, 2011.

Nakao, S., Liu, Y., Tang, P., Chen, C.-L., Zhang, J. and Cocker III, D. R.: Chamber studies of SOA formation from aromatic hydrocarbons: observation of limited glyoxal uptake, Atmos. Chem. Phys., 12(9), 3927–3937, doi:10.5194/acp-12-3927-2012, 2012.

Ng, N. L., Kroll, J. H., Chan, a W. H., Chhabra, P. S., Flagan, R. C. and Seinfeld, J. H.: Secondary organic aerosol formation from m-xylene, toluene, and benzene, Atmos. Chem. Phys., 7(3), 3909–3922, doi:10.5194/acp-7-3909-2007, 2007.

Ng, N. L., Canagaratna, M. R., Zhang, Q., Jimenez, J. L., Tian, J., Ulbrich, I. M., Kroll, J. H., Docherty, K. S., Chhabra, P. S., Bahreini, R., Murphy, S. M., Seinfeld, J. H., Hildebrandt, L., Donahue, N. M., DeCarlo, P. F., Lanz, V. A., Prévôt, A. S. H., Dinar, E., Rudich, Y. and Worsnop, D. R.: Organic aerosol components observed in Northern Hemispheric datasets from Aerosol Mass Spectrometry, Atmos. Chem. Phys., 10(10), 4625–4641, doi:10.5194/acp-10-4625-2010, 2010.

Odum, J. R., Hoffmann, T., Bowman, F., Collins, D., Flagan, R. C. and Seinfeld, J. H.: Gas/Particle Partitioning and Secondary Organic Aerosol Yields, Environ. Sci. Technol., 30(8), 2580–2585, doi:10.1021/es950943+, 1996.

Odum, J. R., Jungkamp, T. P. W., Griffin, R. J., Forstner, H. J. L., Flagan, R. C. and Seinfeld, J. H.: Aromatics, Reformulated Gasoline, and Atmospheric Organic Aerosol Formation, Environ. Sci. Technol., 31(7), 1890–1897, doi:10.1021/es960535l, 1997.

Qi, L., Nakao, S., Malloy, Q., Warren, B. and Cocker III, D. R.: Can secondary organic aerosol formed in an atmospheric simulation chamber continuously age?, Atmos. Environ., 44(25), 2990–2996, doi:10.1016/j.atmosenv.2010.05.020, 2010.

Shah, S. D., Ogunyoku, T. a, Miller, J. W. and Cocker, D. R.: On-road emission rates of PAH and n-alkane compounds from heavy-duty diesel vehicles., Environ. Sci. Technol., 39(14), 5276–84, doi:10.1021/es048086+, 2005.

Song, C., Na, K. and Cocker, D. R.: Impact of the hydrocarbon to NOx ratio on secondary organic aerosol formation, Environ. Sci. Technol., 39(9), 3143–3149, doi:10.1021/es0493244, 2005.

Song, C., Na, K., Warren, B., Malloy, Q. and Cocker, D. R.: Secondary organic aerosol formation from m-xylene in the absence of NOx., Environ. Sci. Technol., 41(21), 7409–16, doi:10.1021/es070429r, 2007.

Takegawa, N., Miyakawa, T., Kawamura, K. and Kondo, Y.: Contribution of Selected Dicarboxylic and ω-Oxocarboxylic Acids in Ambient Aerosol to the m/z44 Signal of an Aerodyne Aerosol Mass Spectrometer, Aerosol Sci. Technol., 41(March 2015), 418–437, doi:10.1080/02786820701203215, 2007.

Tang, P., Nakao, S., Qi, L., Chen, C.-L. and Cocker III, D. R.: Role of Alkyl substituents on Secondary Organic Aerosol Formation from Aromatic Hydrocarbons: Part-II Chemical Composition., 2015.*(In preparation)*

Utembe, S. R., Cooke, M. C., Archibald, a. T., Shallcross, D. E., Derwent, R. G. and Jenkin, M. E.: Simulating secondary organic aerosol in a 3-D Lagrangian chemistry transport model using the reduced Common Representative Intermediates mechanism (CRI v2-R5), Atmos. Environ., 45(8), 1604–1614, doi:10.1016/j.atmosenv.2010.11.046, 2011.

Volkamer, R., Jimenez, J. L., San Martini, F., Dzepina, K., Zhang, Q., Salcedo, D., Molina, L. T., Worsnop, D. R. and Molina, M. J.: Secondary organic aerosol formation from anthropogenic air pollution: Rapid and higher than expected, Geophys. Res. Lett., 33, 7–10, doi:10.1029/2006GL026899, 2006.

Zhang, Y., Liu, P., Queen, A., Misenis, C., Pun, B., Seigneur, C. and Wu, S. Y.: A comprehensive performance evaluation of MM5-CMAQ for the Summer 1999 Southern Oxidants Study episode-Part II: Gas and aerosol predictions, Atmos. Environ., 40(26), 4839–4855, doi:10.1016/j.atmosenv.2005.12.048, 2006.

3.6 Tables and Figures

Table 3.1 Initial experimental conditions and SOA yields for all experiments

Run number	Compounds	Initial PAHs	Initial *m*-Xylene	ΔHC_ PAHs	ΔHC_ *m*-xylene	NO	ΔM_0	SOA yield	Density
		ppb	ppb	μg/m^3	μg/m^3	ppb	μg/m^3		g/cm^3
1784A	naphthalene + *m*-xylene	36.6	114.8	124.3	247.9	12.5	42.0	0.11	1.37
1784B	naphthalene	37.7	-	184.7	-	12.4	39.7	0.21	a
1788A	naphthalene + *m*-xylene	68.6	44.9	209.3	92.2	8.3	61.7	0.20	1.33
1788B	*m*-xylene	-	44.0	-	158.5	8.1	4.8	0.03	b
1791A	naphthalene + *m* -xylene	32.1	94.4	106.8	187.4	8.7	39.4	0.13	1.33
1791B	*m*-xylene	-	91.8	-	248.1	8.7	7.2	0.03	b
1794A	naphthalene + *m* -xylene	49.5	50.0	181.9	117.1	9.5	55.0	0.18	1.34
1794B	naphthalene	50.9	-	226.1	-	9.5	79.9	0.35	a
1797A	naphthalene + *m* -xylene	53.5	50.9	184.8	145.7	11.5	71.3	0.22	1.32
1797B	*m* -xylene	-	58.9	-	201.0	11.5	11.6	0.06	b
1800A	naphthalene + *m* -xylene	30.0	111.2	102.9	242.1	12.2	40.9	0.12	1.33
1800B	naphthalene	29.8	-	148.6	-	12.1	47.8	0.32	a
1959A	naphthalene + *m* -xylene	34.1	110.0	118.8	185.2	12.4	50.3	0.17	1.42
1959B	naphthalene	34.1		156.6	-	12.5	79.0	0.50	a
1804A	1-methylnaphthalene + *m*-xylene	38.2	125.3	152.8	214.0	12.4	123.9	0.34	1.30
1804B	1-methylnaphthalene	38.8	-	203.9	-	12.1	136.3	0.67	c
1805A	1-methylnaphthalene + *m*-xylene	66.5	66.7	227.8	115.9	12.7	155.3	0.45	1.33
1805B	1-methylnaphthalene	65.9	-	303.7	-	12.5	152.8	0.50	c
1808A	1-methylnaphthalene + *m*-xylene	32.8	129.4	122.7	193.0	11.8	81.9	0.26	1.31
1808B	1-methylnaphthalene	34.8	-	176.0	-	11.8	95.1	0.54	c
1976A	1-methylnaphthalene + *m*-xylene	36.5	120.5	161.7	215.1	10.7	137.3	0.36	1.35
1976B	1-methylnaphthalene	38.5	-	214.9	-	11.0	158.8	0.74	c
1978A	1-methylnaphthalene	25.9	-	130.9	-	11.5	112.4	0.86	1.48
1978B	1-methylnaphthalene + *m*-xylene	28.2	68.8	128.1	136.3	11.5	137.5	0.52	
1936A	2-methylnaphthalene + *m*-xylene	36.1	117.8	158.2	234.8	11.5	58.2	0.15	1.37
1936B	2-methylnaphthalene	35.5	-	213.5	-	11.4	84.2	0.39	d
1979A	2-methylnaphthalene + *m*-xylene	48.8	61.3	236.4	134.6	12.6	131.8	0.36	1.38
1979B	2-methylnaphthalene	54.5	-	301.0	-	12.5	151.9	0.50	d
1981A	2-methylnaphthalene + *m*-xylene	26.0	117.0	119.8	226.1	12.4	78.4	0.23	1.35
1981B	2-methylnaphthalene	28.2	-	160.5	-	12.4	134.8	0.84	d
1982A	2-methylnaphthalene	39.0	-	216.0	-	13.0	108.0	0.50	1.44
1982B	2-methylnaphthalene + *m*-xylene	36.9	69.2	188.5	161.6	12.9	103.5	0.30	d

[a] : Assume density for naphthalene is 1.48 g/cm^3 ; [b]: Assume density for *m*-xylene is 1.4 g/cm^3
[c] : Assume density for 1-methylnaphthalene is 1.41 g/cm^3 ; [d]; Assume density for 2-methylnaphthalene is 1.37 g/m^3.

Table 3.2 Initial experimental conditions and SOA yield for PAHs/surrogate mixtures and PAHs/*m*-xylene mixtures photooxidation under H_2O_2 condition

Run number	Compounds	Initial PAHs	Surrogate	ΔHC_ PAHs	ΔHC_ surrogate	NO (ppb)/ H_2O_2 (ppm) /CO(ppm)	ΔM_0	SOA yield	Density
		ppb	ppmC	μg/m^3	μg/m^3	ppb/ppm	μg/m^3		g/cm^3
1814A	naphthalene+surrogate	29.5	1.5	50.8	111.2	H_2O_2 1ppm +CO 50 ppm	3.7	0.07	1.35
1814B	naphthalene	29.5		132.7		H_2O_2 1ppm	73.1	0.55	a
1927A	naphthalene+surrogate	35.5	1.5	105.1	224.7	NO 11.0	24.0	0.07	1.46
1927B	naphthalene	36.8		172.1		NO 11.1	70.0	0.41	a
1932A	1-methylnaphthalene +surrogate	46.5	1.5	188.3	234.5	NO 11.4	117.8	0.28	1.39
1932B	1-methylnaphthalene	46.3		228.8		NO 11.7	166.9	0.73	b
1935A	2-methylnaphthalene +surrogate	34.9	1.5	162.7	222.3	NO 11.9	62.4	0.16	1.37
1935B	2-methylnaphthalene	34.8		176.3		NO 12.0	136.8	0.78	c

Run number	Compounds	Initial PAHs	Initial *m*-Xylene	ΔHC_ PAHs	ΔHC_ *m*-xylene	H_2O_2	ΔM_0	SOA yield	Density
		ppb	ppb	μg/m^3	μg/m^3	ppm	μg/m^3		g/cm^3
2037A	naphthalene+*m*-xylene	33.2	137.8	102.1	318.2	1	86.2	0.21	1.44
2037B	naphthalene+*m*-xylene	34.3	76.0	113.8	191.1	1	103.6	0.34	
2015B	naphthalene	25.3		125.3		1	71.9	0.57	a
2017B	1-methylnaphthalene	40.0		220.0		1	434.4	1.97	b
2018B	2-methylnaphthalene	34.6		189.7		1	136.9	0.72	
2038A	1-methylnaphthalene +*m*-xylene	33.5	119.3	131.6	337.2	1	268.2	0.57	1.42
2038B	1-methylnaphthalene +*m*-xylene	33.4	68.0	145.8	175.5	1	273.6	0.85	
2039A	2-methylnaphthalene +*m*-xylene	30.0	125.7	119.1	320.9	1	139.3	0.32	1.43
2039B	2-methylnaphthalene +*m*-xylene	30.5	74.2	128.4	202.9	1	129.9	0.39	

[a] : Assume density for naphthalene is 1.48 g/cm^3 ; [b]: Assume density for 1-methylnaphthalene is 1.41 g/cm^3 ;
[c] : Assume density for 2-methylnaphthalene is 1.37 g/m^3.

Table 3.3 Predicted organic aerosol formation from PAHs mixture with *m*-xylene

Run number	Compounds	Mixture ratio	Predicted		$Y_{predicted}/Y_{measured}$
			ΔM_{0_PAHs}	$\Delta M_{0\_m\text{-}xylene}$	
			$\mu g/m^3$	$\mu g/m^3$	
	Low NO_x condition				
1784A	naphthalene + *m*-xylene	1:3.3	36.9	30.8	1.61
1788A	naphthalene + *m*-xylene	1.5:1	71.2	13.2	1.37
1791A	naphthalene + *m*-xylene	1:3.3	30.9	22.7	1.36
1794A	naphthalene + *m*-xylene	1:1	59.6	16.1	1.37
1797A	naphthalene + *m*-xylene	1:1	66.0	21.7	1.23
1800A	naphthalene + *m*-xylene	1:4	30.2	29.7	1.47
1959A	naphthalene + *m*-xylene	1:3.3	37.7	24.7	1.24
1804A	1-methylnaphthalene + *m*-xylene	1:3.3	93.8	36.4	1.05
1805A	1-methylnaphthalene + *m*-xylene	1:1	157.7	20.5	1.15
1808A	1-methylnaphthalene + *m*-xylene	1:4	58.6	29.9	1.08
1976A	1-methylnaphthalene + *m*-xylene	1:3.3	105.0	37.3	1.04
1978B	1-methylnaphthalene + *m*-xylene	1:2	83.3	23.6	0.78
1936A	2-methylnaphthalene + *m*-xylene	1:3.3	59.8	32.9	1.59
1979A	2-methylnaphthalene + *m*-xylene	1:1	119.5	23.2	1.08
1981A	2-methylnaphthalene + *m*-xylene	1:4	51.3	34.7	1.10
1982B	2-methylnaphthalene + *m*-xylene	1:2	88.8	26.5	1.11
	H_2O_2 condition				
2037A	naphthalene + *m*-xylene	1:3.3	65.8	87.8	1.78
2037B	naphthalene + *m*-xylene	1:2	82.3	57.2	1.35
2038A	1-methylnaphthalene + *m*-xylene	1:3.3	191.4	143.4	1.25
2038B	1-methylnaphthalene + *m*-xylene	1:2	216.8	75.1	1.07
2039A	2-methylnaphthalene + *m*-xylene	1:3.3	98.1	108.7	1.48
2039B	2-methylnaphthalene + *m*-xylene	1:2	121.8	66.8	1.45

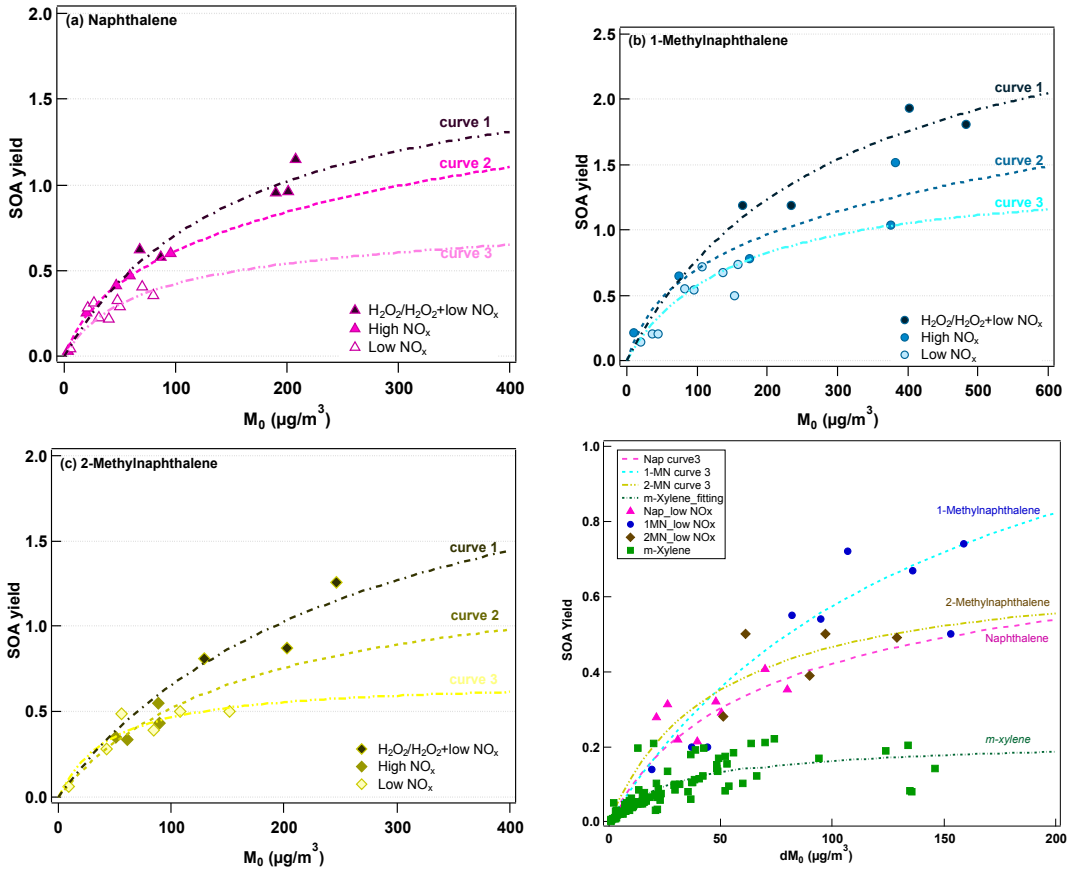

Figure 3.1 Two-product model curves for SOA yield from naphthalene, 1-methylnaphthalene and 2-methylnaphthalene photooxidation under different conditions. Curve 1 represents the H_2O_2/H_2O_2+low NO_x condition, and curve 2 represents the high NO_x (with HONO) condition, and the curve 3 represents the low NO_x condition. Right bottom panel represents the individual PAH and *m*-xylene two-product model curve under low NO_x condition.

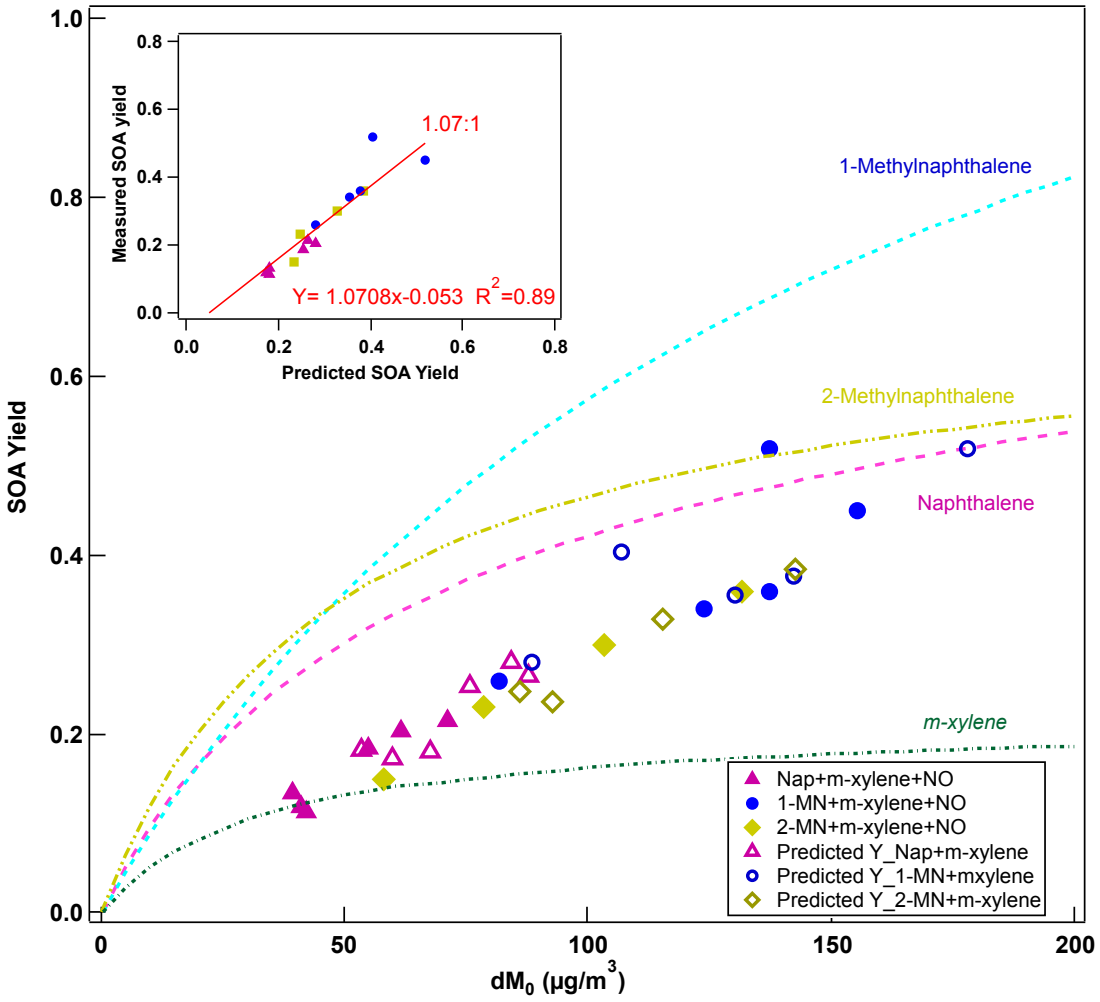

Figure 3.2 Secondary organic aerosol yields as a function of organic aerosol mass concentration (ΔM_0) for each PAHs/*m*-xylene mixture experiment under low NO_x condition. Left upper figure represents the linear relationship of measured SOA yields and predicted SOA yields.

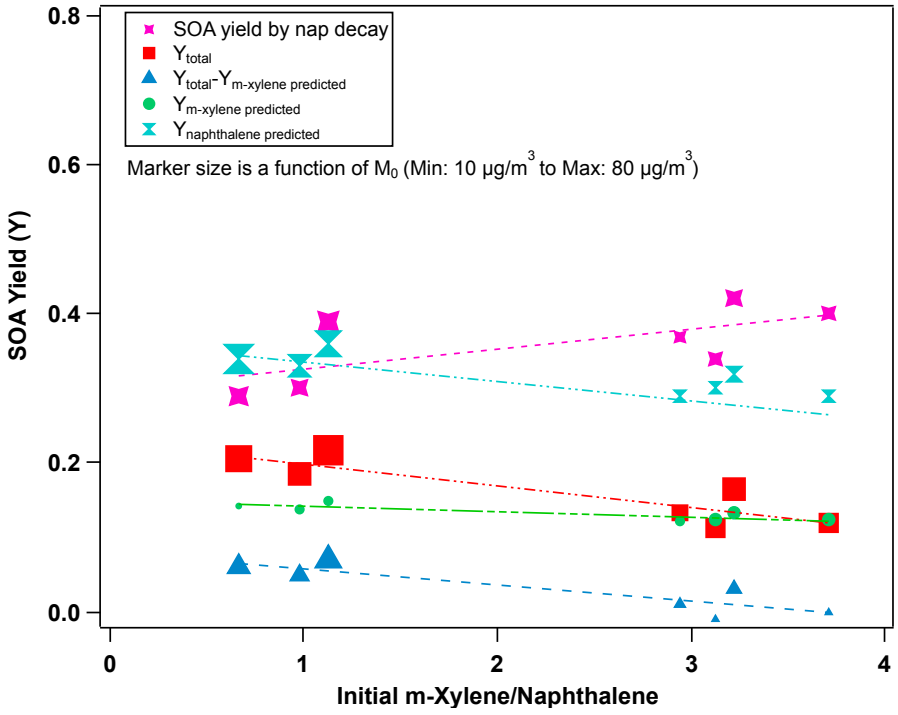

Figure 3.3 Relationship between initial *m*-xylene/naphthalene and SOA yield. Marker size is a function of M_0 (from 10 µg/m^3 to 80 µg/m^3).

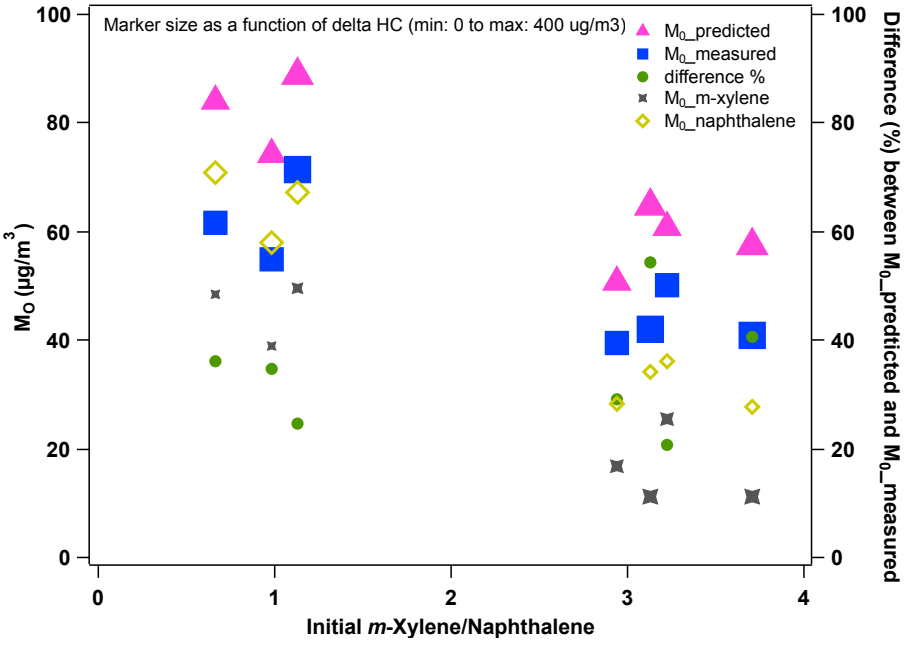

Figure 3.4 Relationship between total organic aerosol mass concentration (M_0) and initial *m*-xylene/naphthalene ratio. ($M_{0\_total\ predicted}$=$M_{0_{m\text{-}xylene\ predicted}}$+ $M_{0\ naphthalene\ predicted}$)

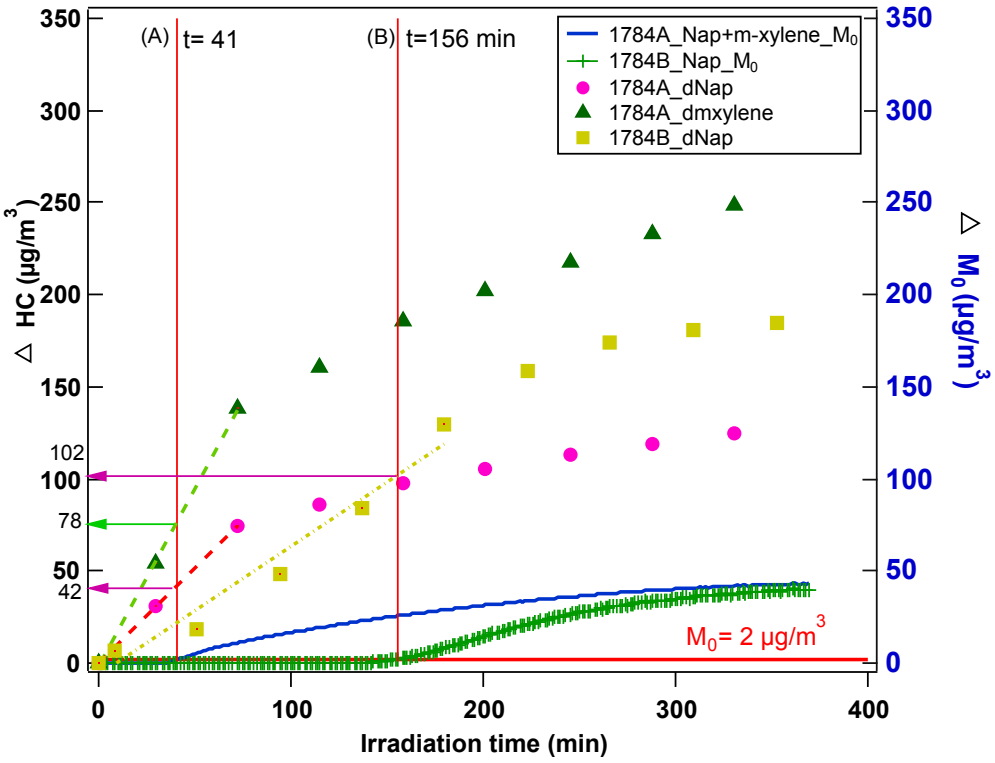

Figure 3.5 Hydrocarbon decays and organic aerosol mass loading of naphthalene and naphthalene+*m*-xylene (mixing ratio: 1:3.3) mixture photooxidation at the first nucleation of total organic aerosol formation at 2 µg/m^3.

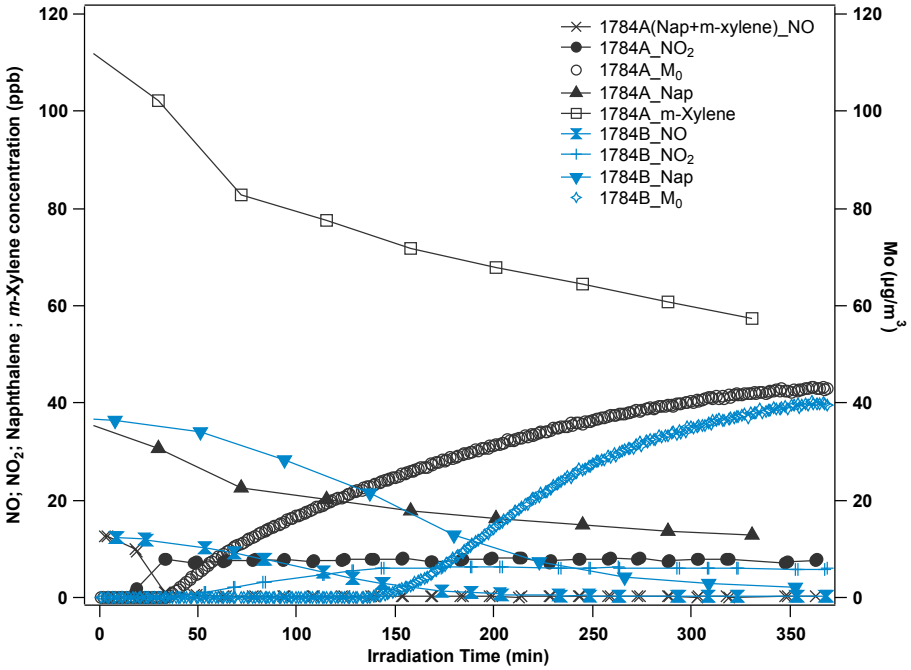

Figure 3.6 Time series of NO, NO_2, naphthalene, and total organic aerosol mass (M_0) formation during naphthalene/*m*-xylene (mixing ratio: 1:3.3, side A) photooxidation and naphthalene only (side B) under low NO_x condition.

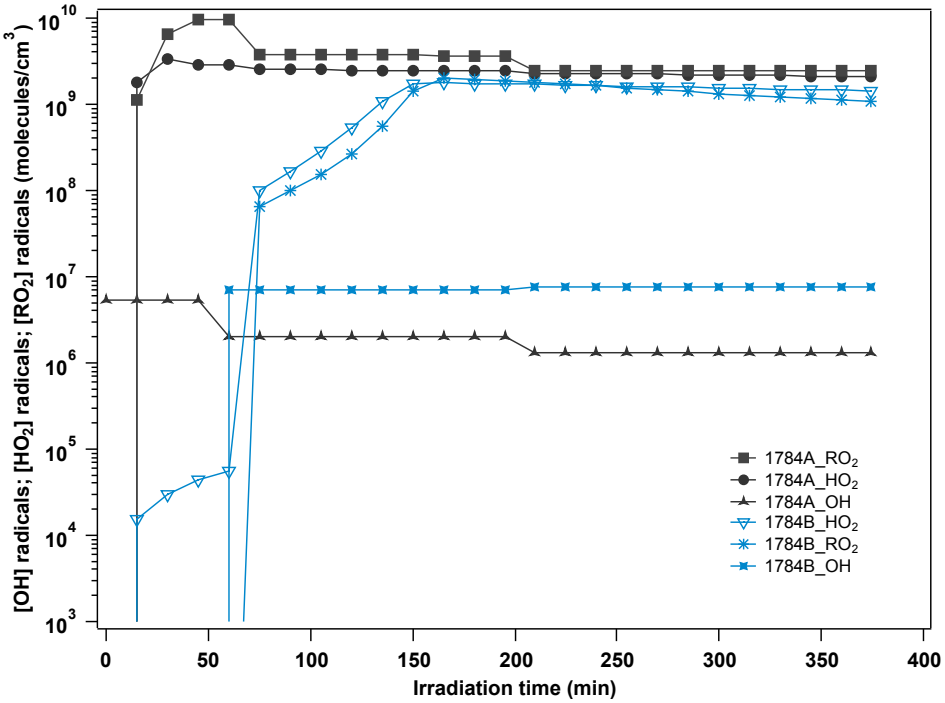

Figure 3.7 Time series of [OH] radicals, [HO_2] radicals, [RO_2] radicals during the course of experiment (run: 1784A and 1784B).

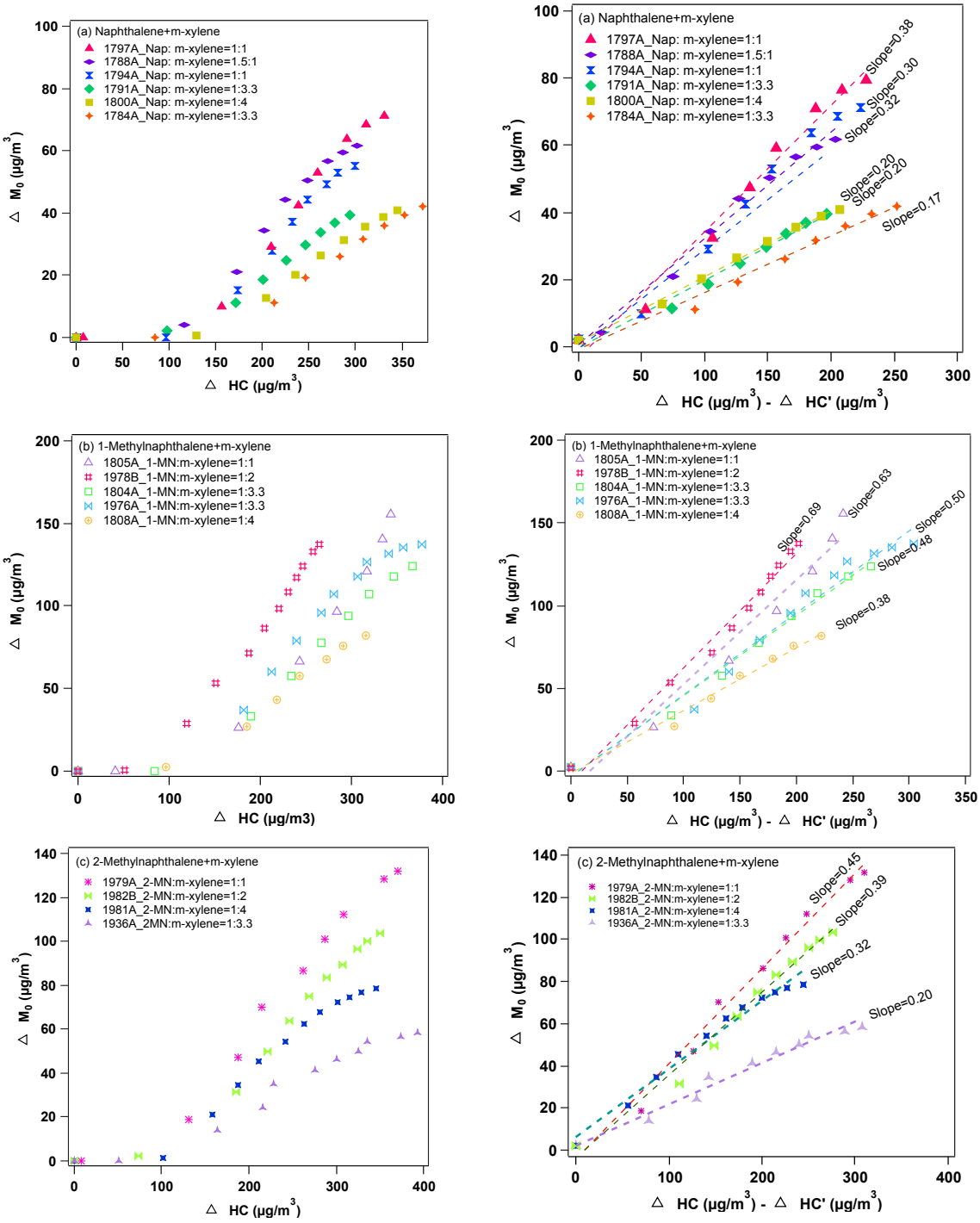

Figure 3.8 SOA mass concentration (ΔM_0) from different PAHs+*m*-xylene mixtures photooxidation experiments as a function of total hydrocarbon consumption. ΔHC' represents the first hydrocarbon decay at the initial lag phase. Right panels represent the liner relationship of ΔM_0 v.s the (ΔHC- ΔHC').

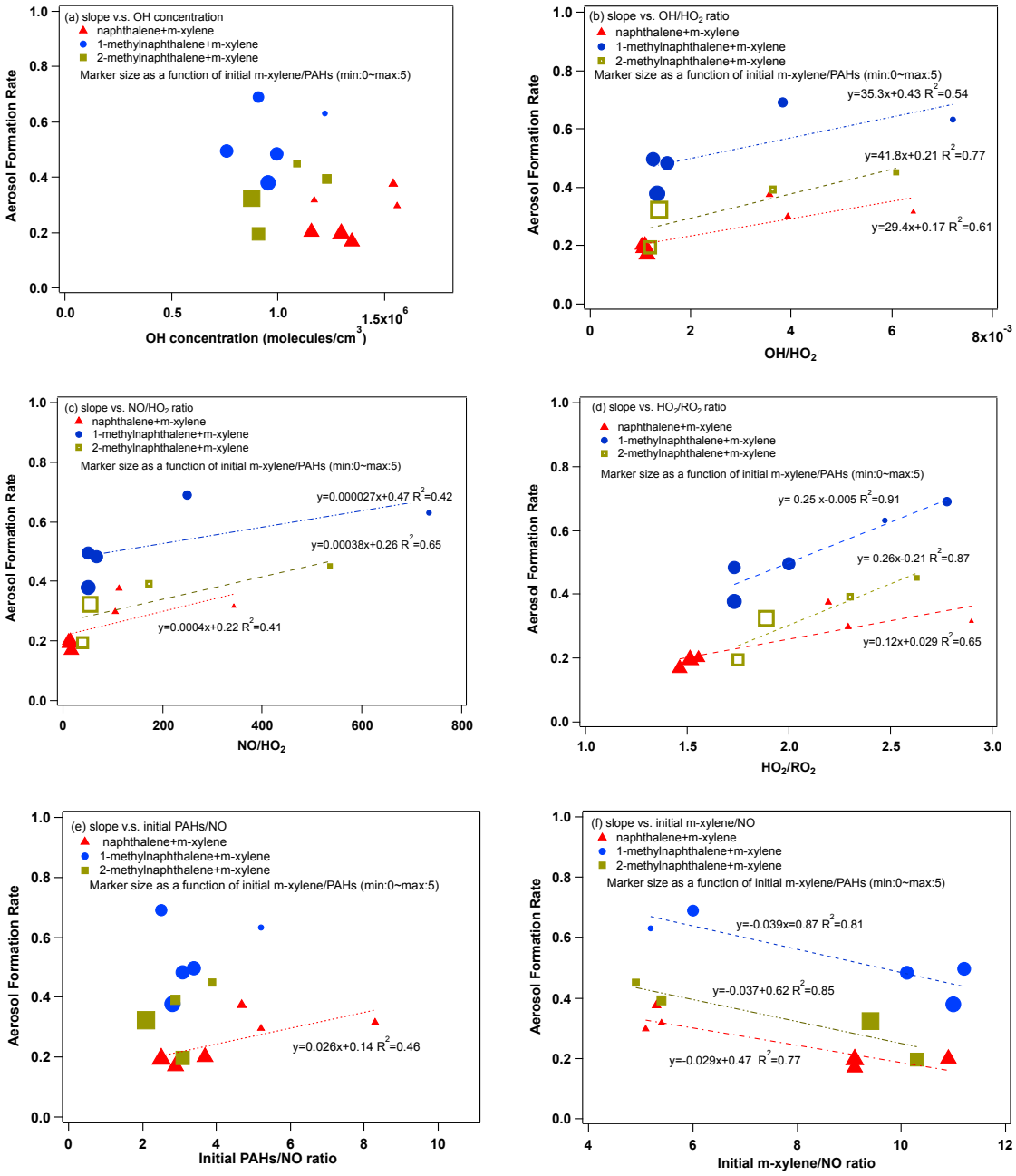

Figure 3.9 SOA formation rate of PAHs/*m*-xylene mixture hydrocarbon reacted after the lag phase versus with (a) the [OH] radical concentration; (b) [OH]/[HO_2] ratio; (c) [NO]/[HO_2] ratio; (d) [HO_2]/[RO_2] ratio; (e) initial PAHs/NO ratio; (f) initial *m*-xylene/NO ratio. Maker size as a function of initial *m*-xylene/PAHs concentration (min:0 ~max:5).

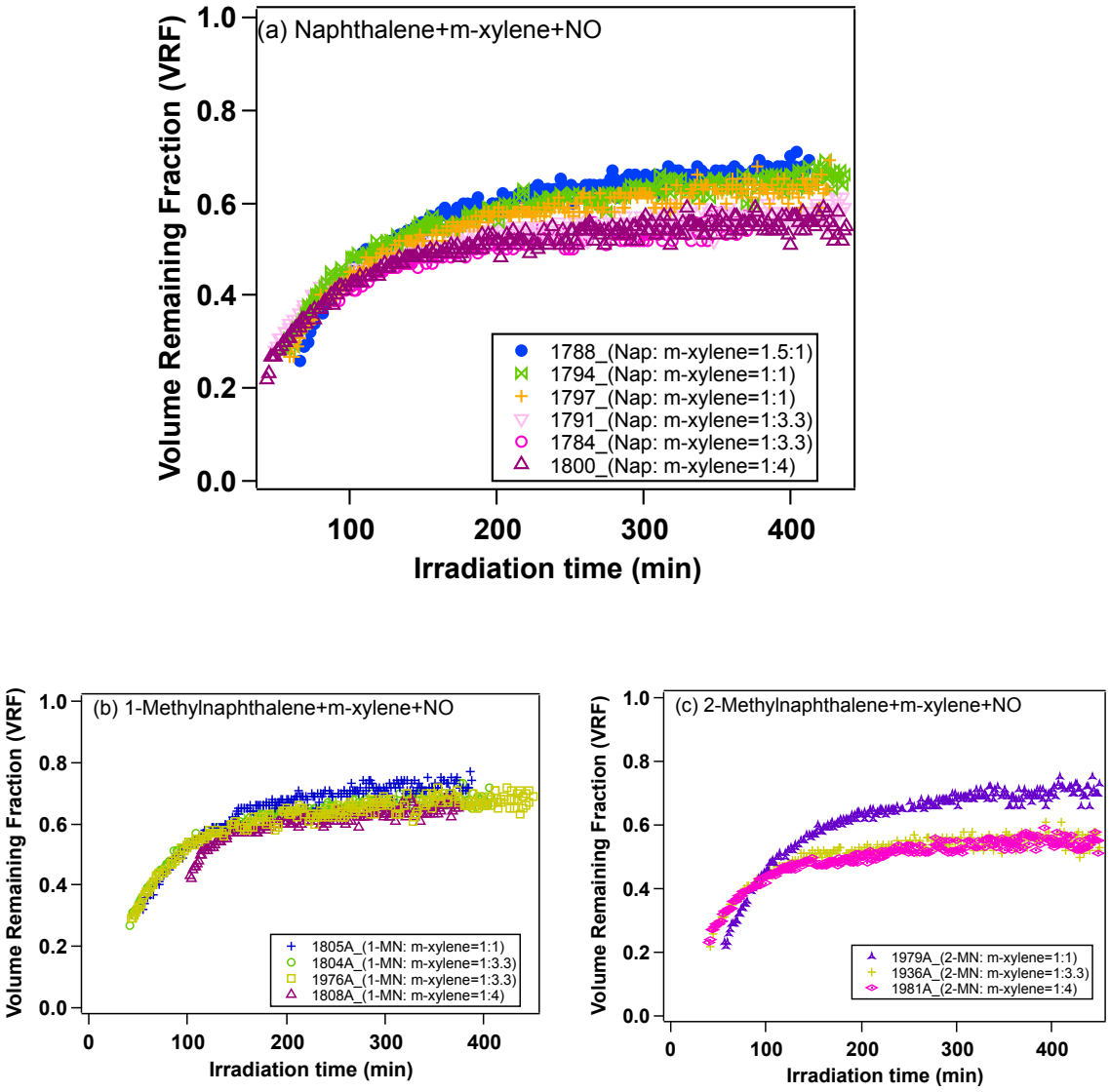

Figure 3.10 Volume remaining fraction (VRF) evolution of SOA from PAHs/*m*-xylene mixtures photooxidation during the course of experiments at different mixing ratios.

(a) EPA1936 (A) 2-methylnaphthalene+m-xylene/low NO_x

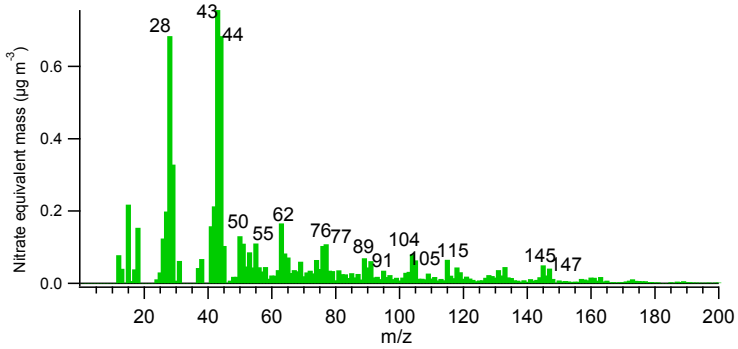

(b) EPA1193 *m*-xylene+NO_x

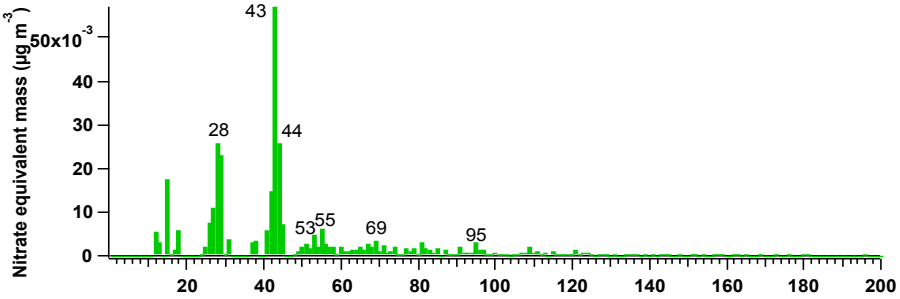

(c) EPA1982 2-methylnaphthalene/low NO_x

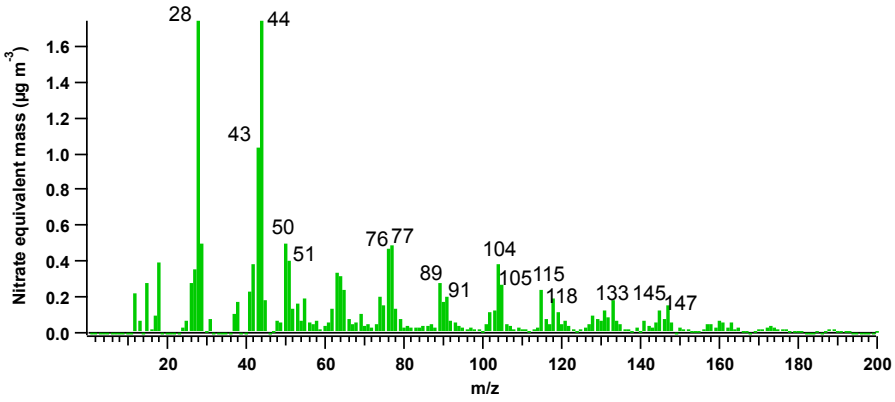

Figure 3.11 Normalized HR-ToF-AMS mass spectra distribution of three representative PAHs with *m*-xylene SOA experiments. (a) 2-methylnaphthalene/*m*-xylene low-NO_x; (b) *m*-xylene low-NO_x; (c) 2-methylnaphthalene low-NO_x.

(a)

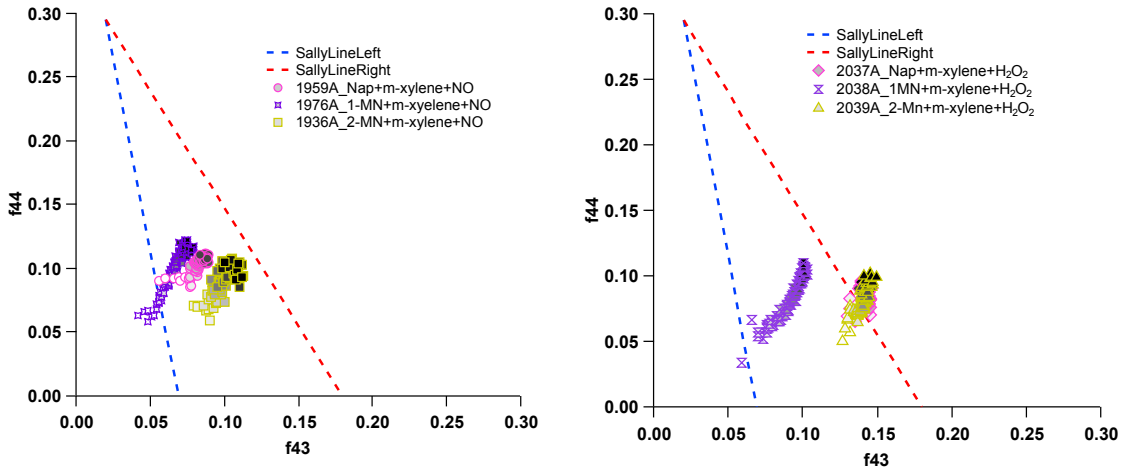

(b)

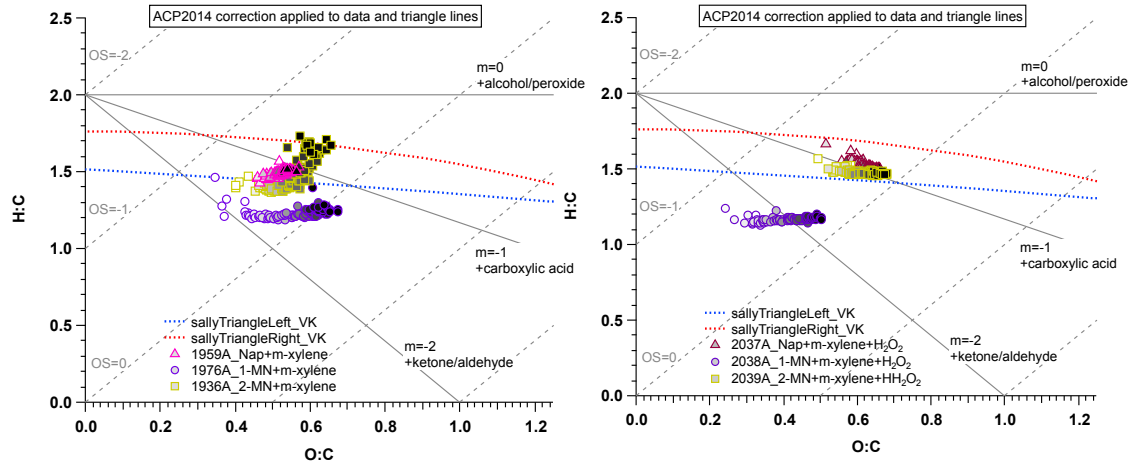

Figure 3.12 (a) Triangle plot for PAHs+*m*-xylene photooxidation under low NO_x and H_2O_2 condition. (b) Van Krevelen diagram for PAHs+*m*-xylene photooxidation under low NO_x and H_2O_2 condition. Blue dashed line and red dashed line represent the left and right line of triangle area developed by (Ng et al., 2010). ACP2014 correction is corrected by ToF-AMS analysis toolkit 1.56D and ToF-AMS HR analysis 1.15D.

3.7 Supporting Information

Table S 3.1 Two-product model curves for SOA yield from individual PAH and *m*-xylene.

Low NO_x condition	Naphthalene	1-Methylnaphthalene	2-Methlnaphthalene	*m*-Xylene
α_1	0.6281	0.9329	0.4515	0.3324
$K_{om,1}$ ($m^3/\mu g$)	0.0014	0.0065	0.0201	0.0000
α_2	0.3813	0.4495	0.2376	0.2103
$K_{om,2}$ ($m^3/\mu g$)	0.0524	0.0065	0.0225	0.0343
High NO_x condition	Naphthalene	1-Methylnaphthalene	2-Methlnaphthalene	
α_1	1.4066	0.8700	1.2056	
$K_{om,1}$ ($m^3/\mu g$)	0.0023	0.0165	0.0063	
α_2	0.4698	2.1234	0.1987	
$K_{om,2}$ ($m^3/\mu g$)	0.0301	0.0008	0.0036	
H_2O_2/H_2O_2+low NO_x condition	Naphthalene	1-Methylnaphthalene	2-Methlnaphthalene	*m*-Xylene
α_1	1.8264	3.0560	0.7110	0.5222
$K_{om,1}$ ($m^3/\mu g$)	0.0063	0.0034	0.0059	0.0061
α_2	0.0029	0.0010	1.7798	0.1038
$K_{om,2}$ ($m^3/\mu g$)	0.0015	0.4729	0.0028	0.1437

Table S 3.2 SOA yield comparison between the end of experiment and the first nucleation

Run number	Compounds	Mixture ratio (ppb:ppb)	End of experiment				First nucleation stage			
			ΔHC PAHs $\mu g/m^3$	ΔHC m-xylene $\mu g/m^3$	total ΔHC $\mu g/m^3$	SOA yield	Irradiation time when M_0>=2 $\mu g/m^3$	ΔHC PAHs $\mu g/m^3$	ΔHC m-xylene $\mu g/m^3$	SOA yield
1784 A	Nap + m-xylene	1:3.3	124.3	247.9	372.2	0.13	41	42	78	0.018
1784 B	Nap		184.7	-		0.21	156	102		0.019
1788 A	Nap+ m-xylene	1.5:1	209.3	92.2	301.5	0.23	69	69	28	0.022
1788 B	m-xylene		-	158.5		0.03	106		103	0.020
1791 A	Nap + m-xylene	1:3.3	106.8	187.4	294.2	0.16	41	37	61	0.016
1791 B	m-xylene			248.1		0.03	74		139	0.014
1794 A	Nap + m-xylene	1:1	181.9	117.1	299.0	0.21	61	39	67	0.020
1794 B	Nap		226.1	-		0.35	132		112	0.018
1797 A	Nap + m-xylene	1:1	184.8	145.7	330.5	0.24	55	60	47	0.019
1797 B	m-Xylene		-	201.0		0.06	59		126	0.015
1800 A	Nap+ m-xylene	1:4	102.9	242.1	345.1	0.14	46	46	92	0.013
1800 B	Nap		148.6	-		0.32	157	79		0.028
1804 A	1-MN+ m-xylene	1:3.3	152.8	214.0	366.8	0.37	45	47	53	0.020
1804 B	1-MN		203.9	-		0.67	104	61		0.033
1805 A	1-MN+ m-xylene	1:1	227.8	115.9	343.7	0.48	55	76	27	0.019
1805 B	1-MN		303.7	-		0.50	89	94		0.021
1808 A	1-MN+ m-xylene	1:4	122.7	193.0	315.7	0.29	40	42	51	0.021
1808 B	1-MN		176.0	-		0.54	94	68		0.029
1976 A	1-MN+ m-xylene	1:3.3	161.7	215.1	376.8	0.36	41	37	35	0.028
1976 B	1-MN		214.9	-		0.74	102	54		0.037
1978 A	1-MN		130.9	-		0.86	92	32		0.062
1978 B	1-MN + m-xylene	1:2	128.1	136.3	264.4	0.52	44	36	27	0.033
1936 A	2-MN + m-xylene	1:3.3	158.2	234.8	393.0	0.15	41	39	46	0.025
1936 B	2-MN		213.5	-		0.39	77	74		0.027
1979 A	2-MN + m-xylene	1:1	236.4	134.6	371.0	0.36	57	34	27	0.033
1979 B	2-MN		301.0	-		0.50	100	74		0.027
1981 A	2-MN+ m-xylene	1:4	119.8	226.1	345.9	0.23	40	43	59	0.019
1981 B	2-MN		160.5	-		0.84	73	64		0.031
1982 A	2-MN		216.0	-		0.50	104	82		0.024
1982 B	2-MN+ m-xylene	1:2	188.5	161.6	350.1	0.30	52	35	39	0.027

Nap: Naphthalene; 1-MN: 1-methylnaphthalene; 2-MN: 2-methylnaphthalene

Table S 3.3 Average radical concentrations and the slopes of SOA formation from hydrocarbon reacted at different initial PAHs/NO and *m*-xylene/NO conditions.

Run number	Compounds	OH ($*10^6$)	HO_2 ($*10^9$)	RO_2 ($*10^9$)	$\frac{OH}{HO_2}$ [a]	Slope [b]	$\frac{PAHs}{NO}$	$\frac{m\text{-xylene}}{NO}$	$\frac{m\text{-xylene}}{PAHs}$
		molecules/cm^3					ratio	ratio	ratio
1784 A	Nap + *m*-xylene	1.35	2.00	1.43	0.0011	0.17	2.9	9.1	3.1
1784 B	Nap	6.51				0.46	3.0		
1788 A	Nap + *m*-xylene	1.17	0.63	0.21	0.0064	0.32	8.3	5.4	0.7
1788 B	m-xylene	3.04				0.05		6.0	
1791 A	Nap + *m*-xylene	1.16	1.74	1.15	0.0010	0.20	3.7	10.9	2.9
1791 B	*m*-xylene	1.63				0.05		10.6	
1794 A	Nap + *m*-xylene	1.56	1.06	0.49	0.0039	0.30	5.2	5.1	1.0
1794 B	Nap					0.71	5.5		
1797 A	Nap + *m*-xylene	1.54	1.21	0.58	0.0036	0.38	4.7	5.3	1.1
1797 B	*m*-xylene	2.79				0.12		5.1	
1800 A	Nap + *m*-xylene	1.30	1.96	1.34	0.0011	0.20	2.5	9.1	3.7
1800 B	Nap					0.67	2.5		
1804 A	1-MN + *m*-xylene	0.995	1.62	1.02	0.0015	0.48	3.1	10.1	3.3
1804 B	1-MN					1.03	3.2		
1805 A	1-MN + *m*-xylene	1.22	0.78	0.34	0.0072	0.63	5.2	5.2	1.0
1805 B	1-MN					0.74	5.3		
1808 A	1-MN + *m*-xylene	0.95	1.63	1.02	0.0013	0.38	2.8	11.0	3.9
1808 B	1-MN					0.84	2.9		
1976 A	1-MN + *m*-xylene	0.761	1.42	0.79	0.0012	0.50	3.4	11.2	3.3
1976 B	1-MN					0.98	3.5		
1978 A	1-MN					1.09	2.3		
1978 B	1-MN + *m*-xylene	0.91	0.89	0.31	0.0038	0.69	2.5	6.0	2.4
1936 A	2-MN+ *m*-xylene	0.908	1.61	0.99	0.0012	0.20	3.1	10.3	3.3
1936 B	2-MN					0.62	3.1		
1979 A	2-MN + *m*-xylene	1.09	0.80	0.31	0.0061	0.45	3.9	4.9	1.3
1979 B	2-MN					0.66	4.4		
1981 A	2-MN + *m*-xylene	0.879	1.52	0.87	0.0014	0.32	2.1	9.4	4.5
1981 B	2-MN					1.40	2.3		
1982 A	2-MN					0.86	3.0		
1982 B	2-MN + *m*-xylene	1.23	1.12	0.51	0.0036	0.39	2.9	5.4	1.9

[a]: Average integrated (OH/HO_2) ; [b] : SOA formation growth slope.

Table S 3.4 Volume remaining fraction of each PAH/*m*-xylene mixture experiment.

Run number	Compounds	mixture ratio	VRF initial	VRF final
1784 A	naphthalene + m-xylene	1:3.3	0.39	0.56
1788 A	naphthalene + m-xylene	1.5:1	0.26	0.69
1791 A	naphthalene + m-xylene	1:3.3	0.28	0.59
1794 A	naphthalene + m-xylene	1:1	0.29	0.66
1797 A	naphthalene + m-xylene	1:1	0.27	0.63
1800 A	naphthalene + m-xylene	1:4	0.22	0.55
1804 A	1-methylnaphthalene + m-xylene	1:3.3	0.27	0.68
1805 A	1-methylnaphthalene + m-xylene	1:1	0.32	0.74
1808 A	1-methylnaphthalene + m-xylene	1:4	0.43	0.65
1976 A	1-methylnaphthalene + m-xylene	1:3.3	0.29	0.69
1936 A	2-methylnaphthalene + m-xylene	1:3.3	0.22	0.59
1979 A	2-methylnaphthalene + m-xylene	1:1	0.23	0.7
1981 A	2-methylnaphthalene + m-xylene	1:4	0.23	0.56

Table S 3.5 Evaluation of cross-reaction effect for PAHs mixture photooxidation.

run ID	**Individual /Mixture**	**f95**		**f(76+104+105)**	**$M_{0\_cross\text{-}reaction}$**		**f44**	**f43**
1193	*m*-xylene+NO	0.83%		0.17%			7.0%	14.0%
1930	*m*-xylene+NO		0.38%					
1661	naphthalene+NO	0.36%		5.42%			13.9%	2.5%
1959	naphthalene+*m*-xylene+NO	**M_0 of m/z95 (μg/m^3)**		**M_0 of (m/z 76+104+105) (μg/m^3)**			11.0%	8.5%
		0.07		1.05				
		M_0 from *m*-xylene (1)	M_0 from *m*-xylene (2)	M_0 contributed from naphthalene	(1)	(2)		
		8.77	19.07	19.31	0.65	-9.66		
		30.5%	66.4%	67.2%				
Two-product model		41.2%		58.8%				
run ID	**Individual /Mixture**	**f95**		**f(76+104+105+115+147)**	**$M_{0\_cross\text{-}reaction}$**		**f44**	**f43**
1978	1-MN+NO	0.17%		5.81%			11.4%	3.6%
1976	1-MN + *m*-xylene+NO	**M_0 of m/z95**		**M_0 of (m/z 76+104+105+115+147)**			11.4%	7.7%
		0.03		0.55				
		M_0 from *m*-xylene (1)	M_0 from *m*-xylene (2)	M_0 contributed from 1-methylnaphthalene	(1)	(2)		
		3.82	8.30	9.47	-2.92	-7.41		
		37%	80%	91%				
Two-product model		26.6%		73.4%				
run ID	**Individual /Mixture**	**f95**		**f(76+104+105+115+147)**	**$M_{0\_cross\text{-}reaction}$**		**f44**	**f43**
1982	2-MN+NO	0.15%		6.54%			12.4%	5.3%
1936	2-MN+ *m*-xylene+NO	**M_0 of m/z95**		**M_0 of (m/z 76+104+105+115+147)**			9.1%	10.6%
		0.03		0.26				
		M_0 from *m*-xylene (1)	M_0 from *m*-xylene (2)	M_0 contributed from 2-methylnaphthalene	(1)	(2)		
		4.11	8.93	3.93	-0.79	-5.61		
		56.6%	123%	54.3%				
Two-product model		35.5%		64.5%				

*m/z fraction was obtained at the end of experiment.

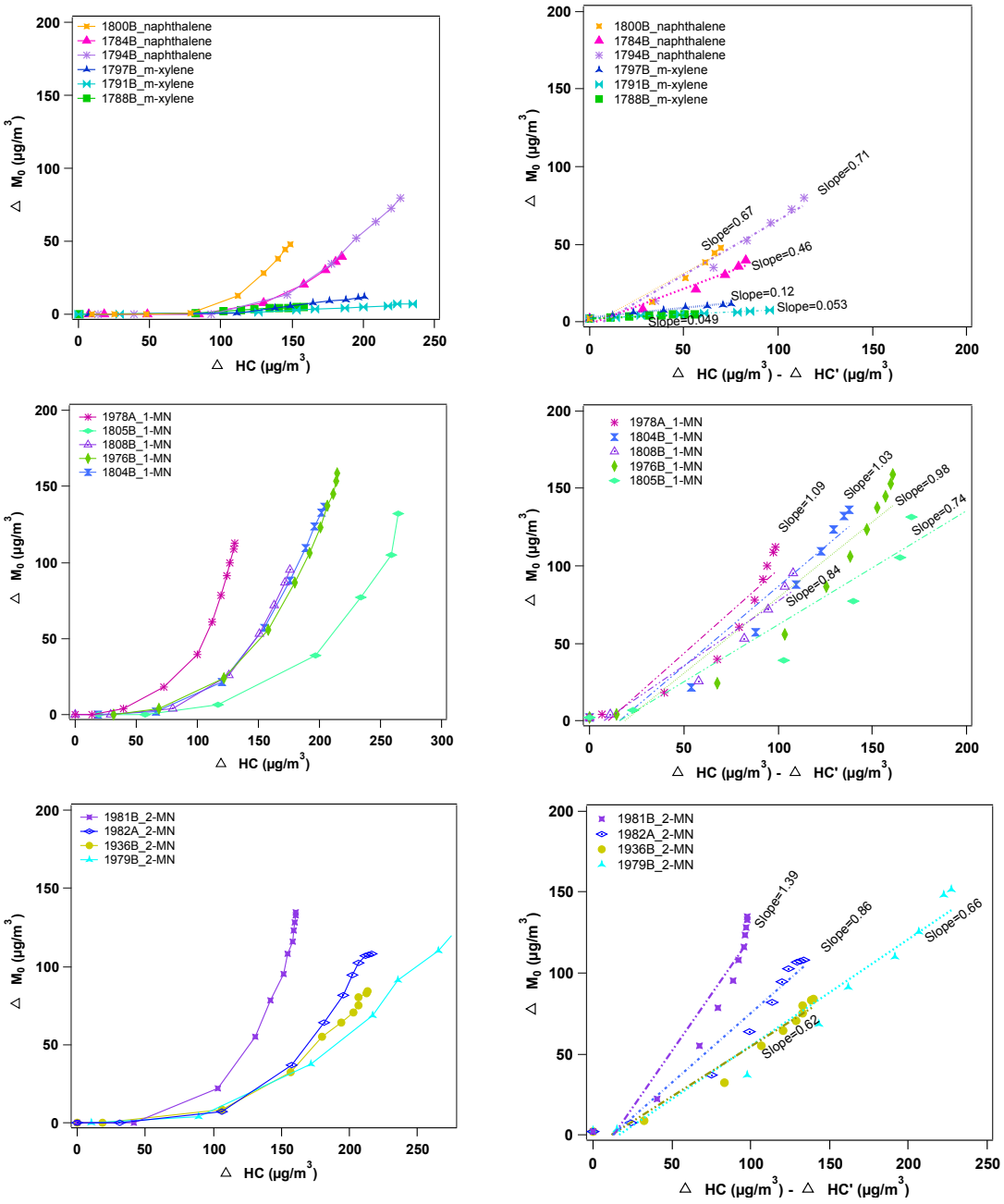

Figure S 3.1 SOA mass concentration (ΔM_0) from different individual PAH and *m*-xylene photooxidation experiments as a function of total hydrocarbon consumption. ΔHC' represents the first hydrocarbon decay at the initial lag phase. Right panels represent the liner relationship of ΔM_0 v.s the (ΔHC- ΔHC').

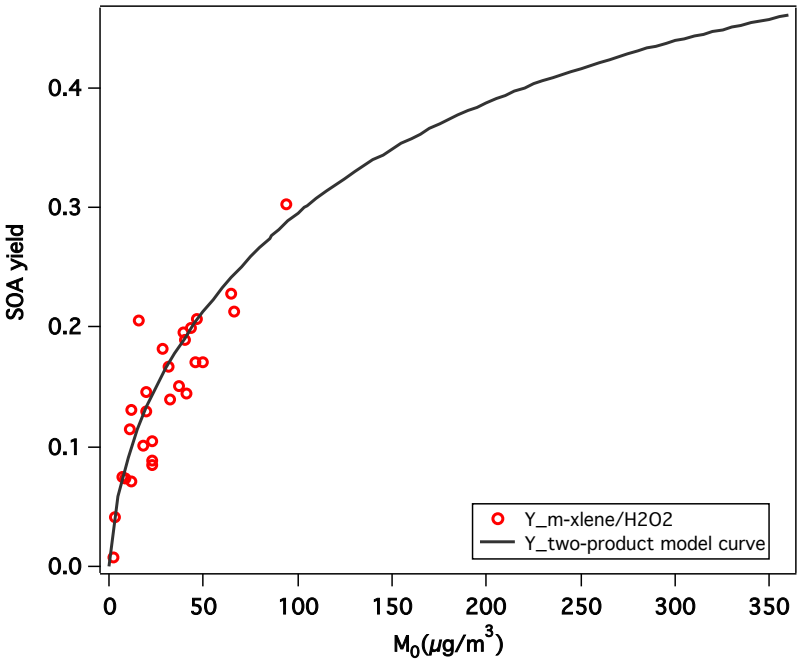

Figure S 3.2 Two-product model for *m*-xylene photooxidation under H_2O_2 condition.

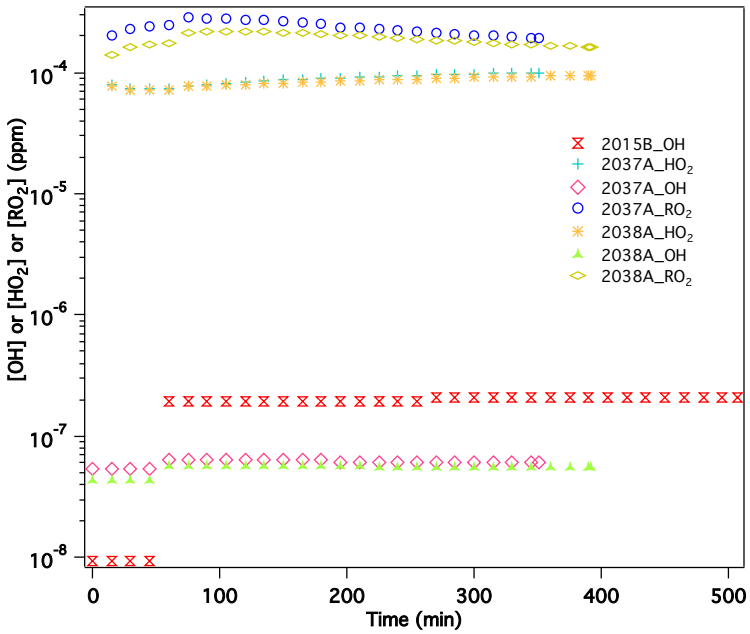

Figure S 3.3 Time series of [OH] radicals, [HO_2] radicals, and [RO_2] radicals during the course of experiments.

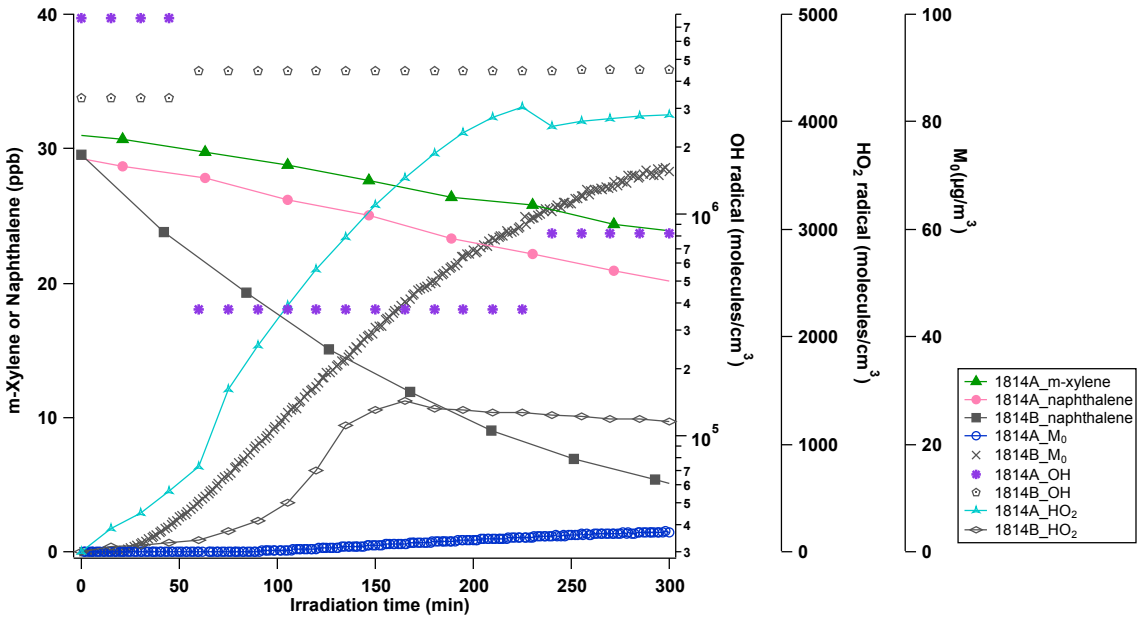

Figure S 3.4 Time series of experimental results during the course of experiment for the naphthalene with/without surrogate under CO/H_2O_2 condition (run: 1814A and 1814B).

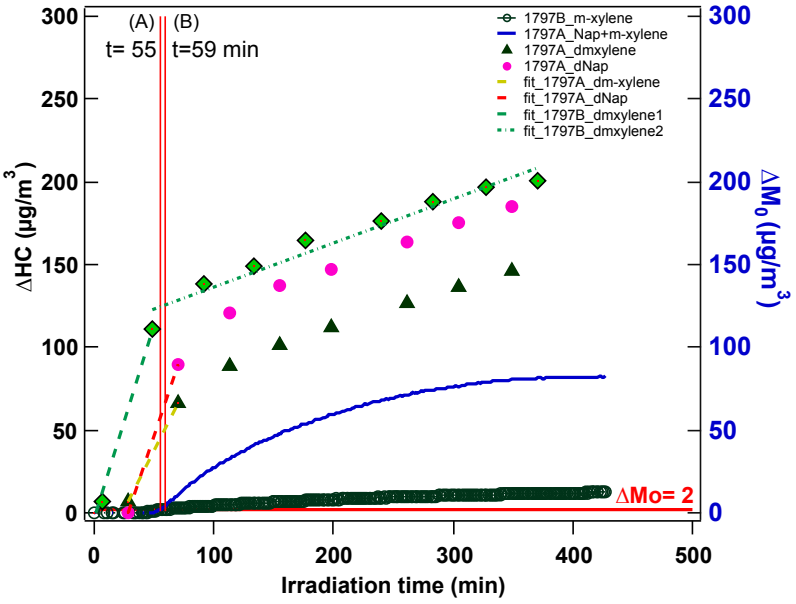

Figure S 3.5 Hydrocarbon decays and total organic aerosol mass concentration of naphthalene and naphthalene/*m*-xylene (mixing ratio: 1:1) photooxidation during the course of experiment.

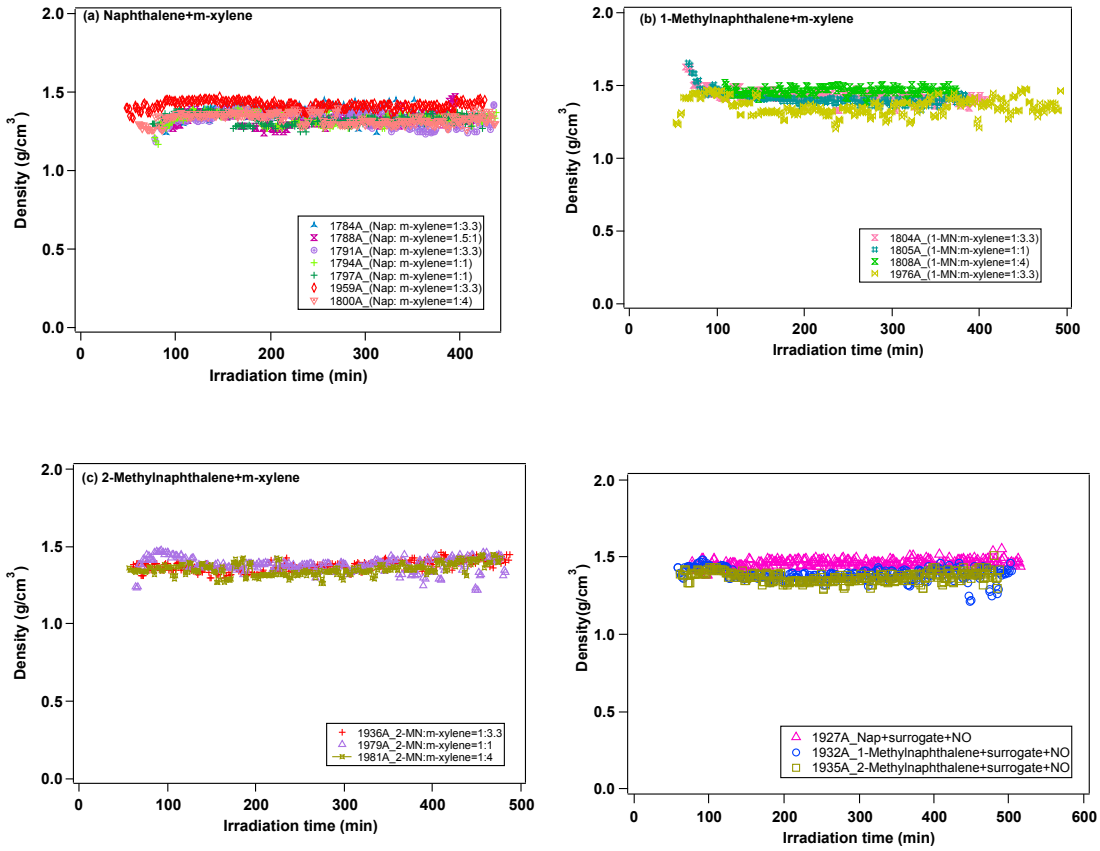

Figure S 3.6 Time series of densities from naphthalene/*m*-xylene, 1-methylnaphthalene/*m*-xylene, 2-methylnaphthalene/*m*-xylene photooxidation, and PAHs with surrogate mixtures photooxidation under low NO_x condition.

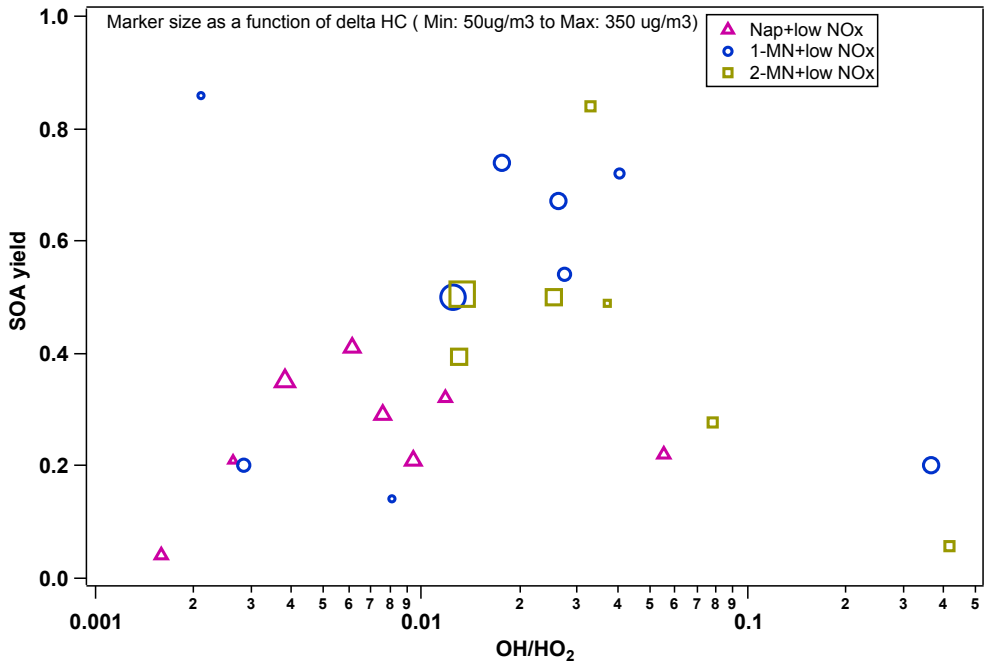

Figure S 3.7 Relationship between [OH]/[HO_2] ratio and SOA yield for individual PAH.

Chapter 4 Secondary Organic Aerosol Potential Formation from Unburned Whole Gasoline and Reference Fuels

4.1 Introduction

An 1990 amendment of U.S. EPA Clean Air Act mandated the use of reformulated gasoline in motor vehicles to reduce urban O_3 formation from gasoline usage. In 1994, Odum et al. (1997) performed chamber experiments on 12 different reformulated gasolines obtained from the Auto/Oil Air Quality Improvement Research Program (AQIRP). Their work showed that the aromatic content of the fuel dominated the SOA formation from atmospheric oxidation of these fuels

These experiments were conducted for relatively high VOC and NO_x concentrations in a VOC:NO_x regime typical of urban atmospheres. Subsequent work by (Song et al., 2005) and others (Hurley et al., 2001; Presto et al., 2005) have since demonstrated unequivocally that VOC:NO_x critically influences the atmospheric chemistry leading to SOA formation and that study of SOA formation at "low" NO_x conditions is critical towards predicting SOA formation from VOCs. Additionally, the U.S. EPA and CARB have continued to promulgate new standards for reformulated and conventional gasolines including increasing oxygenate content while reducing sulfur, olefins, and aromatics. Further, since the 1994 study the fuel additive ethanol has replaced methyl tertiary butyl ether.

The total reactive organic gas (ROG) emissions for gasoline vehicle are ~3.6 times higher than diesel vehicles (110.5 tons/day vs. 30.4 tons/day (CARB, 2011).Further, Bahreini et al. (2012) estimated during the CalNex experiment that the majority of SOA

formation precursors originate from vehicular gasoline vehicles (Bahreini et al., 2012) rather than diesel engines. Currently, reformulated gasoline contains 55~77% of saturated hydrocarbons, 9~36% aromatics, unsaturated hydrocarbons, and less than 10% ethanol (Chin and Batterman, 2012; USEPA, 2008). Harley and Kean (2004) investigated the chemical composition of gasoline and vehicle non-methane organic carbon (NMOC) emissions, which changed significantly during the 1990s, mainly due to California's reformulated gasoline program. Substantial changes include reductions in C_4-C_5 alkenes, benzene, and highly reactive aromatics such as ethyltoluene, diethylbenzene and trimethylbenzene isomers (Harley and Kean, 2004). Isopentane, *n*-butane, *n*-pentane, and MTBE/ethanol accounted for over 60% by mass of the fuel headspace (1995-2001).

Odum et al. (1997) have conducted smog chamber experiments with 12 reformulated gasolines, and using their high and low SOA yield curves and the two-product gas-particle partitioning model was able to predict the SOA formation from whole gasoline solely from fuel's aromatic components. Recently, Jathar et al. (2013) reported that SOA formation from the photooxidation of unburned gasoline is more sensitive to fuel aromatic content (Jathar et al., 2013).

Gasoline volatility is reported as Reid vapor pressure (RVP), which is the vapor pressure of the gasoline blend at 310.93K (100°F). RVP influences engine and evaporative emissions (Hajipour et al., 2014). Summer blend gasoline RVP is lower than winter blend to reduce evaporative emissions, while winter blend gasoline RVP is higher to improve engine operation.

Nowadays, biofuel renewable energy including ethanol is used to reduce carbon emissions (Kiatkittipong et al., 2008). However, the higher vapor pressure of ethanol-containing fuels can increase evaporative emissions (Da Silva et al., 2005) by increasing RVP. Further, Salvo and Geiger (2014) recently reported that ambient ozone concentrations reduced by about 20% as the share of biofuel gasoline rose from 14% to 76% in São Paulo, Brazil.

This work investigated the SOA contribution from current whole gasoline fuels necessary for improving predictions of SOA formation from gasoline fuels needed for inventory and state implement plans (SIP). This study also investigates SOA formation from Southern California summer blend and winter blend gasoline as representatives of reformulated gasoline. This study further provides the understanding of bioethanol fuel affecting SOA formation and O_3 formation. The SOA formation impact from gasoline vapor is expected to differ from previous studies as the chemical composition and our understanding of the relationship between particle formation and atmospheric reactivity has evolved.

4.2 Experimental Methodology

4.2.1 Experimental setup

All experiments were conducted in the UCR/CE-CERT environmental chamber at dry conditions (RH < 0.1%) described in detail by Carter et al. (2005). The facility has a thermally insulated enclosure (27 ± 1 ^{0}C) flushed with continuously purified air (Aadco

737 series (Cleves, Ohio)). Two 90 m^3 2 mil (54 μm) FEP Teflon® film reactors are located in the enclosure along with banks of 115 W Sylvania 350 blacklights.

Three representative Southern California 87 octane summer and winter blend gasolines were collected from commercial company A and are refined to as "summer-blend-A" and "winter- blend A" in this study. An 89 octane gasolines from commercial company B was also collected as "winter blend B". Reference fuel C, an American for Society for Testing and Materials (ASTM) standard fuel, was composed of 50 vol.% toluene and 50 vol.% isooctane. Different ethanol volume percentages were injected with reference fuel C to make E10 (10 vol.% ethanol + 90 vol.% reference fuel C), E15 (15 vol.% ethanol+85 vol.% reference fuel C), E20 (20 vol.% ethanol+ 80 vol.% reference fuel C), E25 (25 vol.% ethanol+75 vol.% reference fuel C), and E50 (50 vol.% ethanol+50 vol.% reference fuel C). Gasoline and reference fuels were injected into the chamber through a heated glass injection manifold system and flushed into the chamber with pure N_2. As needed, 50% (by wt) hydrogen peroxide (H_2O_2) was injected into a glass manifold tube in a 55°C oven and then flushed into the chamber with purified air. NO was prepared by filling a calibrated glass bulb to a known pressure of pure NO and flushed into the chamber with pure N_2.

4.2.2 Instrumentation

Gasoline chemical composition was analyzed using an Agilent 7890A gas chromatography equipped with flame ionization detectors (GC-FID). Standards used in include MA EPH Aliphatic Hydrocarbon Standard at 1000 μg/ml in hexane (RESTEK Corp.), and a certified aromatic mix (benzene, *n*-butylbenzene, *sec*-butylbenzene, *tert*-

butylbenzene, ethylbenzene, isopropylbenzene, 4-isopropryltoluene, naphthalene, *n*-propylbenzene, styrene, toluene, 1,2,4-trimethylbenzene, 1,2,5-trimethylbenzene, *o*-xylene, *m*-xylene, and *p*-xylene all at 200 μg/ml in methanol). Hydrocarbon and inert tracer (perfluorohexane) concentrations within the environmental chamber were measured using dual Agilent 6980 (Palo Alto, CA) gas chromatography (GC) equipped with flame ionization detectors (FID) (light hydrocarbons: 30 m x 0.53 mm GS-Alumina column; C_{5+} alkanes and aromatics: 30 m x 0.53 mm DB-5 column). NO and NO_y-NO were measured by a TECO chemiluminescence NO_x analyzer with an external NO_y to NO converter. Ozone was measured by a Dasibi Environmental Corp. Model 1003-AH O_3 analyzer.

Particle size distributions between 27 and 686 nm were measured by an in-house built Scanning Mobility Particle Sizers (SMPS) described in Cocker et al. (Cocker et al., 2001). Aerosol particle density was measured with an aerosol particle mass analyzer (APM, Kanomax model 3600) and SMPS in series (APM-SMPS). A detailed description of the APM-SMPS system and data procedures are described elsewhere (Malloy et al., 2009; Nakao et al., 2011). Particle volatility was monitored with a volatility tandem differential mobility analyzer (VTDMA) (Nakao et al., 2012). Volume Remaining Faction (VRF) is calculated by taking a (cubed) ratio of particle mobility diameter after the TD (D_{mf}) to initial particle size (D_{mi}), i.e., $VRF = (D_{mf}/D_{mi})^3$. The High-Resolution Time-of-Flight Aerosol Mass Spectrometer (HR-ToF-AMS) can measure the chemical composition and elementary analysis of submicron particles (Aiken et al., 2007, 2008; DeCarlo et al., 2006). Details of the HR-ToF-AMS and software analysis are described in

detail elsewhere (DeCarlo et al., 2006). Data was analyzed with ToF-AMS analysis toolkit squirrel 1.56D /PIKA 1.15D version.

4.2.3 Evaluation Methodology

4.2.3.1 SAPRC 11 model

The SAPRC 11 model was used to predict secondary particulate matter formation, O_3, gases, hydroxyl radical (OH) formation. The SAPRC-11 model is based on a kinetic (O_3) and equilibrium approach (PM). OH concentration is estimated from the decay of toluene. The current completed model version is designated as SAPRC-11 and includes the rate constant and reactions updates based on current data, SAPRC-99 chemical mechanism and chamber evaluations (Carter and Heo, 2013; Carter, 2010).

4.2.3.2 SOA yield and two-product model

SOA yield is calculated as the ratio of organic aerosol formed to hydrocarbon reacted. SOA yield versus organic aerosol mass for individual aromatic precursors is then empirically fit using the two-product model developed by (Odum et al., 1996):

$$Y = M_0 \sum_{i=1} \left(\frac{\alpha_i K_{om,i}}{1+K_{om,i} M_0} \right) \qquad \text{eq (1)}$$

where α_1 and α_2 represents the mass-based stoichiometric coefficients for the formation of two "lumped" products with gas-particle partitioning coefficients $K_{om,1}$ and $K_{om,2}$ ($m^3/\mu g$), respectively. SOA yield from gasoline mixture experiments is then measured as the ratio of the total organic aerosol reacted to total aromatic reacted.

Aromatic hydrocarbons reacted was estimated from initial concentrations of injected gasoline, it's composition, the reaction rate constant (k_{OH}) for each aromatic, and the OH radical concentration (see 4.2.3.2) as equation (2).

$$\frac{d[HC_i]}{dt} = -k_{OH,\,x_i}[OH][HC_i]$$

$$aromatic\ reacted = \sum \Delta HC_i = \Delta HC_{C6\text{-}7} + \Delta HC_{C8\text{-}9} + \Delta HC_{C10+} \qquad \text{eq (2)}$$

4.2.3.3 Volatility Basis Set (VBS)

The volatility basis set approach is similar to "two-product model" and for a given experiment is based on prescribed volatility or saturation concentration (C*) bins where C_i^* ($\mu g/m^3$) is divided into decadal bins as:

$$\{C_i^*\} = \{0.01, 0.1, 1, 10, 100, 1000, 10000, 100000\} \qquad \text{eq (3)}$$

The C* is used with organic aerosol concentration (C_{OA}) to estimate the mass fraction of "*i*" in the aerosol-phase where C_{OA} is related to the total concentration of "*i*" (C_i) as (Donahue et al., 2006, 2011) :

$$\xi_i = \left(1 + \frac{C_i^*}{C_{OA}}\right)^{-1} ;\ C_{OA} = \sum_i C_i\ \xi_i \qquad \text{eq (4)}$$

The mass-based stoichiometric coefficients (α_i) describing the mass-based production of each compound "*i*" is then determined for each fuel from experimental chamber experiments.

4.3 Results and Discussion

4.3.1 SOA yields from whole gasoline vapor

The chemical composition for each carbon category for summer-blend-A, winter-blend-A, and winter-blend-B gasoline are shown in Figure 4.1. The mass composition of each carbon number category along with reaction rate constant (k_{OH}) for each hydrocarbon species category is provided in supporting information (Table S 4.1). The major aromatic hydrocarbon is C_8 (mostly *m*-xylene).

The experimental conditions, fuel injected, initial NO concentration, ΔM_0, total aromatic hydrocarbon reacted (ΔHC_aromatic) and SOA yields from each whole gasoline photooxidation is provided (Table 4.1) for low NO_x conditions. Average OH radical concentrations ranged from 4.34×10^5 ~2.48×10^6 molecules/cm^3. SOA yields reported are based on ΔHC_aromatic and range from 2.11% to 4.82% for winter-blend-A, 2.57% to 5.58% for summer-blend-A, 1.62% to 5.66% for winter-blend-B gasoline photooxidation (Figure 4.2). All aerosol yields fall within the range of $C_{8\text{-}9}$ and C_{10+} two-product model curves developed by (Tang et al., 2015a). This observation strongly supports Odum's earlier study that identified aromatic hydrocarbons as the key class of compounds contributing to the majority of the SOA formation from the atmospheric oxidation of whole gasoline vapor (Odum et al., 1997). The slightly larger from summer-blend-A SOA yields compared to winter-blend-A SOA yields are consisted with higher aromatic content (e.g., C_8 summer: 9.9%; winter: 9.2 %). The key difference between summer-blend and winter-blend gasoline in California is based on the Reid Vapor Pressure (RVP) standard, which is designed to reduce evaporative emissions during the

summer. California's phase 3 Reformulated Gasoline (CaRFG3) regulations (2007) set the RVP limit to 7.0 psi RVP for oxygenated fuels (CARB, 2012).

Previous studies report that decreasing initial NO levels increases SOA yields for individual aromatic compounds as high initial NO reduces SOA formation (Hurley et al., 2001; Song et al., 2005; Ng et al., 2007). . However, as initial NO levels were increased for the whole gasoline experiments, SOA formation and SOA yield increased (Figure 4.2 and Figure 4.3). NO concentrations influences the lifetime and fate of alkylperoxy (RO_2) radicals and hydroperoxide (HO_2) determining the branching between (RO_2+NO) reaction and (RO_2+HO_2) reaction (Kroll and Seinfeld 2008). It has been reported that SOA begins to form only when NO concentrations decreased to sub-ppb level when RO_2+HO_2 reactions and lower volatility dominates (e.g., Hurley et al., 2001; Song et al., 2005; Kroll et al., 2006 ; Ng et al., 2007).

Previous studies have observed that larger alkanes (>C_{12}) have the opposite dependence as individual aromatics on SOA formation with SOA yields increasing with increasing NO_x levels (Lim and Ziemann 2005). The increasing SOA yields with increasing NO_x level are more consistent with observed SOA NO_x trends in this study for whole gasoline vapors photooxidation. This suggests that the gasoline major components may be decreasing the radical chemistry thereby influencing observed SOA trends from that of individual aromatic experiments. Further evaluation of the OH and HO_2 radical concentrations shows that they are relatively lower for the lower NO condition, leading to slower formation of semivolatile compounds. Two example NO and organic aerosol mass formation traces are provided (Figure S 4.1). Reacting hydrocarbons begin to form SOA

as NO decreased to sub-ppb level for the lower initial NO (9 ppb) experiment (1852A) consistent with traces from classical single aromatic hydrocarbon experiments. However, in the experiment (1937A) with the same amount of fuel injected but with higher NO (173 ppb) present after only 84% reduction of NO SOA growth starts to increase. This suggests organic nitrates ($RONO_2$) produced from RO_2+NO reaction may be contributing to SOA formation.

The influence of alkanes on aromatic mixtures was also examined by evaluating SOA from aromatic hydrocarbon mixture (C_6~C_9) a photooxidation experiment with without *n*-hexane addition (run: 2054A and 2054B, Figure S 4.2). This experiment reveals that *n*-hexane suppresses both OH radical concentration and SOA formation, leading to the SOA mass from photooxidation of aromatic hydrocarbon mixture. Hence, individual SOA experiments for aromatic species may not reflect SOA formation from these precursors leading to the possibility that offsetting effects (decreased SOA from aromatics plus additional SOA precursors in fuel) may be leading to observations that gasoline SOA formation is predicted by aromatic compounds alone.

4.3.2 Two-product model prediction

SOA yield was predicted using the stoichiometric coefficients and partitioning coefficients developed in Tang et al. (2015a) using a two product empirical fit. Yields curves were lumped into three aromatic carbon number groups ($C_{6\text{-}7}$, $C_{8\text{-}9}$, and C_{10+}).

The gasoline photooxidation experiments in this work were conducted at the same experimental conditions (NO_2 photolysis rate, dry (RH<0.1%), temperature, and without

seed aerosol) as the Tang et al. (2015a). Predicted aerosol yields for the gasoline experiments based on aromatic content alone overestimated the measured SOA formation by ~ 1.4 times (Figure 4.4, slope 1.362). The overestimate, as noted in the previous section, is likely in past due to changes in reactivity conditions due to non-aromatic species present.

Aerosol yield two-product model fits are higher for individual aromatics than in the original work by Odum et al (1997). Significant environmental impacts (lower temperature and higher light intensity) are likely the cause of the higher aerosol formation for individual aromatic species than in the Odum et al (1997) work. A slope of 0.923 (Figure 4.4) was observed by Odum et al (1997) leading to the observation that aromatics alone could be used to predict whole gasoline formation. Given that changes to gas-phase chemistry are expected as noted above, it is possible that the excellent previous agreement may have in past been due to competing experimental biases caused by challenges of a less environmentally controlled (light and temperature) use of the Odum et al (1997) high yield (C_6, C_7 aromatics) and low yield (C_{8+} aromatics) leads to underprediction of ~ 35 % (Figure 4.4) of SOA from gasoline in the current work. These differences are likely due to the much higher temperatures that the Odum et al (1997) work was conducted at (~ 40 ° C vs. 25° C).

4.3.3 Volatility basis set (VBS) evaluation for SOA yields for whole gasoline vapor

Recently, Jathar et al. (2013) reported a volatility basis set parametrization to predict SOA yield from unburned gasoline using four semivolatile SOA products with

effective saturation concentrations (C*) of 0.1, 1, 10, and 100 μg/m^3. Using these values the SOA in the current data set is underpredicted by ~ 22% (Figure S 4.3, slope 0.78). The difference is attributed to Jather et al (2013) use of SOA yields gasoline mixtures reacted at high NO_x conditions while SOA yields from this study are from whole gasoline at low NO_x conditions. The current study VBS starts with 8 products with effective saturation concentration (C*) of 0.1, 1, 10, 10^2, 10^3, 10^4, 10^5, and 10^6 μg/m^3. Measured SOA yields were fit to determine the stoichiometric mass coefficients ($\alpha_1 \sim \alpha_8$) (equation (5)):

$$Y = \frac{C_{OA}}{\Delta HC_{aromatics}} = \frac{\sum_i C_i \xi_i}{\Delta HC_{aromatics}} = \frac{\sum_i \left(1+\frac{C_i^*}{C_{OA}}\right)^{-1} \times \alpha_i \times \Delta HC_{aromatics}}{\Delta HC_{aromatics}} = \sum_i \left(1 + \frac{C_i^*}{C_{OA}}\right)^{-1} \times \alpha_i \qquad \text{eq (5)}$$

Two-products were found sufficient to describe the SOA formation from the photooxidation of whole gasoline vapor: $\alpha_3 = 0.0466$ and $\alpha_4 = 0.0474$ for the 10 and 100 μg/m^3 C* bin, respectively (Figure 4.5). Experiment 1897B, for example, winter-blend-A with total organic aerosol (C_{OA}= 39.1 μg/m^3) and reacted 748 μg/m^3 aromatic hydrocarbons and shows 80% (mass-based) of product is condensed in bin 3 (C*=10 μg/m^3) while and 28% (mass-based) of product is condensed in bin 4 (C*=100 μg/m^3) (Figure 4.5).

4.3.4 SOA yields from reference fuels

SOA yields from reference fuel (50: 50 toluene: isooctane) photooxidation under low NO_x condition range from 3.3% to 11.0%. No SOA yield is observed from individual isooctane (2,2,4-trimethylpentane) photooxidation under low NO_x and H_2O_2 (Figure 4.6

(a), Table 4.2), indicating that SOA formation from reference fuel is from toluene photooxidation. The aerosol formation from the reference fuel (irregardless of ethanol content) coincides with C_{6-7} two-product model accounting only for toluene reacted (Figure 4.6 (b)) except for the two largest fuel injections. Overall aerosol formation (based on total fuel injected) decreased with increasing ethanol. However, increasing ethanol increased ozone formation (Figure S 4.4), which could impact achievement of O_3 standard in urban area.

An ambient surrogate was introduced to this study to simulate the reactivity of South Coast air. The surrogate is comprised of n-butane, trans-2-butene, propene, ethene, m-xylene, 1,2,4-trimethylbenezene, toluene, 2-methyl-butane, methylcyclopentane, 1-pentene, 2-butanone, isoprene. SOA yield from reference fuel with surrogate photooxidation was observed to range from 5.1% to 7.7% by accounting for toluene and isooctane reacted. Even though more mixture compounds were mixed in the system, these precursors still formed similar amount of organic aerosols.

4.3.5 Volatility and density evolution

An VTDMA was used to measure the volatility of SOA from gasoline and reference fuels photooxidation during the course of experiments. Volume remaining fraction (VRF) increases from 0.21 to 0.46 for summer-blend-A, 0.22 to 0.42 for winter-blend-A, 0.22 to 0.38 for winter-blend-B fuel (Figure 4.7). SOA from summer-blend photooxidation produced lower volatility products than winter-blend gasoline consistent

with the RVP differences in the fuel specification. VRF gradually increased over the course of the experiment with slightly higher VRF for larger injections.

Density changes during the course of experiments for summer- and winter-blend gasoline, reference fuels and the different ethanol blends (Figure 4.8). Average particle density was slightly higher in winter-blend-A gasoline (ρ=1.48 g/cm^3) than summer-blend-A gasoline (ρ=1.43 g/cm^3) (Figure 4.8(a)). Pure reference fuel photooxidation produced slightly larger average density than fuels with ethanol addition (Figure 4.8(b)) with the average density decreasing for increasing ethanol content (Figure S 4.5).

4.3.6 Chemical composition properties

Previous studies have widely used Aerodyne HR-ToF-AMS for characterizing chemical composition of ambient and laboratory organic aerosol (OA) such as triangular plot of f_{44} vs. f_{43} (Ng et al. 2010; Chhabra et al. 2011), elementary analysis of atomic oxygen-to-carbon (O:C), hydrogen-to-carbon (H:C), organic mass-to-organic carbon (OM:OC) ratios (Aiken et al., 2007, 2008; Chhabra et al., 2010), and the average oxidation state of carbon ($\overline{OS}_c \approx 2\ O/C - H/C$) (Kroll et al., 2011). The HR-ToF-AMS was used in this study to investigate chemical composition of organic aerosol from gasoline and reference fuel photooxidation. The SOA mass spectra from both summer-blend-A and winter-blend-B photooxidation under the low NO_x condition shows *m*/*z* 43 and *m*/*z* 44 as the major organic aerosol fragments along with *m*/*z* 55, *m*/*z* 57, and *m*/*z* 71 fragments possibly from aromatic hydrocarbon with ethyl or propyl substituents (Sato et al., 2010; Tang et al., 2015b) (Figure 4.9 and Figure 4.10). The m/z 43 ($C_2H_3O^+$ or $C_3H_7^+$)

fragment is a marker ion of oxidized OA from nonacid oxygenated species (Ng et al., 2010) while *m*/*z* 44 (CO_2^+) is a marker ion of oxidized OA commonly from the fragmentation of carboxylic acids (Takegawa et al., 2007). Ng et al. (2010) has investigated ambient oxygenated organic aerosol (OOA) which was characterized in a "triangle region" of f_{44} versus f_{43}, and can be deconvolved into low volatility OOA (LVOOA; $f_{44} \approx 0.17 \pm 0.04$) and semi-volatile OOA (SVOOA; $f_{44} \approx 0.07 \pm 0.04$). Figure 4.11 (upper panel) shows that SOA from three representative gasolines lies on the lower side of triangle area (SVOOA) while summer-blend-A gasoline lies on the right dash line, suggesting that more non-acid oxidized OA is generated from the summer-blend-A. Jathar et al. (2013) recently reported that commercial summer-blend gasoline SOA sit in a similar region suggesting that the f_{43} and f_{44} signal of SOA from unburned gasoline was similar to that from the oxidation of toluene and *m*-xylene. However, in this work SOA from aromatic mixture sits right hand side of gasoline (higher f_{43}). To further compare with aromatic mixture and gasoline, the mass-to-charge distribution of organic aerosol from photooxidation of whole gasoline and aromatic mixtures with *n*-hexane was compared as Figure 4.12. The *m*/*z* fragment of SOA from whole gasoline and aromatic mixtures with *n*-hexane has high linear relationship with R^2=0.94, suggesting that SOA from whole gasoline exhibits similar chemical composition as SOA from aromatic hydrocarbons photooxidation. Additionally, the reference fuel SOA sits on the middle of triangle area, and it is observed that E50-blend fuel has highest f_{44} than other blends and with the increasing of ethanol percentage the f_{44} slightly increases, indicating SOA from ethanol-blend fuel leading to more products from carboxylic acids.

The Van Krevelen diagram (H:C versus O:C) was first applied to the AMS measurement by Heald et al. (2010), who observed a slope of -1 from field and laboratory organic aerosol characterizes atmospheric aging, which involves volatilization, oxidation, mixing or condensation of further products. Recently, Canagaratna et al. (2014) reported a new AMS "Improved calibration" method to reproduce O:C and H:C values 28% and 14% higher than "Aiken-Ambient" method to account for HO_2 produced from thermally dehydration and CO from decarboxylation (Chen et al., 2015). Chen et al. (2015) further revisited and corrected the elementary composition of organic aerosol from ambient and laboratory measurement noting a -0.6 slope in the Van Krevelen diagram. All the data from current study falls on the 0 to -1 slope suggesting organic aerosol functionalized by alcohol/peroxide or carboxylic acids addition.

4.4 Conclusion

This study revisited prediction of the SOA formation from whole gasoline vapor photooxidation by the two-product model and explored the SOA and O_3 formation from ethanol-blended reference fuels. The empirical two-product model overpredicted the SOA yields from reformulated whole gasoline vapors photooxidation when estimated by the SOA formation from individual aromatic hydrocarbons, suggesting that non-aromatic precursors impact the overall gas reactivity reducing the SOA formation from the aromatic precursors. Odum's (1997) low yield curve and high yield curve was applied to and found to underpredict SOA formation from reformulated gasoline in this study due to differences including higher NO_x level, precursor concentrations, and higher VOC/NO_x

condition. SOA formation was observed to increase as initial NO_x concentration increased, opposite of the trend noted by previous studies of individual aromatic compounds. This further demonstrates the above observations that alkanes or other species are influencing the system reactivity (including NO_x effects) preventing accurate estimates of aerosol formation from individual aromatic precursors.

4.5 References

Aiken, A. C., DeCarlo, P. F. and Jimenez, J. L.: Elemental analysis of organic species with electron ionization high-resolution mass spectrometry., Anal. Chem., 79(21), 8350–8, doi:10.1021/ac071150w, 2007.

Aiken, A. C., Decarlo, P. F., Kroll, J. H., Worsnop, D. R., Huffman, J. A., Docherty, K. S., Ulbrich, I. M., Mohr, C., Kimmel, J. R., Sueper, D., Sun, Y., Zhang, Q., Trimborn, A., Northway, M., Ziemann, P. J., Canagaratna, M. R., Onasch, T. B., Alfarra, M. R., Prevot, A. S. H., Dommen, J., Duplissy, J., Metzger, A., Baltensperger, U. and Jimenez, J. L.: O/C and OM/OC ratios of primary, secondary, and ambient organic aerosols with high-resolution time-of-flight aerosol mass spectrometry, Environ. Sci. Technol., 42(12), 4478–4485, doi:10.1021/es703009q, 2008.

Bahreini, R., Middlebrook, A. M., de Gouw, J. A., Warneke, C., Trainer, M., Brock, C. A., Stark, H., Brown, S. S., Dube, W. P., Gilman, J. B., Hall, K., Holloway, J. S., Kuster, W. C., Perring, A. E., Prevot, A. S. H., Schwarz, J. P., Spackman, J. R., Szidat, S., Wagner, N. L., Weber, R. J., Zotter, P. and Parrish, D. D.: Gasoline emissions dominate over diesel in formation of secondary organic aerosol mass, Geophys. Res. Lett., 39, L06805, doi:10.1029/2011GL050718, 2012.

Canagaratna, M. R., Jimenez, J. L., Kroll, J. H., Chen, Q., Kessler, S. H., Massoli, P., Hildebrandt Ruiz, L., Fortner, E., Williams, L. R., Wilson, K. R., Surratt, J. D., Donahue, N. M., Jayne, J. T. and Worsnop, D. R.: Elemental ratio measurements of organic compounds using aerosol mass spectrometry: characterization, improved calibration, and implications, Atmos. Chem. Phys. Discuss., 14(13), 19791–19835, doi:10.5194/acpd-14-19791-2014, 2014.

CARB: EMFAC 2011 Data, Calif. Air Resour. Board [online] Available from: http://www.arb.ca.gov/jpub/webapp/EMFAC2011WebApp/, 2011.

CARB: The California Reformulated Gasoline Regulations. [online] Available from: http://www.arb.ca.gov/fuels/s2250-2298-regdoc.htm#currentregs, 2012.

Carter, W. P. L.: Development of a condensed SAPRC-07 chemical mechanism, Atmos. Environ., 44(40), 5336–5345, doi:10.1016/j.atmosenv.2010.01.024, 2010.

Carter, W. P. L. and Heo, G.: Development of revised SAPRC aromatics mechanisms, Atmos. Environ., 77, 404–414, doi:10.1016/j.atmosenv.2013.05.021, 2013.

Carter, W. P. L., CockerIII, D. R., Fitz, D. R., Malkina, I. L., Bumiller, K., Sauer, C. G., Pisano, J. T., Bufalino, C. and Song, C.: A new environmental chamber for evaluation of gas-phase chemical mechanisms and secondary aerosol formation, Atmos. Environ., 39(40), 7768–7788, doi:10.1016/j.atmosenv.2005.08.040, 2005.

Chen, Q., Heald, C. L., Jimenez, J. L., Canagaratna, M. R., Zhang, Q., He, L.-Y., Huang, X.-F., Campuzano-Jost, P., Palm, B. B., Poulain, L., Kuwata, M., Martin, S. T., Abbatt, J. P. D., Lee, A. K. Y. and Liggio, J.: Elemental Composition of Organic Aerosol: The Gap Between Ambient and Laboratory Measurements, Geophys. Res. Lett., (1), n/a–n/a, doi:10.1002/2015GL063693, 2015.

Chhabra, P. S., Flagan, R. C. and Seinfeld, J. H.: Elemental analysis of chamber organic aerosol using an aerodyne high-resolution aerosol mass spectrometer, Atmos. Chem. Phys., 10(9), 4111–4131, doi:10.5194/acp-10-4111-2010, 2010.

Chhabra, P. S., Ng, N. L., Canagaratna, M. R., Corrigan, a. L., Russell, L. M., Worsnop, D. R., Flagan, R. C. and Seinfeld, J. H.: Elemental composition and oxidation of chamber organic aerosol, Atmos. Chem. Phys., 11(17), 8827–8845, doi:10.5194/acp-11-8827-2011, 2011.

Chin, J. Y. and Batterman, S. A.: VOC composition of current motor vehicle fuels and vapors, and collinearity analyses for receptor modeling, Chemosphere, 86(9), 951–958, doi:10.1016/j.chemosphere.2011.11.017, 2012.

Cocker, D. R., Flagan, R. C. and Seinfeld, J. H.: State-of-the-art chamber facility for studying atmospheric aerosol chemistry, Environ. Sci. Technol., 35(12), 2594–2601, doi:10.1021/es0019169, 2001.

DeCarlo, P. F., Kimmel, J. R., Trimborn, A., Northway, M. J., Jayne, J. T., Aiken, A. C., Gonin, M., Fuhrer, K., Horvath, T., Docherty, K. S., Worsnop, D. R. and Jimenez, J. L.: Field-deployable, high-resolution, time-of-flight aerosol mass spectrometer, Anal. Chem., 78(24), 8281–8289, doi:10.1021/ac061249n, 2006.

Donahue, N. M., Robinson, a L., Stanier, C. O. and Pandis, S. N.: Coupled partitioning, dilution, and chemical aging of semivolatile organics, Environ. Sci. Technol., 40(8), 2635–2643, doi:10.1021/es052297c, 2006.

Donahue, N. M., Epstein, S. a., Pandis, S. N. and Robinson, a. L.: A two-dimensional volatility basis set: 1. organic-aerosol mixing thermodynamics, Atmos. Chem. Phys., 11(7), 3303–3318, doi:10.5194/acp-11-3303-2011, 2011.

Hajipour, S., Satyro, M. a. and Foley, M. W.: Uncertainty analysis applied to thermodynamic models and fuel properties - Natural gas dew points and gasoline reid vapor pressures, Energy and Fuels, 28(2), 1569–1578, doi:10.1021/ef4019838, 2014.

Harley, R. A. and Kean, A. J.: Chemical Composition of Vehicle-Related Volatile Organic Compound Emissions in Central California. [online] Available from: http://www.arb.ca.gov/airways/ccos/docs/II5_0014_Aug04_fr.pdf, 2004.

Heald, C. L., Kroll, J. H., Jimenez, J. L., Docherty, K. S., DeCarlo, P. F., Aiken, a. C., Chen, Q., Martin, S. T., Farmer, D. K. and Artaxo, P.: A simplified description of the evolution of organic aerosol composition in the atmosphere, Geophys. Res. Lett., 37(L08 803), doi:10.1029/2010GL042737, 2010.

Hurley, M. D., Sokolov, O. and Wallington, T. J.: Organic aerosol formation during the atmospheric degradation of toluene, Environ. Sci. Technol., 35(7), 1358–1366, doi:10.1021/es0013733, 2001.

Jathar, S. H., Miracolo, M. a, Tkacik, D. S., Donahue, N. M., Adams, P. J. and Robinson, A. L.: Secondary organic aerosol formation from photo-oxidation of unburned fuel: experimental results and implications for aerosol formation from combustion emissions., Environ. Sci. Technol., 47(22), 12886–93, doi:10.1021/es403445q, 2013.

Kiatkittipong, W., Thipsunet, P., Goto, S., Chaisuk, C., Praserthdam, P. and Assabumrungrat, S.: Simultaneous enhancement of ethanol supplement in gasoline and its quality improvement, Fuel Process. Technol., 89(12), 1365–1370, doi:10.1016/j.fuproc.2008.06.007, 2008.

Kroll, J., Donahue, N. and Jimenez, J.: Carbon oxidation state as a metric for describing the chemistry of atmospheric organic aerosol., Nat. Chem., 3(February), 133–139, doi:10.1038/nchem.948, 2011.

Kroll, J. H. and Seinfeld, J. H.: Chemistry of secondary organic aerosol: Formation and evolution of low-volatility organics in the atmosphere, Atmos. Environ., 42(16), 3593–3624, doi:10.1016/j.atmosenv.2008.01.003, 2008.

Kroll, J. H., Ng, N. L., Murphy, S. M., Flagan, R. C. and Seinfeld, J. H.: Secondary organic aerosol formation from isoprene photooxidation., Environ. Sci. Technol., 40(6), 1869–1877, doi:10.1021/es0524301, 2006.

Lim, Y. Bin and Ziemann, P. J.: Products and mechanism of secondary organic aerosol formation from reactions of n-alkanes with OH radicals in the presence of NO_x, Environ. Sci. Technol., 39(23), 9229–9236, doi:10.1021/es051447g, 2005.

Malloy, Q. G. J., Nakao, S., Qi, L., Austin, R., Stothers, C., Hagino, H. and Cocker, D. R.: Real-Time Aerosol Density Determination Utilizing a Modified Scanning Mobility Particle Sizer—Aerosol Particle Mass Analyzer System, Aerosol Sci. Technol., 43(7), 673–678, doi:10.1080/02786820902832960, 2009.

Nakao, S., Shrivastava, M., Nguyen, A., Jung, H. and Cocker, D.: Interpretation of Secondary Organic Aerosol Formation from Diesel Exhaust Photooxidation in an Environmental Chamber, Aerosol Sci. Technol., 45(8), 964–972, doi:10.1080/02786826.2011.573510, 2011.

Nakao, S., Liu, Y., Tang, P., Chen, C.-L., Zhang, J. and Cocker III, D. R.: Chamber studies of SOA formation from aromatic hydrocarbons: observation of limited glyoxal uptake, Atmos. Chem. Phys., 12(9), 3927–3937, doi:10.5194/acp-12-3927-2012, 2012.

Ng, N. L., Kroll, J. H., Chan, a W. H., Chhabra, P. S., Flagan, R. C. and Seinfeld, J. H.: Secondary organic aerosol formation from m-xylene, toluene, and benzene, Atmos. Chem. Phys., 7(3), 3909–3922, doi:10.5194/acp-7-3909-2007, 2007.

Ng, N. L., Canagaratna, M. R., Zhang, Q., Jimenez, J. L., Tian, J., Ulbrich, I. M., Kroll, J. H., Docherty, K. S., Chhabra, P. S., Bahreini, R., Murphy, S. M., Seinfeld, J. H., Hildebrandt, L., Donahue, N. M., DeCarlo, P. F., Lanz, V. a., Prévôt, a. S. H., Dinar, E., Rudich, Y. and Worsnop, D. R.: Organic aerosol components observed in Northern Hemispheric datasets from Aerosol Mass Spectrometry, Atmos. Chem. Phys., 10(10), 4625–4641, doi:10.5194/acp-10-4625-2010, 2010.

Odum, J. R., Hoffmann, T., Bowman, F., Collins, D., Flagan, R. C. and Seinfeld, J. H.: Gas/Particle Partitioning and Secondary Organic Aerosol Yields, Environ. Sci. Technol., 30(8), 2580–2585, doi:10.1021/es950943+, 1996.

Odum, J. R., Jungkamp, T. P. W., Griffin, R. J., Forstner, H. J. L., Flagan, R. C. and Seinfeld, J. H.: Aromatics, Reformulated Gasoline, and Atmospheric Organic Aerosol Formation, Environ. Sci. Technol., 31(7), 1890–1897, doi:10.1021/es960535l, 1997.

Presto, A. A., Huff Hartz, K. E. and Donahue, N. M.: Secondary organic aerosol production from terpene ozonolysis. 2. Effect of NOx concentration, Environ. Sci. Technol., 39(18), 7046–7054, doi:10.1021/es050400s, 2005.

Salvo, A. and Geiger, F. M.: Reduction in local ozone levels in urban São Paulo due to a shift from ethanol to gasoline use, Nat. Geosci., 7(6), 450–458, doi:10.1038/NGEO2144, 2014.

Sato, K., Takami, A., Isozaki, T., Hikida, T., Shimono, A. and Imamura, T.: Mass spectrometric study of secondary organic aerosol formed from the photo-oxidation of aromatic hydrocarbons, Atmos. Environ., 44(8), 1080–1087, doi:10.1016/j.atmosenv.2009.12.013, 2010.

Da Silva, R., Cataluña, R., Menezes, E. W. De, Samios, D. and Piatnicki, C. M. S.: Effect of additives on the antiknock properties and Reid vapor pressure of gasoline, Fuel, 84(7-8), 951–959, doi:10.1016/j.fuel.2005.01.008, 2005.

Song, C., Na, K. and Cocker, D. R.: Impact of the hydrocarbon to NO_x ratio on secondary organic aerosol formation, Environ. Sci. Technol., 39(9), 3143–3149, doi:10.1021/es0493244, 2005.

Takegawa, N., Miyakawa, T., Kawamura, K. and Kondo, Y.: Contribution of Selected Dicarboxylic and ω-Oxocarboxylic Acids in Ambient Aerosol to the m/z44 Signal of an Aerodyne Aerosol Mass Spectrometer, Aerosol Sci. Technol., 41(March 2015), 418–437, doi:10.1080/02786820701203215, 2007.

Tang, P., Nakao, S., Chen, C.-L., Carter, W. and Cocker III, D. R.: Role of Alkyl Substituents on Secondary Organic Aerosol Formation from Aromatic Hydrocarbons: Part-I Aerosol Formation Potential in the Presence of NO_x., 2015a. *(In preparation)*

Tang, P., Nakao, S., Qi, L., Chen, C.-L. and Cocker III, D. R.: Role of Alkyl substituents on Secondary Organic Aerosol Formation from Aromatic Hydrocarbons: Part-II Chemical Composition., 2015b. *(In preparation)*

USEPA: SPECIATE Version 4.2, U.S. Environ. Prot. Agency [online] Available from: http://www.epa.gov/ttn/chief/software/speciate/, 2008.

4.6 Tables and Figures

Table 4.1 Experimental conditions and results of SOA formation from whole gasoline

Run number	Fuel injected	$NO_{initial}$	Average OH[a]	ΔHC (aromatics)	M_0 [b]	SOA yield[c]	Density	O_3	Predicted SOA yield	$Y_{predicted}/Y_{measured}$
	($\mu g/m^3$)	(ppb)	(molecules/cm^3)	($\mu g/m^3$)	($\mu g/m^3$)		(g/cm^3)	(ppb)		
Winter blend A										
1852 A	1928	9	4.51E+05	249	5.3	2.13%	1.46	63	1.54%	0.72
1852 B	1928	15	6.23E+05	338	7.1	2.11%		92	2.04%	0.97
1857 A	1928	32	9.25E+05	499	16.2	3.25%	1.52	160	4.13%	1.27
1857 B	1928	46	1.14E+06	521	16.5	3.17%		203	4.20%	1.32
1865 A	1928	45	1.18E+06	552	24.9	4.52%	1.44	197	5.65%	1.25
1865 B	1928	104	1.80E+06	735	34.6	4.70%		342	7.27%	1.55
1897 A	1928	100	1.86E+06	804	39.1	4.86%	1.48	344	7.84%	1.62
1897 B	1928	68	1.55E+06	748	35.0	4.68%		268	7.27%	1.55
1937 A	1928	115	1.92E+06	820	39.6	4.82%	1.48	324	7.92%	1.64
1937B	1928	173	2.48E+06	913	41.0	4.49%		406	8.28%	1.85
Summer blend A										
1918 B	2025	23	7.52E+05	464	16.7	3.59%		126	4.15%	1.16
1920 A	2025	92	1.52E+06	621	30.8	4.95%	1.44	312	6.55%	1.32
1920 B	2025	45	9.60E+05	473	21.5	4.54%		195	5.00%	1.10
1921 A	2025	61	1.21E+06	598	33.4	5.58%	1.44	234	6.82%	1.22
1921 B	2025	11	4.34E+05	285	7.9	2.77%		75	2.20%	0.79
2046A	2025	55	1.64E+06	597	15.3	2.57%	1.40	200	4.00%	1.56
2046 B	2025	55	1.43E+06	708	19.2	2.72%	1.40	212	4.85%	1.79
Winter blend B										
1856 A	1693	9	6.06E+05	296	4.8	1.62%	1.43	62	1.57%	0.97
1856 B	2098	23	8.37E+05	366	9.9	2.79%		132	3.03%	1.12
1862 A	2227	27	7.82E+05	372	11.6	3.10%	1.47[e]	141	3.39%	1.09
1862 B	2774	41	1.08E+06	476	17.9	3.76%		192	4.88%	1.30
1870 A	2861	61	1.53E+06	487	14.9	3.06%	1.50	225	4.26%	1.39
1875A	2860	55	1.27E+06	492	20.1	4.09%	1.49	220	5.38%	1.32
1875B	3346	107	1.73E+06	584	23.9	4.09%		336	6.20%	1.52
1904A	3102	71	1.39E+06	538	28.2	5.24%	1.48	293	6.81%	1.30
1904B	3117	79	1.48E+06	543	30.7	5.66%		315	7.20%	1.27
Mixture compounds[d]	HCi	$NO_{initial}$	Average OH[a]	ΔHC (aromatics)	M_0 [b]	SOA yield[c]	Density	O_3	Predicted SOA yield	$Y_{predicted}/Y_{measured}$
	($\mu g/m^3$)	(ppb)	(molecules/cm^3)	($\mu g/m^3$)	($\mu g/m^3$)		(g/cm^3)	(ppb)		
2054A	1156	21	1.14E+06	437	30.6	7.01%	1.44	79	8.38%	1.20
2054B	1157+ n-hexane 384	21	8.76E+05	328	17.2	5.25%		84	5.73%	1.09

a: Hydroxyl radical concentration is predicted by SAPRC11 model.

b: Organic aerosol mass concentration (M_0) is obtained by PM volume wall-loss corrected concentration multiplies average density.

c: SOA yield is the ratio of M_0 divided by ΔHC (aromatics).

d: Mixture compounds include 12% benzene, 20% toluene, 61% *m*-xylene, and 7% 1,2,4-trimethylbenzene.

e: Assume average density is the average of winter blend B SOA densities.

Table 4.2 Experimental conditions and results of SOA formation from reference fuels

Run number	Fuel	Initial toluene (ppb)	Initial isooctane (ppb)	ΔHC_ toluene μg/m³	ΔHC_ isooctane μg/m³	ΔHC μg/m³	NO ppb	H_2O_2 ppm	ΔM_0 μg/m³	SOA yield	SOA yield/ by toluene	Density g/cm³	O_3 ppb
1884A	Reference fuel	446.2	291.1	482.9	256.8	739.7	55.6		56.4	7.6%	11.7%	1.54	187
1884B	Reference fuel+E10	411.1	262.1	505.9	271.2	777.1	55.4		38.6	5.0%	7.6%		195
1890A	Reference fuel	154.1	105.8	247.1	137.6	384.8	57.9		42.2	11.0%	17.1%	1.54	195
1890B	Reference fuel+E10	160.9	109.2	274.9	155.6	430.5	57.0		42.0	9.8%	15.3%		202
1953A	Reference fuel	189.9	123.9	284.0	151.5	435.5	55.4		32.9	7.6%	11.6%	1.49	157
1953B	Reference fuel+E15	130.0	84.5	201.2	108.4	309.5	55.1		21.8	7.0%	10.8%		165
1954A	Reference fuel+E15	141.3	92.7	188.9	101.3	290.1	25.4		19.1	6.6%	10.1%	1.48	122
1954B	Reference fuel	174.9	113.8	233.0	124.9	357.9	25.6		23.1	6.5%	9.9%		115
1955A	Reference fuel+E20	125.4	80.6	137.0	72.0	209.0	10.2		11.2	5.4%	8.2%	1.47	91
1955B	Reference fuel	124.3	80.3	140.9	76.0	216.9	10.2		11.0	5.1%	7.8%		77
1956A	Reference fuel+E25	124.4	82.4	159.9	86.5	246.3	23.3		13.9	5.6%	8.7%	1.47	121
1956B	Reference fuel	124.7	82.7	184.2	100.1	284.3	23.3		17.6	6.2%	9.5%		108
1958A	Reference fuel+E50	145.6	98.6	99.0	55.0	154.0	22.5		3.4	2.2%	3.4%	1.42	124
1958B	E100						22.4		0	0.0%	0.0%		88
1971A	Reference fuel+E10	149.2	101.7	184.1	99.7	283.8	22.6		9.5	3.3%	5.2%	1.49	131
1971B	Isooctane + Ethanol 30ul +H_2O_2		553.2		722.2	722.2	22.3	2	0.01	0.0%			206
1966A	Isooctane + NO +1ppm H_2O_2 middle		575.8		615.6	615.6	63.2	1	0.03	0.0%			340
1966B	Isooctane + NO+1ppm H_2O_2 middle		577.0		473.4	473.4	22.5	1	0.01	0.0%			171
1997A	Reference fuel+surrogate 1ppmC	178.2	54.5	180.1	43.4	223.5	55.0		12.5	5.6%	6.9%	1.46	209
1997B	Reference fuel+surrogate 1ppmC	160.3	54.7	252.3	71.6	323.9	54.7		24.8	7.7%	9.8%		175
2002A	Reference fuel+surrogate 2ppmC	195.0	109.1	158.9	67.8	226.7	55.8		11.3	5.0%	7.1%	1.43	201
2002B	Reference fuel+surrogate 2ppmC	161.6	109.9	257.5	145.1	402.7	55.9		20.4	5.1%	7.9%		171

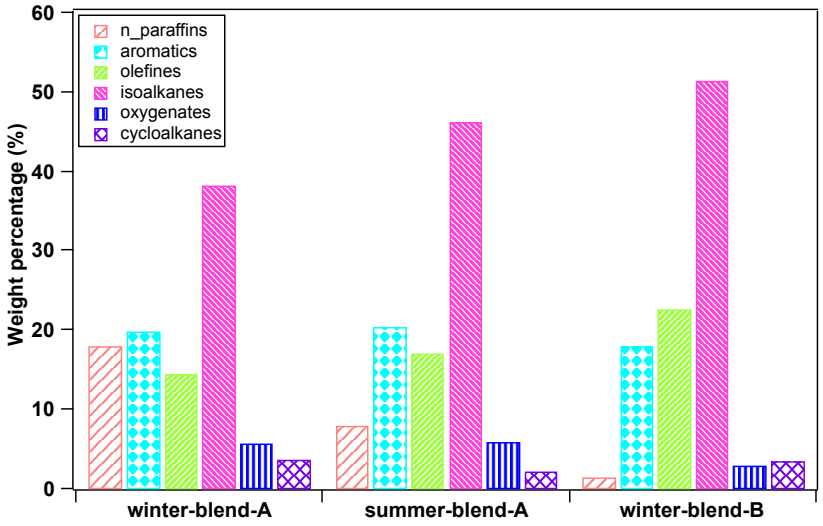

Figure 4.1 Chemical compositions of winter-blend-A, summer-blend-A, and winter-blend-B gasoline.

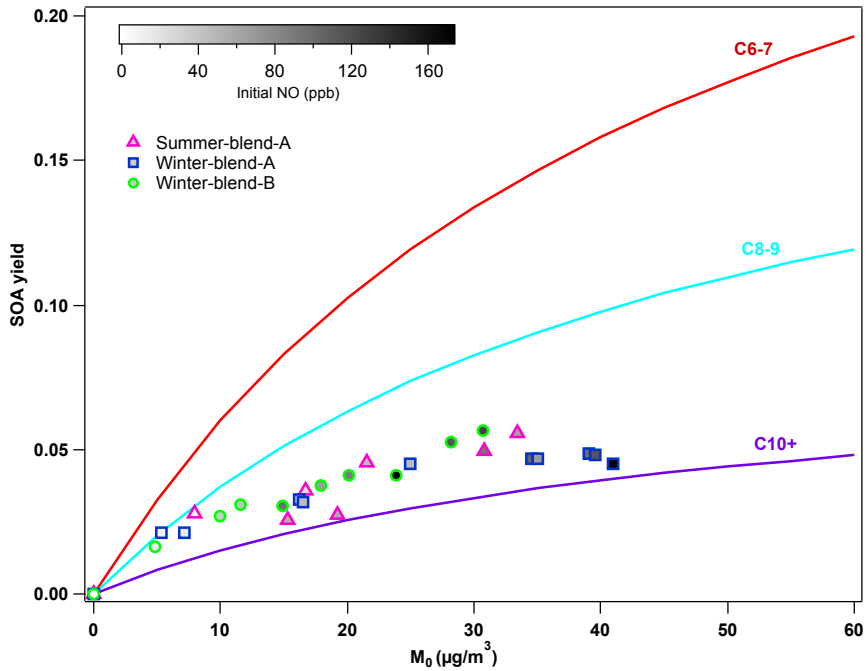

Figure 4.2 SOA yields from different California whole gasoline vapor photooxidation. One-product model SOA yield curves for aromatics $C_{6\text{-}7}$ curve, $C_{8\text{-}9}$ curve, and C_{10+} curve were developed by Tang et al. (2015a). Stoichiometric coefficient α_1 and partitioning coefficient K_{om1} is 0.345, 0.021 for $C_{6\text{-}7}$ curve, 0.214 and 0.021 for $C_{8\text{-}9}$, 0.086 and 0.021 for C_{10+} curve, respectively.

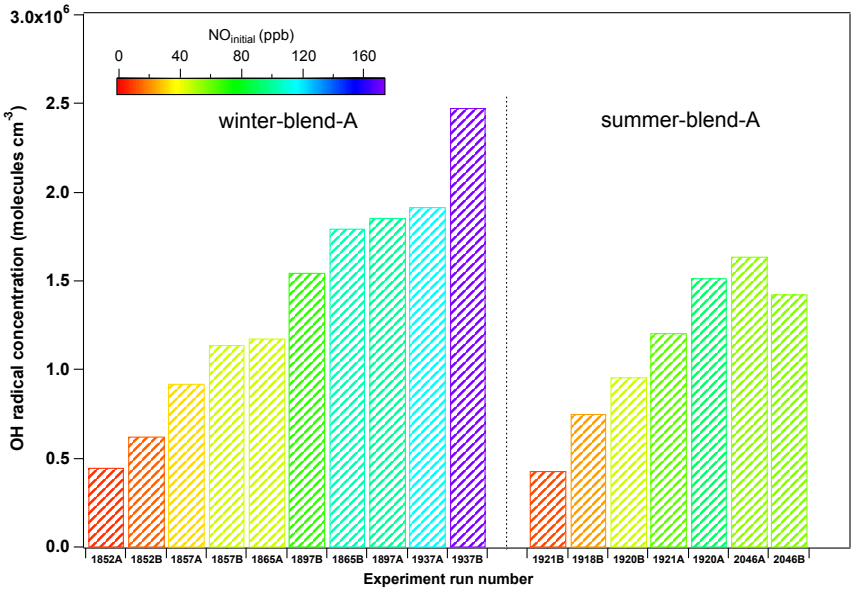

Figure 4.3 Average OH radical concentration with initial NO concentration for winter-blend-A and summer-blend-A photooxidation. Each column represents each experiment and colors by initial NO concentration.

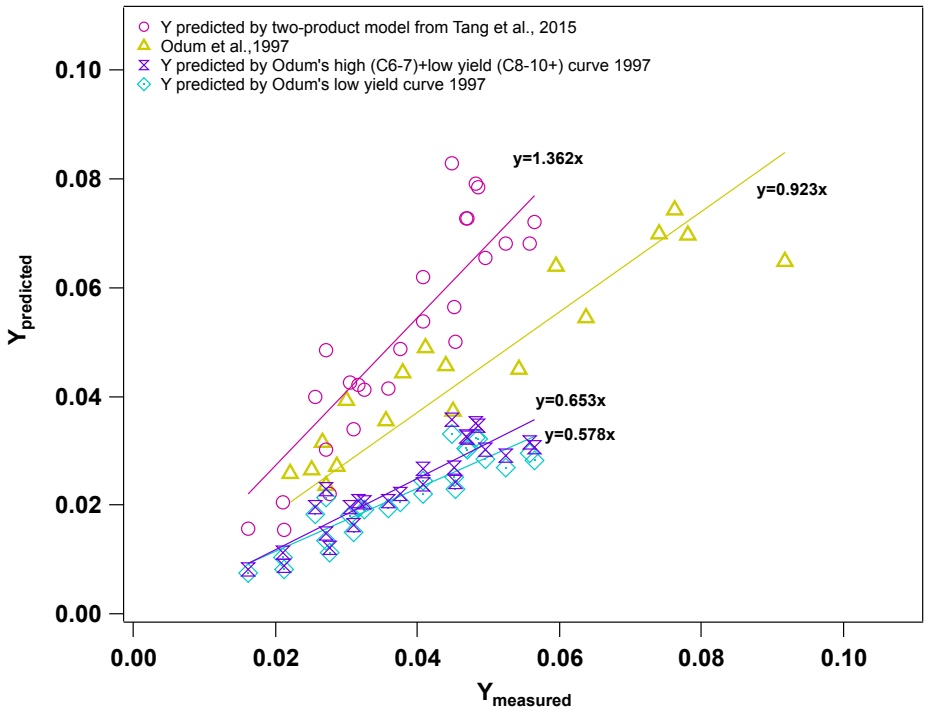

Figure 4.4 Relationship between predicted SOA yields and measured SOA yields by two-product model curves.

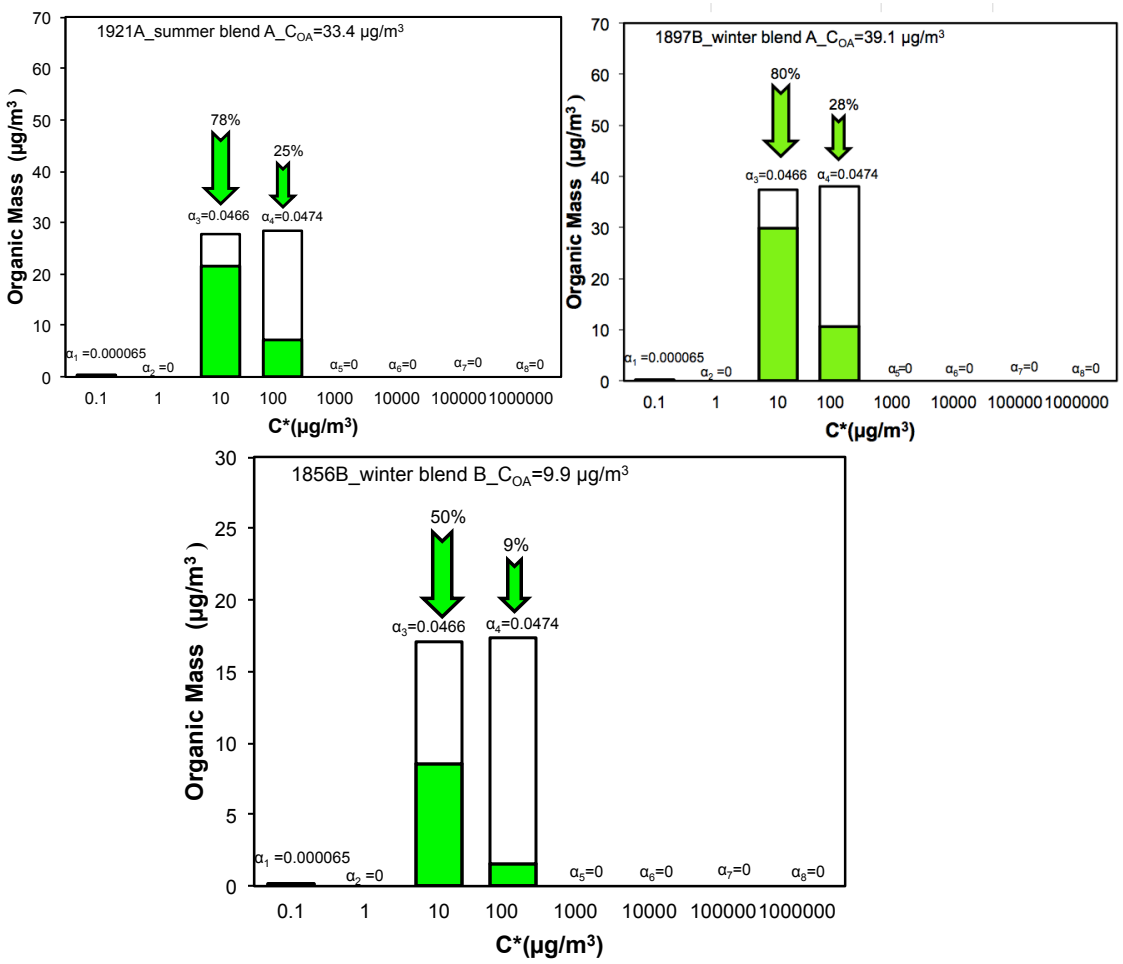

Figure 4.5 Volatility basis set (VBS) distribution from three representative whole gasoline photooxidation experiments.

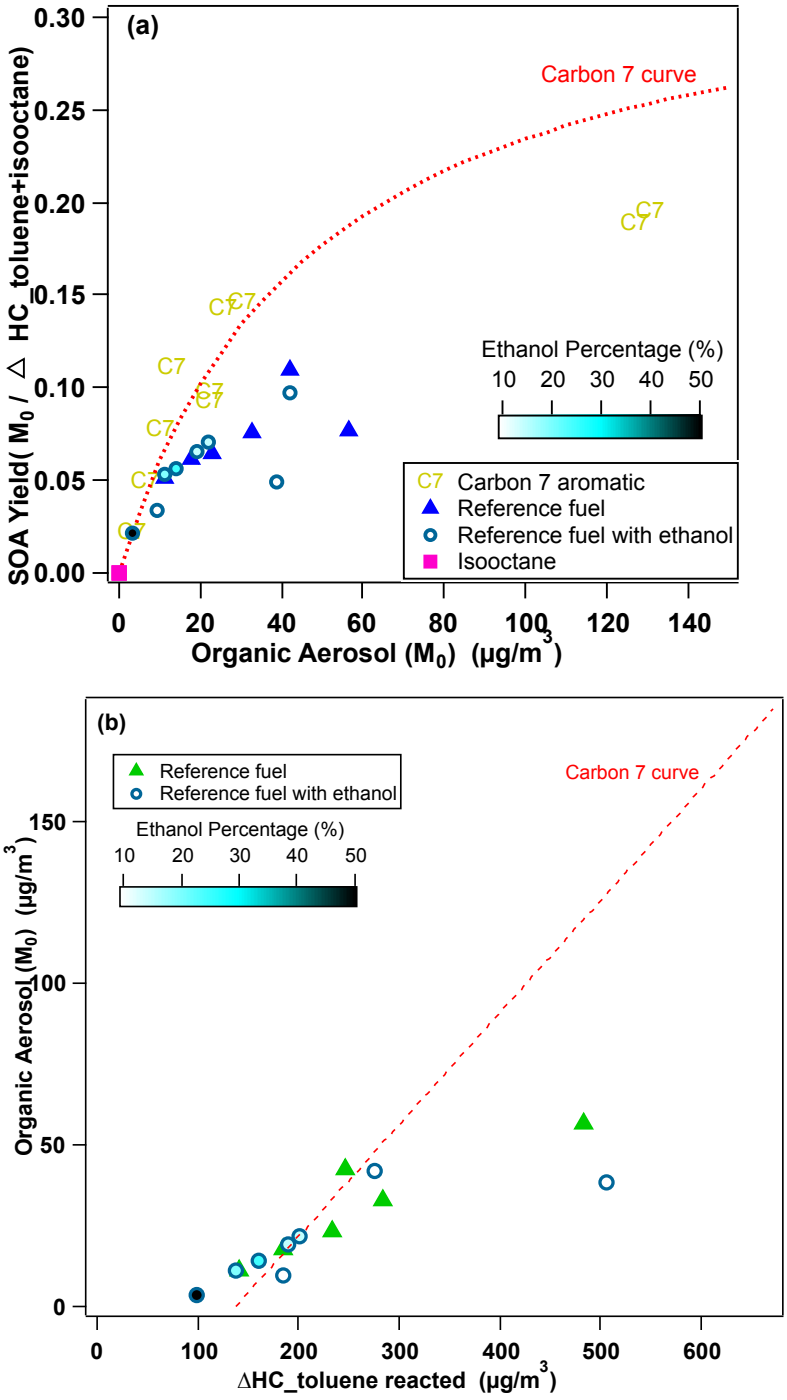

Figure 4.6 SOA yields and total aerosol formation (M_0) from reference fuel C and different ethanol blends photooxidation under low NO_x condition. (a) SOA yield is calculated by M_0 /$\Delta HC_{(toluene\ +isooctane)}$. (b) M_0 vs. $\Delta HC_{(toluene)}$. Carbon 7 curve is obtained from Tang et al. (2015a).

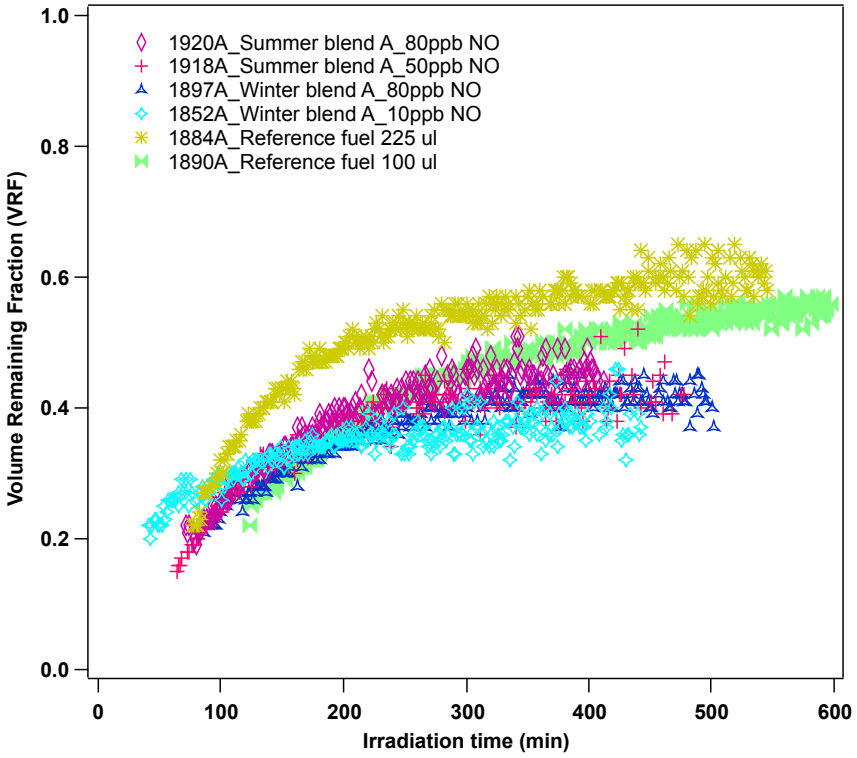

Figure 4.7 Time series of volume remaining fraction (VRF) of SOA of photooxidations from whole gasoline vapor and reference fuels at low NO_x condition.

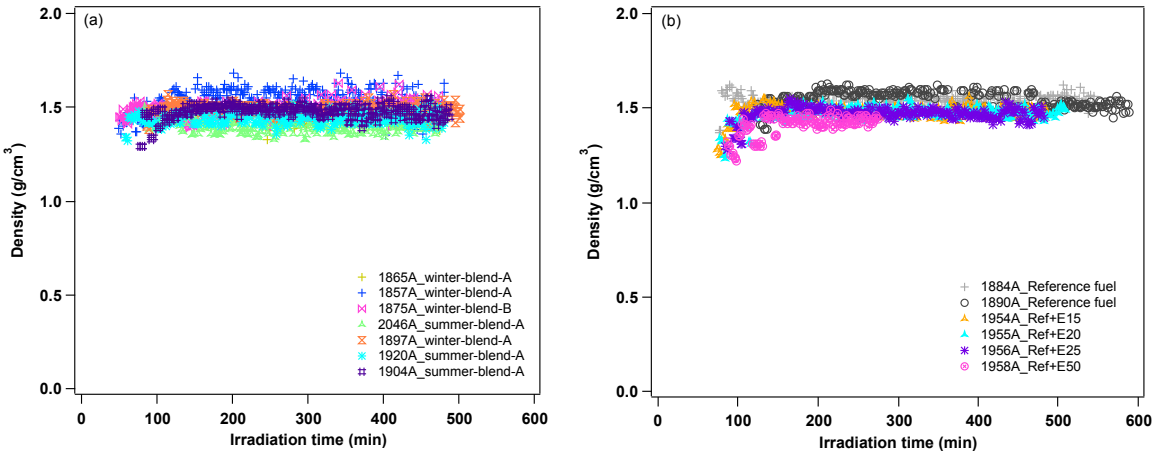

Figure 4.8. Time series of density of SOA formation from (a) winter- and summer-blend gasoline and (b) reference fuels with different ethanol blends photooxidation under low NO_x condition.

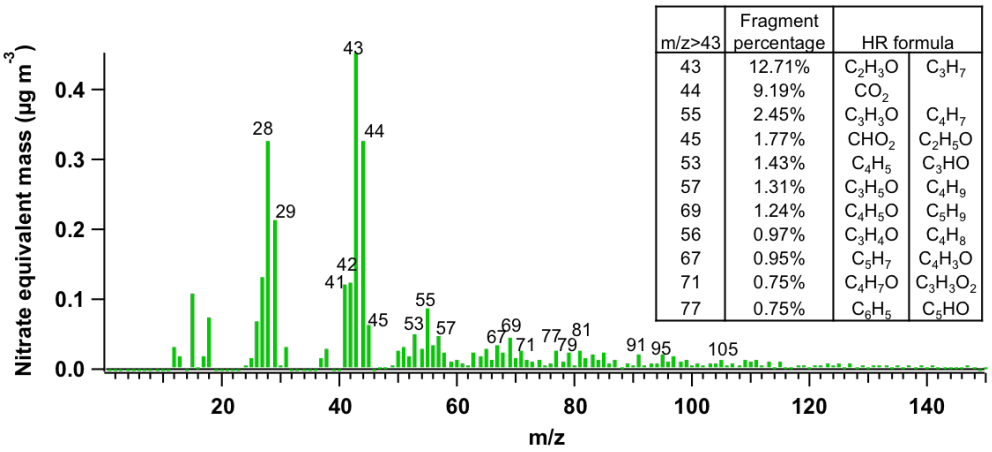

m/z>43	Fragment percentage	HR formula	
43	12.71%	C_2H_3O	C_3H_7
44	9.19%	CO_2	
55	2.45%	C_3H_3O	C_4H_7
45	1.77%	CHO_2	C_2H_5O
53	1.43%	C_4H_5	C_3HO
57	1.31%	C_3H_5O	C_4H_9
69	1.24%	C_4H_5O	C_5H_9
56	0.97%	C_3H_4O	C_4H_8
67	0.95%	C_5H_7	C_4H_3O
71	0.75%	C_4H_7O	$C_3H_3O_2$
77	0.75%	C_6H_5	C_5HO

Figure 4.9 Average mass-to-charge distribution from summer-blend-A photooxidation under low NO_x condition. (run: 2046B, w mode)

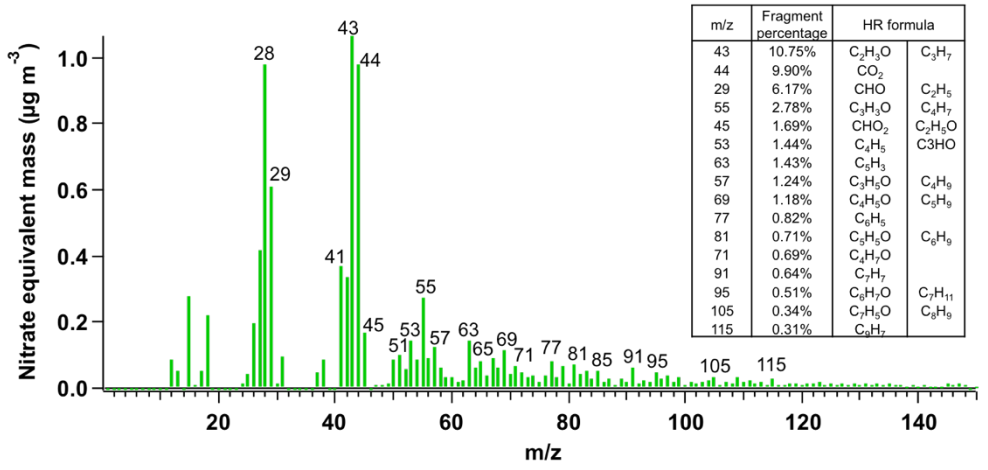

m/z	Fragment percentage	HR formula	
43	10.75%	C_2H_3O	C_3H_7
44	9.90%	CO_2	
29	6.17%	CHO	C_2H_5
55	2.78%	C_3H_3O	C_4H_7
45	1.69%	CHO_2	C_2H_5O
53	1.44%	C_4H_5	C3HO
63	1.43%	C_5H_3	
57	1.24%	C_3H_5O	C_4H_9
69	1.18%	C_4H_5O	C_5H_9
77	0.82%	C_6H_5	
81	0.71%	C_5H_5O	C_6H_9
71	0.69%	C_4H_7O	
91	0.64%	C_7H_7	
95	0.51%	C_6H_7O	C_7H_{11}
105	0.34%	C_7H_5O	C_8H_9
115	0.31%	C_9H_7	

Figure 4.10 Average mass-to-charge distribution from winter blend A photooxidation under low NO_x condition. (run: 1937A, w mode)

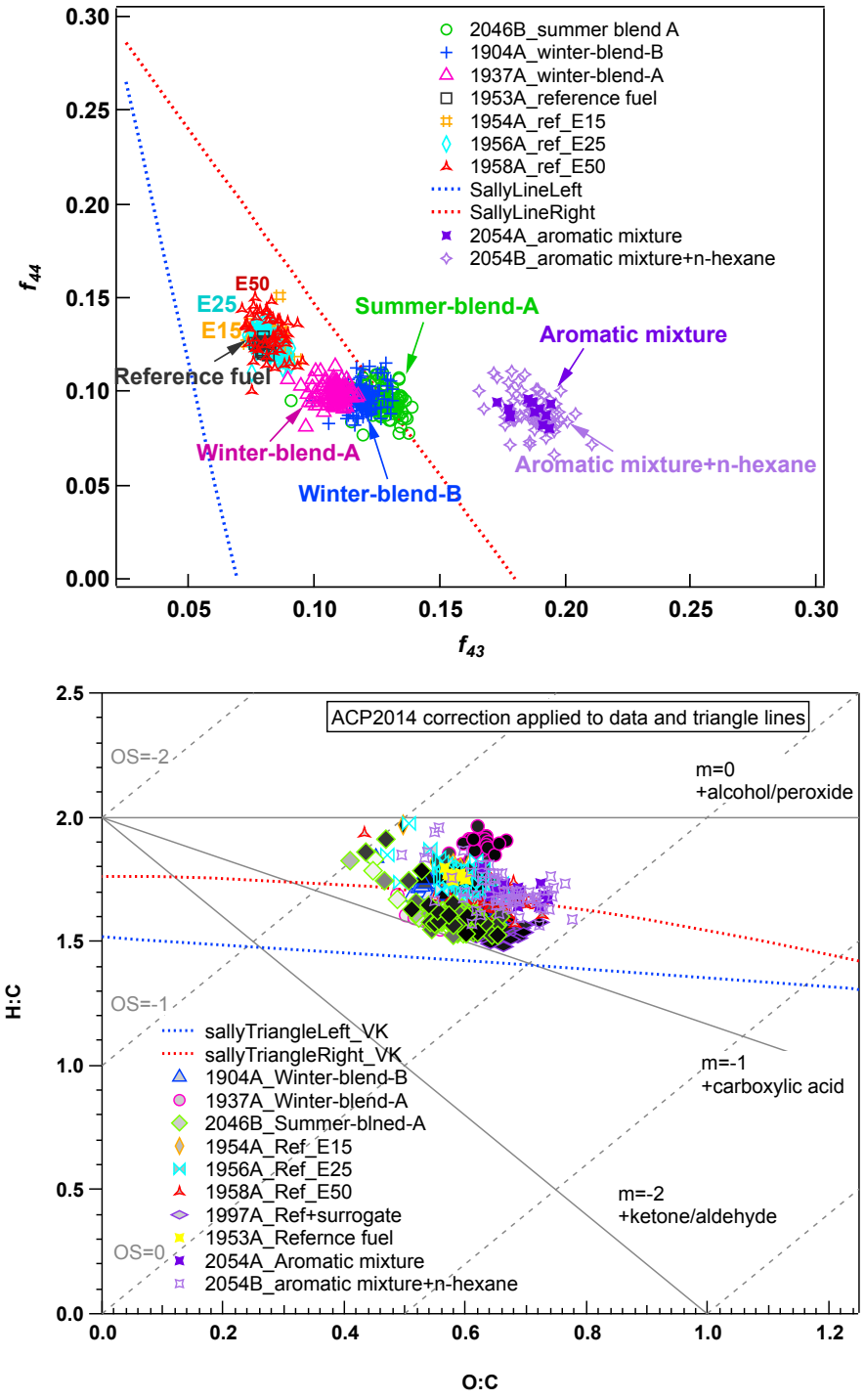

Figure 4.11 Triangle plot (f_{44} vs. f_{43}) and Van Krevelen diagram (H:C vs. O:C) for SOA of photooxidation from whole gasoline vapor and reference fuels with different blends. (ACP2014 correction applied to data and triangle lines was created by ToF-AMS-Analysis Toolkit 1.56D and HR Analysis 1.15D) (Canagaratna et al., 2014)

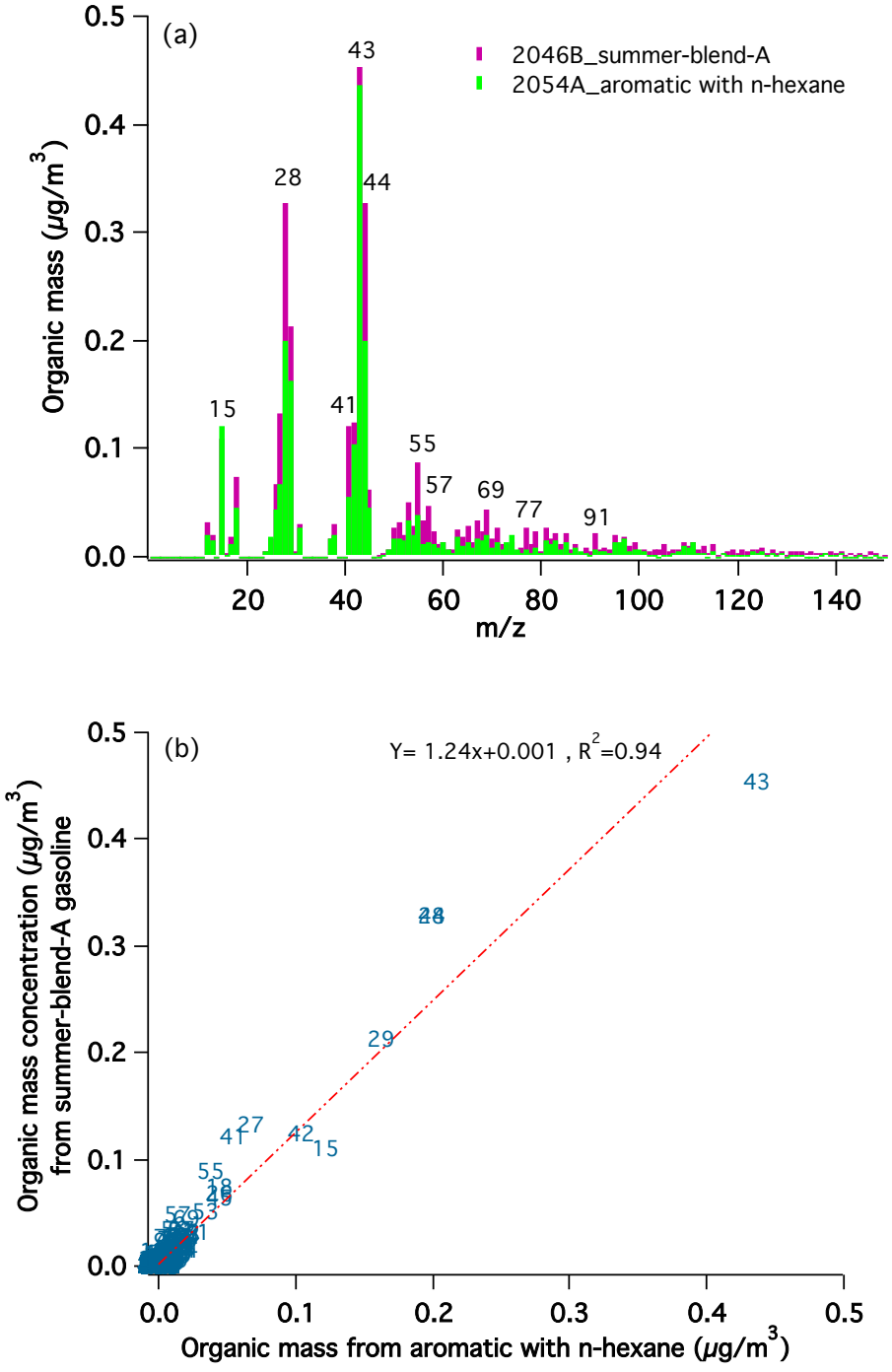

Figure 4.12 (a) Mass spectra distribution of organic aerosol from photooxidation of whole gasoline and aromatic mixture with *n*-hexane. (b) Mass-to-charge distribution relationship between gasoline and aromatic mixture with *n*-hexane.

4.7 Supporting Information

Table S 4.1 Chemical composition and reaction rate constant for whole gasoline

Species	Winter-blend-A Mass %	Summer-blend-A Mass %	Winter-blend-B Mass %	k_{OH} surrogate[a]	k_{OH} (cm^3 $molecules^{-1}$ s^{-1})[a]
C4 Paraffin	3.9	5.3	5.3	C4 iso/cyclo alkane	2.63E-12
C5 Paraffin	11.8	0.1	0.1	C5 iso/cyclo alkane	3.95E-12
C6 Paraffin	5.0	13.4	13.0	C6 iso/cyclo alkane	5.34E-12
C7 Paraffin	8.2	7.6	7.4	C7 iso/cyclo alkane	6.81E-12
C8 Paraffin	14.5	16.2	18.2	C8 iso/cyclo alkane	8.35E-12
C9 Paraffin	4.9	3.7	2.7	C9 iso/cyclo alkane	9.96E-12
C10 Paraffin	0.2	0.2	0.0	C10 iso/cyclo alkane	1.17E-11
C11+ Paraffin	0.2	0.2	0.0	C11 iso/cyclo alkane	1.34E-11
C6 Aromatic	1.9	1.6	1.6	benzene	1.22E-12
C7 Aromatic	3.0	2.9	2.8	toluene	5.63E-12
C8 Aromatic	9.2	9.9	9.5	C8 aromatic	9.98E-12
C9 Aromatic	1.1	1.2	1.0	C9 Aromatic	1.88E-11
C10 Aromatic	1.8	1.8	1.2	C10 Aromatic	3.30E-11
C11+ Aromatic	2.4	2.5	1.5	C11+ Aromatic	5.50E-11
Olefines	14.2	15.6	21.3	Olefines	3.70E-11
C5 Clycloalkane	0.0	0.0	0.0	C5 iso/cyclo alkane	3.95E-12
C6 Clycloalkane	1.2	1.2	2.7	C6 iso/cyclo alkane	5.34E-12
C7 Clycloalkane	0.3	0.3	0.3	C7 iso/cyclo alkane	6.81E-12
C8 Clycloalkane	1.9	0.7	0.4	C8 iso/cyclo alkane	8.35E-12
C9 Clycloalkane	0.1	0.0	0.0	C9 iso/cyclo alkane	9.96E-12

a: literature values (Jathar et al., 2013)

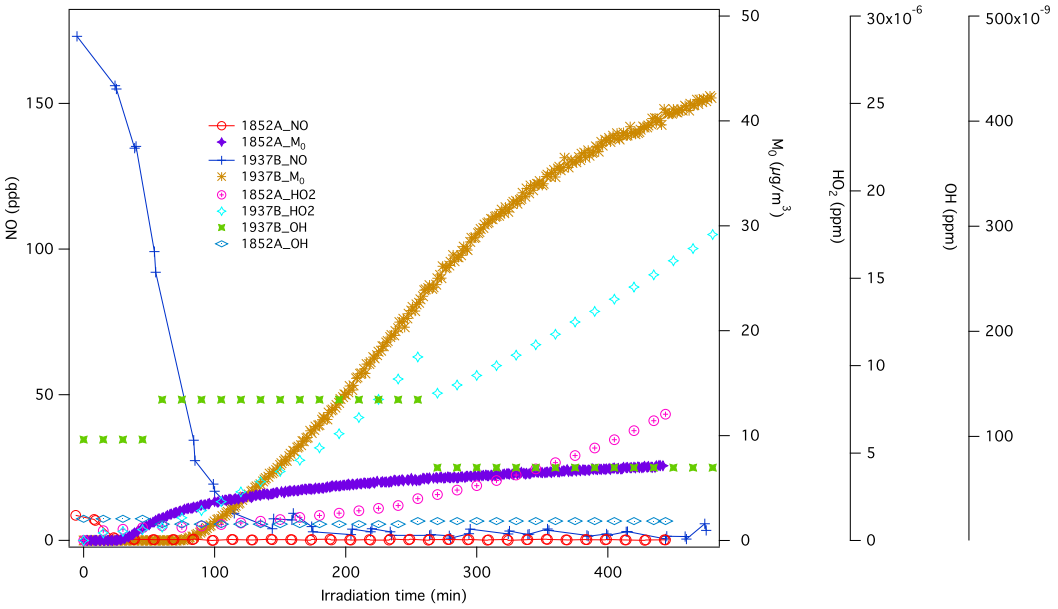

Figure S 4.1 Time series of NO consumption and total organic aerosol formation (ΔM_0) from winter-blend-A gasoline photooxidation.

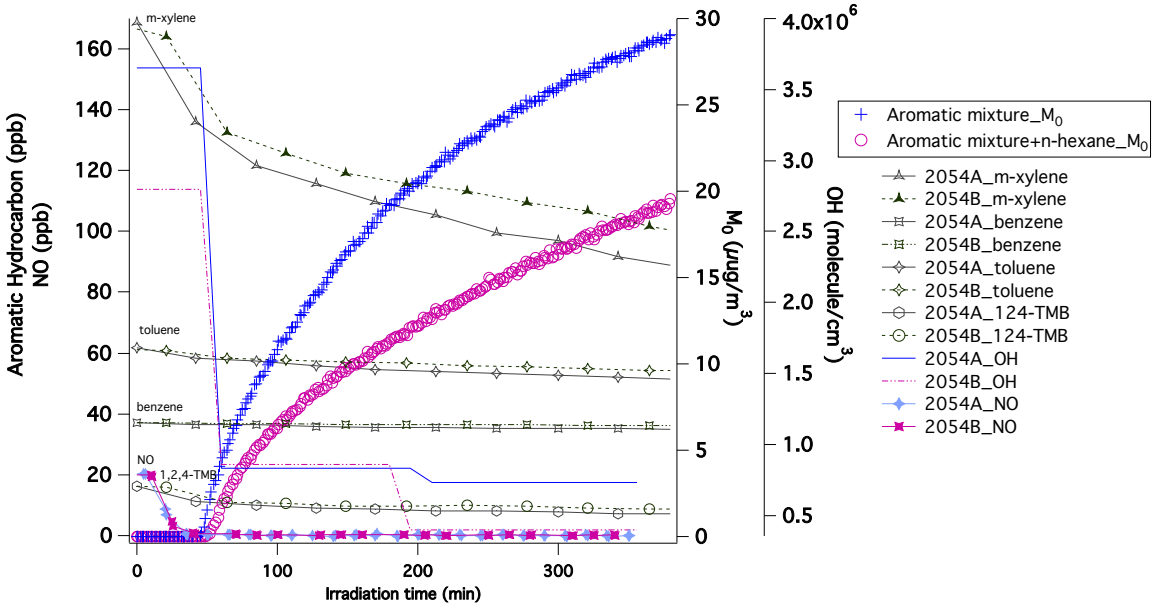

Figure S 4.2 Time series of NO, hydrocarbon decays, OH radicals, total organic aerosol mass concentration during the course of experiment.

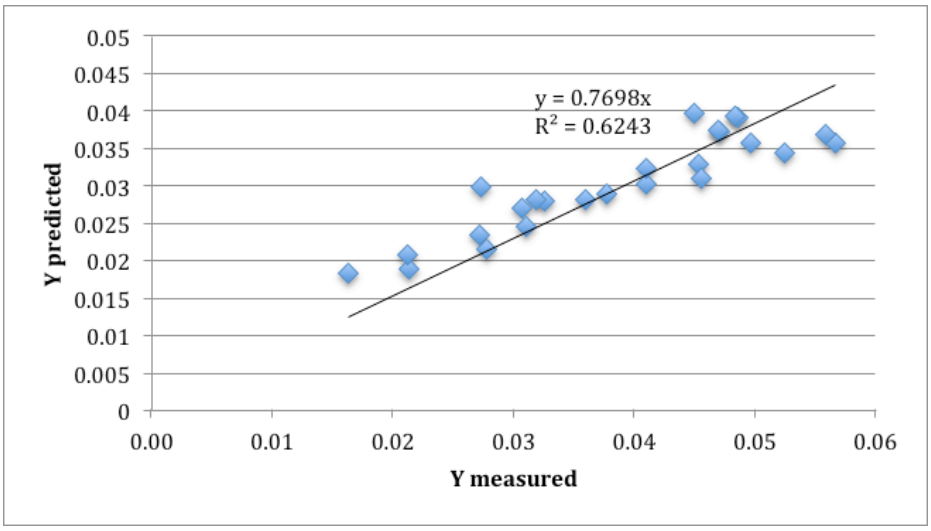

Figure S 4.3 Relationship of predicted SOA yields and measured SOA yields. (Predicted SOA is calculated using VBS parametrization by Jather et al (2013))

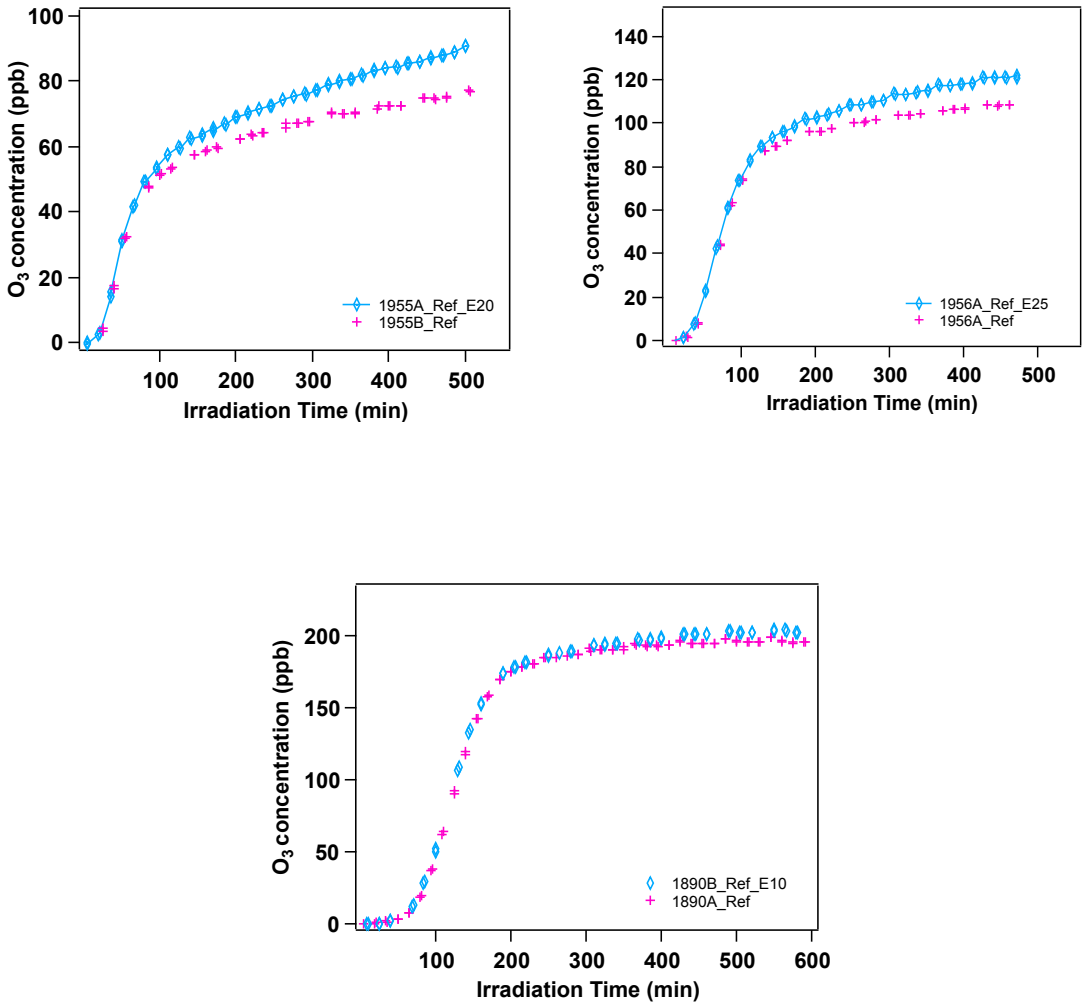

Figure S 4.4 Ozone formation from photooxidation of reference fuels with different ethanol blends.

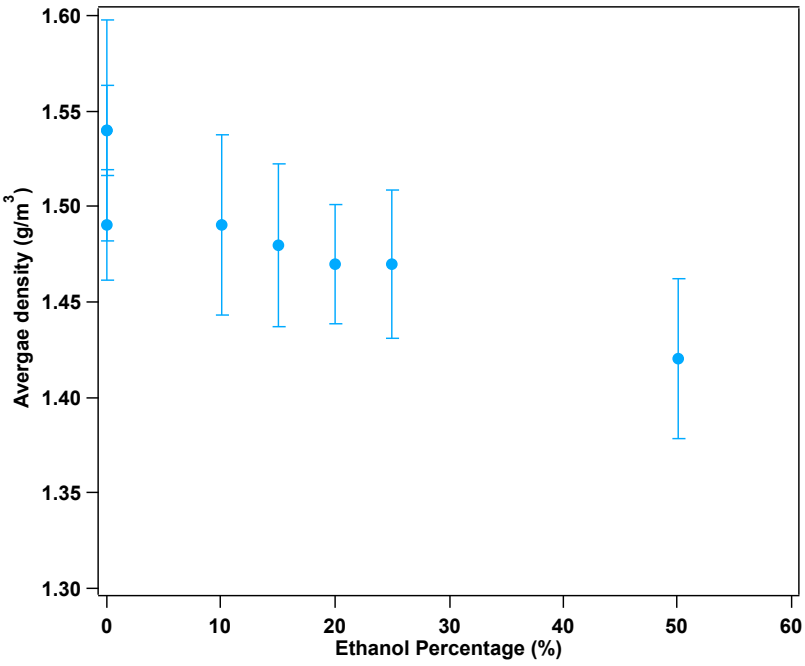

Figure S 4.5 Relationship between average density and ethanol percentage from reference fuels and reference fuels with ethanol addition.

Chapter 5 Summary of Dissertation

This thesis enhances our understanding of secondary organic aerosol (SOA) formation from select anthropogenic sources including polycyclic aromatic hydrocarbons (PAHs), PAHs mixed with *m*-xylene and an atmospheric surrogate, and unburned whole gasoline vapors. Major SOA chemical characteristics and physical properties were explored along with SOA formation within the UCR CE-CERT environmental chamber.

Chapter 2 investigated the SOA yield and chemical characteristics of SOA formation from naphthalene and two methyl substituted naphthalenes, 1-methylnaphthalene and 2-methylnaphthalene in the presence of NO_x and absence of NO_x conditions. The SOA yield is very high for all three PAHs precursors: 1-methylnaphthalene > 2-methylnaphthalene ~ naphthalene for all atmospheric conditions studies. SOA yields were substantially greater than 1.0 under H_2O_2 (ultra low NO_x) and low NO_x +H_2O_2 conditions for all three PAH precursors. OH concentration was observed to be a key factor in SOA formation from the PAH precursors. SOA from both 1-methylnaphthlaene and 2-methylnaphthalene high NO_x photooxidation was observed to be fractal-like indicating coagulating solid SOA particles. Formation of fractal SOA particles requires careful evaluation of SOA density to accurately represent SOA mass yields. It also suggests that chemical reactions in solid particles are surface-limited. The elemental and chemical composition analysis of HR-ToF-AMS revealed that oxygen-to-carbon ratio (O/C), average oxidation state of carbon, and aerosol time based triangle plot suggest that SOA aged during the experiment and is consisitent with observations of decreasing SOA volatility over the course of the experiments. Additionally, an indicator

of *m/z* 104 associated with the phthalic acid or phthalic anhydride product from PAHs SOA was observed by HR-ToF-AMS. The observation of a lower density fractal particle during 1-methylnaphthalene and 2-methylnaphthalene high NO_x photooxidation experiments suggests that previous studies not directly measuring density likely grossly over predict SOA formation.

Chapter 3 extended SOA formation from individual PAH photoxidation to that mixed with *m*-xylene and/or surrogate addition for simulating atmospheric condition. Experiments with different mixing ratios between PAHs and *m*-xylene indicate that the addition of *m*-xylene to PAH photooxidation experiments suppressed SOA formation from the PAH precursor. The SOA growth rate relationship of aerosol mass concentration (ΔM_0) versus hydrocarbon reacted (ΔHC) from different PAHs-*m*-xylene mixture is correlated with initial *m*-xylene/NO, PAHs/NO, $[OH]/[HO_2]$ ratio, $[NO]/[HO_2]$ ratio and $[HO_2]/[RO_2]$ ratio. It is observed that higher *m*-xylene/PAHs ratios and higher initial *m*-xylene/NO ratios lead to lower net SOA formation. The chemical composition characteristics such as f_{44} versus $f_{43,}$ H/C ratio, O/C ratio, and the oxidation state of the carbon ($\overline{OS_c}$) showed that PAHs-*m*-xylene SOA continuously ages and the SOA exhibits characteristics of both individual precursors. The atmospheric surrogate mixture chosen for the surrogate/PAH mixtures was based on the surrogate used to develop the Carter O_3 reactivity scales. Our results showed that the surrogate mixture photooxidation also suppressed SOA formation from PAHs by influencing gas-phase chemical reactivity.

Chapter 4 revisited the secondary organic aerosol (SOA) formation from reformulated whole gasoline vapor. SOA yields from select Southern California summer-

and winter-blend gasoline vapor photooxidation experiments under varying low NO_x condition range from 1.62% to 5.66%. SOA yields increased with increasing initial NO, which is reverse of observed trend with individual aromatic hydrocarbon chamber experiments. Three SOA yield curves (aromatics C_{6-7}, C_{8-9}, $C_{10+)}$ obtained previously for 17 individual aromatic hydrocarbons chamber experiments are overpredicted SOA formation from whole gasoline vapor by ~36%. Further, n-alkane addition was found to suppress SOA formation from the photooxidation of a mixture of aromatics. SOA from whole gasoline vapor and reference fuels were characterized as semivolatile oxygenated organic aerosol (SVOOA) by examining the "triangle plot" (f_{44} vs. f_{43}), the "Van Krevelen" (H:C vs. O:C) diagram, and volatility basis set.

In the future, the impact of gas-phase product chamber wall loss on SOA formation from aromatic hydrocarbons and PAHs can be investigated to further our understanding of aerosol formation underestimation based on two-product model prediction failure. In addition, diesel exhaust/diesel vapor emission is another major contribution of SOA source in urban area. It is expected that SOA formation from unburned diesel vapor will differ from whole gasoline vapor. Moreover, a direct measurement of OH and HO_2 radicals in aromatic or PAHs photooxidation system is necessary to further understand the effect of radicals on SOA formation.